Title
Development of Diverse Hydrogels from the Protean Polymer, Elastin-like Polypeptide

Author
Desai, Malav Sanjiv

Publication Date
2017

Peer reviewed|Thesis/dissertation

Development of Diverse Hydrogels from the Protean Polymer, Elastin-like Polypeptide

By

Malav S. Desai

A dissertation submitted in partial satisfaction of the

requirements for the degree of

Joint Doctor of Philosophy with University of California, San Francisco

in

Bioengineering

in the

Graduate Division

of the

University of California, Berkeley

Committee in charge:

Professor Seung-Wuk Lee, Chair
Professor Tejal Desai
Professor Ting Xu

Fall 2017

Development of Diverse Hydrogels from the Protean Polymer, Elastin-like Polypeptide

by

Malav S. Desai

To Elaine & my parents

Abstract

Development of Diverse Hydrogels from the Protean Polymer, Elastin-like Polypeptide

by

Malav S. Desai

Joint Doctor of Philosophy in Bioengineering with University of California, San Francisco

University of California, Berkeley

Professor Seung-Wuk Lee, Chair

Hydrogels have been used to develop scaffolds to address challenges in tissue engineering and drug delivery for several decades. The major advantage of using hydrogels is that their high water content and low stiffness enables them to mimic tissue-like environments. In my work, I develop four unique hydrogels using a single polymer, elastin-like polypeptide. The first challenge I address is that of hydrogel extensibility. Typical hydrogels cannot undergo large strains, which limits their durability and applicability to active tissues such as muscles. I use ELP to create a rubber-like elastic hydrogel that can stretch to 15 times its original length. Unlike most previous ELP hydrogels, our gels can reach such high strains due to the well-defined structure of our materials with minimal crosslinks. Next, I focus on developing an adhesive hydrogel using ELP. Unlike most adhesives, especially protein-based adhesives, our adhesive hydrogels are flexible and deswell in physiological conditions. This improves their potential for success in practical applications. We also developed a self-healing hydrogel by combining ELP with bioglass. Unlike other strategies that use reversible physical bonds, we use pH driven reversible Schiff base formation to synthesize hydrogels. Bioglass raises the localized pH to yield ideal conditions that favor gelling in our system. We also show that our materials can self-heal after being severed, which makes them durable and ideal for topical applications. Finally, we employ our efforts in the design and synthesis of protein-based beads for biolaser development. These devices are stimuli-responsive, which makes them ideal for optical sensing applications for biomolecule sensing and the flexibility of the hydrogels also makes them suitable for studying cellular biophysics. Through my dissertation, I hope to convey the versatility of ELP and the potential of structural design that can lead to the development of hydrogels with diverse functions.

Table of contents

List of figures

List of tables

Acknowledgments

First and foremost, I would like to acknowledge my mentor, Prof. Seung-Wuk Lee. I joined his lab in 2012 wanting to learn material design using genetic engineering and recombinant proteins. But, reflecting on my experience, the more important thing I learned is true independence in thought and problem solving. Over the years, Prof. Lee reminded me that Ph.D. is a degree in philosophy; my goal should be to learn how to think about scientific topics and the challenges at hand. Once I learn that skill, I can go out into the world and tackle any problem I take on. I hope to carry forward his enthusiasm for research, and his drive to invent and innovate through multi-disciplinary research. I would also like to thank my thesis committee members, Prof. Tejal Desai and Prof. Ting Xu, for their support through this process. Of course, I am also grateful for the support of my qualifying exam committee members, Prof. Song Li, Prof. Kevin Healy, Prof. Tamara Alliston and Prof. Alex Zettl.

I thank my labmates for making this experience so unique in many ways. My journey began with Eddie, Woojae, Byungyang and Jinwoo, all of whom went on to bigger and better things soon after I joined. But I am thankful for the warm and welcoming environment they created. I continued my journey with Kwang and Hyo Eon, who always inspired me with their hard work and dedication. The second half of my journey was with Juhun and Ju-Hyuck. I thoroughly enjoyed working with both of them and I certainly appreciate the respect they have shown me as a researcher. I am also thankful to Moon Kee and Hwa Hui for being so kind and helpful. I hope that I pass on my experience to them and I wish them great success as they carry the lab forward. I would also like to acknowledge Kyle, Tae Won and Julio for working with me and helping with my research. I hope I was able to teach them something useful and I wish them success in their future.

I wanted to dedicate this paragraph to my dear friend and mentor, Eddie. My wife, Elaine always jokes that I talk about Eddie like my big brother and I guess it is true. Eddie has been my role model and I am always inspired by his creativity in problem solving. I am truly grateful for all that Eddie has taught me and for introducing me to the once unknown world of elastin. And I cannot thank him enough for all the time he put aside to discuss my research and help me even after he moved on to his next adventures. I wish him success with everything he does.

I would like to thank all my friends in the program. I am so grateful to be surrounded by the smartest people in the world. Thanks to Harrison, Freeman, Daniel, Tuan, Ann, Harrison C. and Kunwoo for helping me and being there for me since when I first moved to the bay area. I enjoyed all our movie nights and social gatherings. I would also like to thank Paul for being such a great friend. Paul introduced me to climbing and it was a great way to manage stress and stay healthy. I also thank Paul for helping me machine parts for my experimental setups and always being there when I needed. I am also thankful to my fellow climbers, Kevin, Nicole, George, Preeya and Eda. I also thank the TableScope team, led by Arunan. It was such a fruitful experience working with Arunan, Matt, Kevin, Nicole and Ryan to create a real device that is on display in the

Deutsches Museum. I thank Xinyi for being so supportive and baking all the delicious desserts. It was so great that so many of our friends were also able to join me and Elaine for our wedding all the way in India. I am grateful to Hong, Jessie, Cade, and so many others who made my experience so wonderful. I have always been inspired by everyone's achievements and I can only hope that I made a difference in their lives.

I would like to thank my family members, who have always been there for me and believed in me. I am grateful to my uncle and aunt, Dewang and Rupal, for hosting me when I came to the US and for their continued support in everything I do. I also thank my uncle and aunt, Rashmin and Jyoti, for being there for me and helping me get settled in the US. I thank my cousins, Avi, Aakash and Aanal for their kinship. They made me feel at home even though I was so far away from home. And last year, my family expanded as Elaine and I tied the knot. I am thankful to my in-laws, Cheewai and Meiling, for being so supportive and making me feel at home whenever I am with them. I am also grateful to Victoria (the good twin) and Mark. Victoria and Mark are always there when I need help and I am proud to have both of them in my life. Finally, I would like to thank my parents, grandparents and my aunt, Pallavi. All of them played crucial roles in my childhood and continue to root for me in whatever I do. I am so grateful for the sacrifices my parents have made for me. They worked so hard to make my life easy. I cannot even comprehend what they went through to send their only child so far away. I can only hope that I have lived up to their expectations and continue to do so in the future.

Lastly, I want to thank my wife, Elaine. I have thoroughly enjoyed the years we have spent together and getting married to her was a dream come true. Elaine has been my inspiration to work hard and enjoy life. I am eternally grateful that she decided to find part-time work at the dining hall in Rutgers where I worked. Ever since, she has been the light that perpetually brightens each day of my life and I cannot imagine my life without her. I hope that we continue bringing out the best in each other and make each other proud.

Chapter 1 Protein biomaterials – hydrogel design and applications

1.1 Hydrogels

Water is an essential part of biological systems. Without water, the protein based tissues would be brittle and unable to support the cells they host. Although cells can typically maintain their surroundings, recovery from significant damage requires intervention. And the goal of this intervention is to replace the damaged tissues with a support structure that not only mimics the tissue, but also allows cells to penetrate, repopulate and replace the support with natural tissue.[1-4] Hydrogels are ideal for this need due to their high water content and a myriad series of available polymers, design strategies and cell-/tissue-specific interactions.[4-6]

In my thesis, I will mainly focus on the use of polymer chains to synthesize hydrogels. Polymer chains can be used to form stable networks by crosslinking them using physical or chemical bonds. Design of such a hydrogel requires the selection of at least two important parameters: type of polymer and crosslinking scheme. Synthetic polymers, such as polyethylene glycol, are readily available or can be synthesized using readily available components. The ability to tailor the composition of synthetic polymers and copolymers is an obvious advantage for designing unique hydrogels with properties such as controlled degradation, crosslink-density, adhesion or anti-fouling and cell-interactions. Alternately, natural polymers can also be used to synthesize hydrogels.[7] Nature-derived polymers such as polysaccharides and proteins are also readily available. Natural polymers can also be customized to display functional molecules and many already show great biocompatibility and safe degradation.[7] Both synthetic and natural polymer chains can be crosslinked using either physical crosslinks, such as hydrophobic interactions, ionic interactions and hydrogen bonding, or chemical crosslinks, through reactions such as Michael reaction, Diels-Alder reaction, Click chemistry and others or enzymatic reactions using transglutaminase, peroxidase, tyrosinase and others.[8]

Despite the fact that there are many materials and strategies that can be used to create a functional hydrogel, these strategies have unresolved complications that impedes their application. For example, synthetic polymers cannot be directly degraded by the cells and the management of degradation products is another issue altogether.[1] On the other hand, in addition to difficulty with degradation, natural polymers can show batch-to-batch variability depending on the source of the material and the method of extraction.[9,10] Theoretically, the use of proteins to replace damaged tissues makes logical sense because proteins are the polymers produced and used by our cells for support. However, the use of animal-derived proteins such as gelatin, collagen, α-elastin and other proteins also suffer from batch-to-batch variability as they are already in their mature and fully crosslinked form and require random hydrolysis for extraction.[7] Additionally, animal-derived proteins carry the risk of disease transfer from the host animal.

Recombinant proteins are an excellent alternative to the standard polymer choices.[11] Similar to natural proteins, recombinant proteins are composed of the same amino acid monomers. Yet, the synthesis of recombinant proteins begins with the design of the protein genes. The genes are then inserted into a host organism that expresses the prescribed protein. This process gives us the ultimate precision to control the sequence of the protein at the molecular level. Moreover, the expressed polymer chains are monodispersed both chemically and physically unlike other synthetic and natural polymers. I believe that recombinant proteins have great potential in the future even though it has met with limited adoption due to the need for specialized skills and the high cost of scaling up.[12]

1.2 Recombinant structural proteins

Proteins are an essential part of all biological systems. They have diverse and intricate life sustaining functions and have evolved tremendously to make us all fit for survival. Among the numerous proteins that exist, structural proteins are of particular interest in the design of nanomaterials for bioengineering and medicine. By understanding and using the naturally occurring proteins as a starting point to design new materials, we can improve upon evolution and design solutions that currently do not exist. The proteins that will be discussed in this review are the mammalian elastin and collagen as well as insect-derived silk and resilin. These proteins have been studied extensively and have been employed as scaffolds for tissue engineering and drug delivery.[13] Protein-based polypeptide (PBP) materials possess various advantageous features: 1) genetic engineering allows for the synthesis of precisely designed sequences, 2) recombinantly expressed PBPs enable preparation of monodispersed stock materials, and 3) careful sequence selection can facilitate mimicking natural extracellular matrix without the fear of rejection and disease transmission compared to allo- & xeno- grafts or the intricate chemical synthesis involved in synthetic scaffolds. Additionally, PBPs are easy to employ in biomedical applications due to their innate biocompatibility and biodegradability.[14,15]

PBPs described here are relatively simple polypeptides composed of the identified consensus sequences that hold the major properties of their host protein such as elasticity of elastin and strength of silk. Recombinantly expressed PBPs can either be full protein genes for instance recombinant tropoelastin and recombinant collagen or the fully synthetic versions composed of tandemly repeated consensus sequences. The fully synthetic PBPs are of great interest as they allow for the incorporation of functionalities abnormal to their natural counterpart, for example, cell adhesive resilin[16] and silk[17] or hydroxyapatite binding elastin.[18] The idea of incorporating functional modules into recombinant PBPs is nothing new, however creating more comprehensive PBPs with multiple functionalities is a growing field.[19] The development of more extracellular matrix-like PBPs is possible as now a single network of PBP can contain cell adhesion sites, biomolecule binding sites, matrix metalloprotease sites, etc. Additionally, combining multiple structural motifs to create PBPs such as silk-elastin,[20] silk-collagen,[21]

and even resilin-elastin-collagen[22] has led to self-assembling novel materials with previously unobserved properties.

We will first provide brief backgrounds for each of the four structural proteins followed by updates on the types of strategies being used for developing PBP-based tissue engineering materials. This is followed by a description of a range of modular PBPs developed for similar applications and future prospective on the field. Comprehensive collections of research for each PBP such as elastin,[13,14,23-27] collagen,[13,27,28] silk,[13,27,29-32] and resilin[13,33,34] can be found in recent reviews.

1.2.1 Elastin & Elastin-like polypeptides (ELP)

Elastin is one of the major mammalian structural proteins present in blood vessels, lung epithelium, skin, and other tissues to provide them with high elasticity and resilience.[35] The highly repetitive elastin proteins are secreted by cells in their vicinity and crosslinked soon after. This crosslinked (or mature) elastin is fibrous and hydrophobic making it insoluble and difficult to isolate and sequence. In order to study elastin, it was critical to isolate the 72 kDa soluble protein known as tropoelastin upon secretion from cells.[35,36] Tropoelastin is composed of lysine-rich hydrophilic crosslinking domains and elastic hydrophobic domains. Once outside the cell, lysine is enzymatically converted to allysine (a reactive moiety that forms desmosine or isodesmosine crosslinks) by lysyl oxidase, a copper-dependent enzyme.[36] As a result, soluble tropoelastin was first isolated from copper-deficient pigs by Sandberg and co-workers.[37,38] This was a major breakthrough in identifying the protein sequence and genes expressing this highly repetitive protein. Since then, there have been numerous studies about the biochemistry and structure of tropoelastin increasing our understanding of the role of elastin and its potential to solve problems.

As mentioned, tropoelastin is a highly repetitive protein with hydrophilic and hydrophobic domains. The hydrophilic domains mainly contain a series of lysine residues interspersed with alanine, while the hydrophobic domains contain repetitive sequence units such as the tetra-, penta- and hexa-peptides ‘VPGG’, ‘VPGVG’ and ‘VAPGVG’, respectively.[36] The hydrophobic domains are the source of elasticity and the unique thermo-responsiveness of proteins related to elastin. These two properties are recaptured within recombinantly produced elastin-like polypeptides or ELP (also known as elastin-like recombinamer, ELR) that commonly use the hydrophobic domain derived pentapeptide repeats ‘VPGVG’ or more generally ‘VPGXG’ (‘X’ can be any amino acid except proline).[14](Figure 1.1) In mammalian tissues, the intriguing thermal response of tropoelastin is critical for mature elastin formation as the phenomenon localizes the secreted tropoelastin until crosslinking. Localization occurs as tropoelastin phase-separates into a coacervated state above its characteristic transition temperature (T_t). This phenomenon is fully reversible and is known as inverse temperature transition (ITT).[36] Thus, ELPs also have ITT and numerous sequences produced over years of research show that this ITT depends on the sequence (*i.e.* hydrophilicity of the guest residue ‘X’) and the length/molecular weight (M_w) of the ELP, as well as the pH and ionic strength of the environment.[39,40]

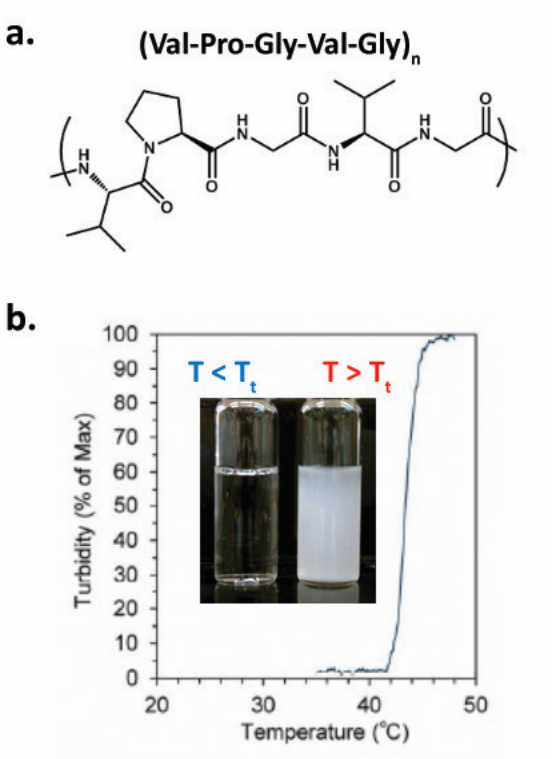

Figure 1.1 Elastin-like polypeptide sequence and stimuli-response. *a) Consensus sequence derived from tropoelastin (Val-Pro-Gly-Val-Gly) can be tandemly repeated to synthesize elastin-like polypeptides (ELPs). (b) Stimuli-responsive properties of the ELPs, which exhibit inverse temperature transition. They are highly soluble in low temperature and coacervate above low critical solution temperature (T_t). Reprinted (adapted) with permission from Wang E., Desai M.S., Lee S.-W. Light-Controlled Graphene-Elastin Composite Hydrogel Actuators. Nano Lett 2013, 13(6):2826–2830. doi:10.1021/nl401088b. Copyright 2013 American Chemical Society.*

Understanding the mechanisms for the properties of elastin and its derivatives has been a challenge as the protein cannot be crystallized making structure determination and visualization challenging. Although only supported by circumstantial evidence, Urry and coworkers have claimed from early on that elastin has a β-spiral structure with 'VPGV' sequences creating type II β-turns.[41] Nonetheless this is not probable because a rigid β-spiral structure with intra-chain hydrogen-bonding would contradict the rubber like entropic mechanism observed for the elasticity of the protein; for example, stretching a single tropoelastin chain using an atomic force microscope does not produce a saw-tooth profile expected from unfolding of secondary or tertiary structures but instead shows single and repeatable change in cantilever deflection.[42] Recent studies using complex 2D NMR modalities to determine distances between ^{13}C-^{1}H and ^{13}C-^{15}N as well as to observe ^{15}N within labeled elastin reveal the lack of a β-spiral structure but indicate that the entropically driven elasticity mechanisms rely on the entropy of water around hydrophobic elastin segments as opposed to the entropy of intra-chain hydrogen bonding.[43,44] This conclusion agrees with the tropoelastin chain stretching experiment in which elastin returns to its original conformation or something similar after the chain is

relaxed. Additionally, it also helps explain the thermo-responsiveness of elastin that depends on the changes in the entropy of water molecules resulting from the changes in water/elastin hydrogen bonding stability as the temperature increases. The theory can also be used to explain the increases in the proportions of ordered structures as seen in Fourier transform infrared (FTIR) and circular dichroism spectra resulting from elastin dehydration during its ITT that likely concentrates β-turns as the protein coacervates.[45,46]

In biomaterial research, three main derivatives of elastin have been utilized: α-elastin, recombinant human tropoelastin (rTE), and ELP (or ELR). The commercially available α-elastin is obtained from processed mature elastin derived from bovine tissues, however these polypeptides have predefined sequences, a broad distribution of M_w and can have batch-to-batch variability as they are tissue derived.[47] rTE and ELP allow for better control of polypeptide dispersity with the fully synthetic ELP being the most biochemically customizable.[14] Recombinant expression of elastin derivatives is mainly done in engineered *E. coli* with relative ease of protein purification due to the thermo-responsiveness of elastins.[14] As will be discussed in section 1.3.1, elastins are extremely valuable for making highly extensible structures as well as for stimuli-responsive applications including stimuli-triggered self-assembly and molecule delivery. Outside of their usefulness as structural proteins, the thermo-responsive ELP sequences can also be used as fusion tags for purification of other recombinantly expressed proteins. Examples include purification of thioredoxin and tendamistat as shown by Meyer *et al*., and more recently to purify beak and feather virus capsid proteins expressed in tobacco plants by Duvenage *et al*.[48,49]

1.2.2 Collagen & Collagen-like polypeptides (CLP)

Collagen is the most abundant structural protein in mammalian tissues. The characteristic structure of collagen is the triple helix composed of three separate α chains that form homotrimers if the chains are identical or heterotrimers if they are different.[50] (Figure 1.2) In addition to the six α chains, α1 thru α6, further complexity arises as α chains can be composed of different domains due to alternative splicing of exons.[50] The variety of triple helices can then assemble into higher ordered supramolecular structures like fibrils, beaded filaments, anchoring fibrils, networks and hexagonal networks in addition to fibril associated collagens with interrupted triple helices (FACITs) that latch onto assembled fibrils.[50] So far, 29 different types of collagen have been identified serving different purposes in tissues.[50,51] Among these, collagen type I is a major component forming tissues such as skin, tendons, blood vessels, organs and bone. Collagen type III is also present in many tissues alongside collagen type I, while collagen type II makes up majority of the cartilage tissues as well as vitreous humour in the eye.[52,53] Due to the relative abundance and applicability of these three types of collagen, they have been used in biomedical research as well as for more basic research to understand collagen structure and stability.

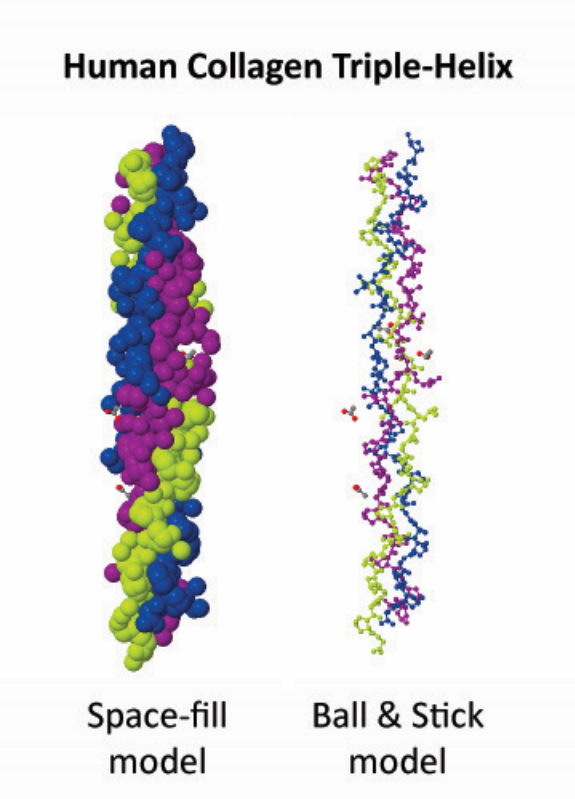

Figure 1.2 Human collagen structures that are visualized using PDB: IBKV in two different forms: Space-fill model (left) and Ball & Stick model (right).

The polypeptide chains of collagen are composed of highly repetitive tripeptide of the general from 'GXY'.[50,54] The presence of hydroxyproline (O) at 'X' and proline at 'Y' is relatively common in collagen sequences. Through studies of chemically synthesized collagen-mimetic peptides (CMP) of the form $[GOP]_n$, researchers have identified that hydroxyproline and proline are critical for the stability of mammalian collagen triple helices as the residues constrict the conformation of the chains to entropically stabilize the structure even at 37°C.[28,55] The stereoelectronic effects of the electronegative hydroxyl group on the hydroxyproline has been indicated to promote the trans-isomer of the hydroxyprolyl amide bond thus increasing triple helix stability.[28,56] Although this knowledge is valuable, recombinant synthesis of collagen-like polypeptides (CLP) still remains a challenge. Chemical synthesis allows the use of hydroxyproline, an unnatural amino acid, however CMP/CLP is of limited length as well as expensive to produce in large quantities. Biological systems such as *E. coli* lack prolyl 4-hydroxylase required for post-translational modification of proline to hydroxyproline and the high G-C content of CLP genes also limits the size of peptide that can be successfully expressed. Other organisms such as plants and yeast have thus been commonly used to express CLP with the drawback of increased genetic complexity.

A solution to this problem came to light upon the identification of collagen-like sequences in bacteria such as *Streptococcus pyogenes*, *Bacillus anthracis*, *Clostridium perfringens*, etc.[57-59] This bacterial protein capable of forming triple helices is naturally expressed on the cell walls of the host bacteria and is used by the bacteria to anchor onto

human cells.[58] These proteins are also composed of repeating 'GXY' triplets with 'X' and 'Y' positions having high frequencies of charged amino acids such as lysine, glutamic acid, aspartic acid as well as rigid proline residues. The presence of charged residues enables bacterial collagen to mimic mammalian collagen-like triple helical structures without the need for hydroxyproline.[59] This phenomenon has also been replicated using chemically synthesized CMPs containing charged amino acids instead of $[GOP]_n$ sequence.[56] The bacterial collagens have been shown to have melting temperatures around 35°C to 39°C,[58,59] which is quite remarkable as it makes this simple and scalable recombinant CLP useful for biomedical applications. Currently, a critical property missing from bacterial collagen is that the protein cannot undergo mammalian collagen-like hierarchical assembly into complex structures.[58] However, research using CMPs or model collagen-like particles to understand collagen stability and self-assembly is already underway and will help determine the criteria useful for future design and tuning of bacterial CLPs.[56,60,61]

1.2.3 Silk & Silk-like polypeptides (SLP)

Silk is one of the most important and ancient insect-derived protein materials used by humans. The protein has come a long way from being used in textiles to being FDA approved for use in various biomedical applications.[29] Silk is expressed by many insects as a supportive structural material and it has piqued the interest of many due to its astonishing properties. It is extremely tough with high strength and elasticity, properties that tend to be mutually exclusive. In fact, silk can be compared to and has been shown to surpass the properties of materials such as tensile steel and kevlar.[29] Among the different sources of silk, silkworm silk and spider silk have been studied heavily with dragline spider silk being the toughest of all types.[29] Several domains and consensus repeat units have been identified in natural sequences of spider silk, for example rigid β-sheet forming '$[A]_n$' and '$[GA]_n$' repeats, highly elastic β-spiral forming 'GPGGX' and 'GPGQQ' repeats, 3_{10} helix forming 'GGX' repeats, charged non-repetitive spacers, and N- & C-terminal domains critical for pH responsive fiber spinning in insect glands.[29,32,62] (Figure 1.3)

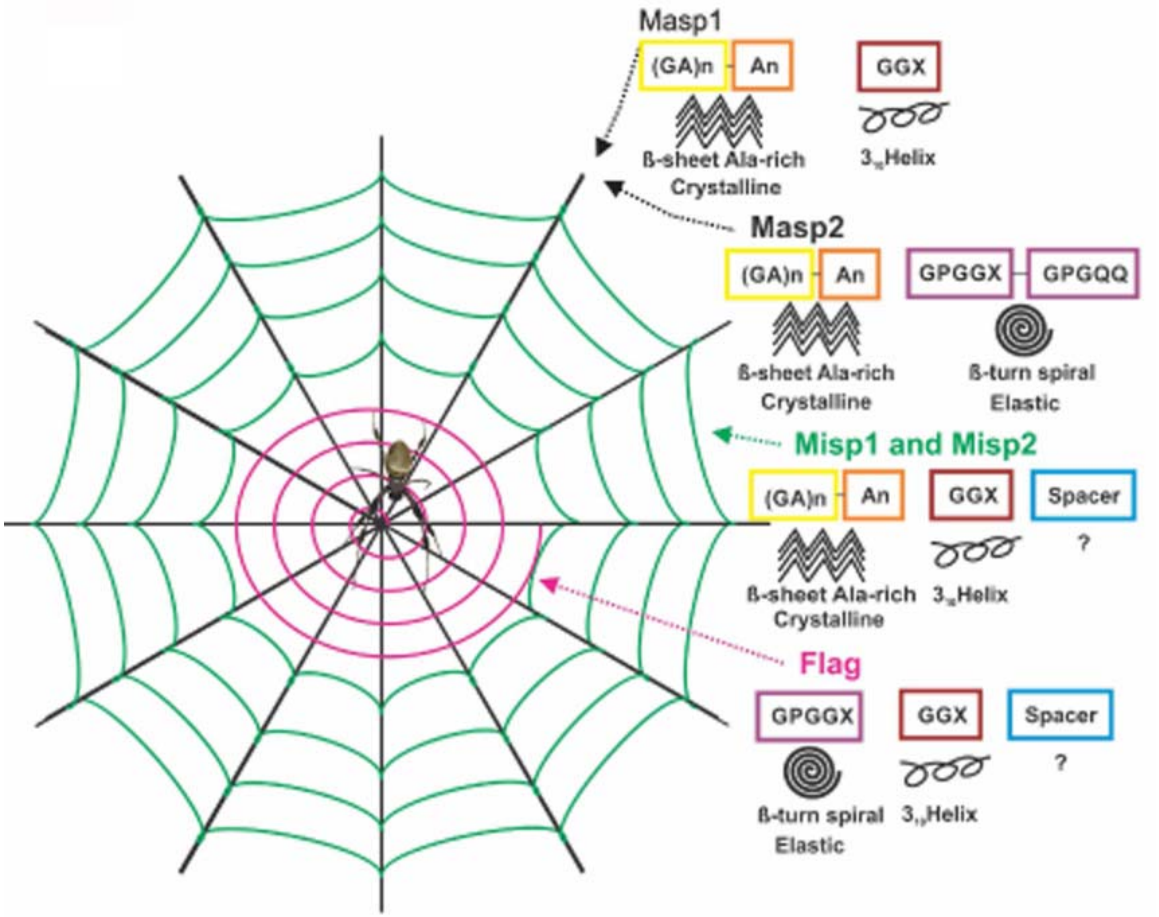

Figure 1.3 Schematic showing the different types of silks spun by spiders. *Each type of silk has different modular domains that vary the strength, elasticity, and adhesiveness of the silk. Reprinted (adapted) with permission from Tokareva O., Michalczechen-Lacerda V.A., Rech E.L., Kaplan D.L. Recombinant DNA production of spider silk proteins. Microb Biotechnol 2013, 6(6):651–663. doi:10.1111/1751-7915.12081. Copyright 2013 John Wiley and Sons.*

The mechanical properties of silk depend on the order and proportions of crystalline and elastic domains involved, thus making the proteins intrinsically modular. Spiders alone combine these different modules in varying proportions to create an assortment of silks for example: dragline silk from major ampullate glands, viscid silk from flagelliform glands, and adhesive silks from aggregate and piriform glands as well as accessory silks such as tubiliform silk from cylindrical glands and capture silk from aciniform glands.[63,64] Among these proteins, the dragline silks: major ampullate spidroin 1 & 2 form the toughest fibers and are therefore used extensively for recombinant expression.[64] Highly extensible silks have also been studied by recombinant expression of flagelliform silk containing the elastic 'GPGGX' repeats.[65] Recently, a chimeric silk composed of a combination of major ampullate spidroin 2 and flagelliform silk modules was also created to show the formation of a highly extensible yet strong silk-like polypeptide (SLP) with a young's modulus of 4.6 GPa, toughness of 93.5 MJ/m^3 and extensibility of 80.3 %.[66] Although individually, the native dragline (10 GPa; 160 MJ/m^3; 27-35 %, resp.) and flagelliform (0.003 GPa; 150 MJ/m^3; 200-270 %, resp.) silks have

higher toughness and excel in young's modulus and failure strain, respectively, the properties of the chimeric SLP are remarkable considering that it is only 1/5th of the native protein length.[66]

Chimeric and multimeric SLPs combining multiple properties in a single polypeptide will be extremely valuable in the future especially if the hurdle of recombinant expression is overcome. SLP length is a critical factor defining its mechanical properties, but longer proteins are challenging to express due to factors such as highly repetitive gene sequences rich in guanine-cytosine pairs, high glycine content, and insoluble expression products.[67,68] Fortunately, over time, longer SLPs have been expressed in a variety of hosts such as bacteria (*E. coli*), transgenic silkworms, transgenic plants and mammalian cells.[67] Recently, Xia *et al*. successfully expressed a full length 284.8 kDa SLP composed of major ampullate spidroin 1 derived sequence from *Nephila clavipes* using engineered *E. coli*.[68] Compared to this, the more commonly expressed SLPs using similar sequences tend to be in the range of 60 – 130 kDa.

In addition to the protein sequence and length, silk properties are also affected by the process of fiber spinning. As revealed through studies of spider silk glands, a highly concentrated aqueous silk dope undergoes phase separation and transitions to a solid from due to ion exchange, acidification, and water removal as it travels out from ampulla (sac) through a tapered duct.[69] It is proposed that the amphiphilic silk proteins are able to form micelles with semi-crystalline domains and these micelles further organize into stable supramolecular assemblies via the N- and C- terminal domains.[69] As the solution travels through the tapered duct, the micelles elongate and fuse due to phase separation and transition of the dope solution into a solid fiber.[69] The increasing shear forces and post-draw stretching further help align crystalline domains of silk giving the fibers their remarkable properties.[70,71] Attempts have been made to copy this process, however obtaining highly concentrated silk dopes (up to 50 % w/v in silk glands) is not yet possible.[72] Being able to fully replicate such a process would greatly improve the properties of synthetic silks to match or even surpass the properties of natural silk fibers.

An alternative to the more conventional silks is silk produced by bees, hornets and ants.[73] Unlike the β-sheet rich spider and silkworm silks, these silks have four proteins each with a central α-helical structure that induces the formation of coiled-coils. The coiled-coil silks are weaker but more elastic than spider and silkworm silk. For example, hand-drawn fibers from honeybee larvae have a tensile strength of 132 MPa and failure strain of 204% in dry conditions.[73] These silks are also readily expressed in *E. coli* due to the small protein size (30-45 kDa for each of the four proteins) compared to the full length major ampullate spidroin proteins (250-320 kDa) that require genetically modified *E. coli* for expression.[67,68,74] Additionally, due to sequence similarity among the four proteins it was found that a single protein can also accomplish the same coiled coil structure eliminating the need to express all four proteins in *E. coli* for silk fiber formation.[75] Although these small and elastic silk proteins are still relatively unexplored in the field of bioengineering, they may be useful alternatives to keep in mind for future applications due to their proven biocompatiblity.[76]

1.2.4 Resilin & Resilin-like polypeptides (RLP)

Resilin is a highly resilient protein that is also a critical component for the extraordinary abilities of insects to fly, move and produce sound.[77] Among the structural proteins described so far, resilin is the newest member to be recombinantly expressed. It was only about a decade ago that resilin from *Drosophila melanogaster* was expressed using *E. coli*, a critical milestone that boosted structural studies of this protein and interest in its use for bioengineering applications.[77] The protein is composed of three segments with the hydrophilic N-terminal segment being highly elastic, hydrophobic mid-segment containing chitin binding sequence and the hydrophilic C-terminal segment that can reversibly undergo conformational changes indicating energy storage.[77,78] (Figure 1.4) The phenomenon of energy storage in the C-terminal segment has been explained by thermally induced changes in its conformation from random coil to β-turns that reverses when the protein is cooled. This reversible transition can also be observed when a gel made of the full protein or just the C-terminal segment is mechanically stretched indicating that this mechanical energy may be also be absorbed. Qin *et al*. drew a correlation that similar to the heat absorbed during conformational changes with thermal input, energy from a mechanical input is absorbed and stored in resilin; the stored energy can be released and use for mechanical work upon removal of this input.[78] Thus, for insects, resilin is not only a soft highly extensible spacer, but it reversibly stores energy that is used to give a significant boost to the moving appendages enabling insects to jump and/or fly with great efficiency.

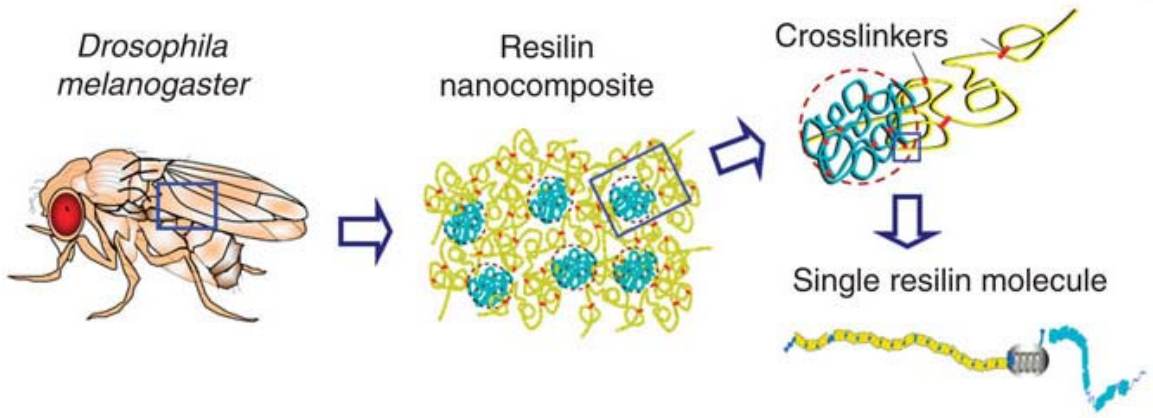

Figure 1.4 Resilin structure from Drosophila melanogaster. *A single molecule of resilin (bottom right) contains three segments: elastic segment (yellow) from exon 1, chitin binding segment (gray) exon 2, and energy storing segment (blue) exon 3. Resilin molecules crosslinked via dityrosine bridges organize into a nanocomposite structures due to self-association of exon 3 protein segment and give insects remarkable abilities of locomotion, flight and sound production. Reprinted (adapted) with permission from Qin G., Hu X., Cebe P., Kaplan D.L. Mechanism of resilin elasticity. Nat Commun 2012, 3:1003. doi:10.1038/ncomms2004. Copyright 2012 Nature Publishing Group.*

Recombinantly expressed resilin-like polypeptide or RLP is composed of tandem repeats of consensus sequences from the N-terminal segment of resilin. These include *D. melanogaster* derived 'GGRPSDSYGAPGGGN' as well as *Anopheles gambiae* derived

'AQTPSSQYGAP' repeating units.[33] RLP using both of these sequences have been shown to have similar elastomeric properties. In addition to the elastomeric properties, resilin and RLP are also thermo-responsive. Similar to elastin and ELP, resilin and RLP sequences undergo a sharp transition from hydrophilic to hydrophobic above a transition temperature, a property known as lower critical solution temperature (LCST). However, unlike elastin, resilin and RLP also undergo a similar transition when cooled below a second transition temperature, a phenomenon known as upper critical solution temperature (UCST). Due to the presence of many hydrophilic residues in RLP sequences, the LCST of the protein occurs at a relatively high temperature of 70°C, while UCST occurs below 6°C.[79] One last property of natural resilin is that it undergoes fluorescence resulting from its dityrosine crosslinks. The phenomenon can be replicated in RLP when it is crosslinked via tyrosine residues.[77]

1.3 Design and applications of protein hydrogels

1.3.1 Elastin & Elastin-like polypeptides

Recombinant tropoelastin (rTE) has helped reveal many properties of elastin and its derivatives. Along with basic biological studies, rTE has also been used to develop various tissue engineering substrates. The advantages of using rTE are that it does not induce blood clot formation due to its low thromogenicity,[80,81] it forms compliant structures,[82] and it is compatible with many cell-types including vascular endothelial and smooth muscle cells.[82-84] Additionally, rTE also contains a hydrophilic cell-interactive C-terminal domain with positively charged 'GRKRK' domain that induces cell adhesion via integrin binding.[35,36,85] The first example of rTE based scaffolds is electrospun fabrics composed of rTE.[82-84] rTE has mainly been spun in 1,1,1,3,3,3–hexafluoro-2-propanol (HFIP) followed by crosslinking (necessary fiber stability) with amine reactive 1,6-diisohexanecyanate and glutaraldehyde (GTA),[84] and disuccinimidyl suberate.[82,83] The disuccinimidyl suberate crosslinked electrospun fabrics formed using 15 % w/v solutions are soft as revealed by tensile testing of phosphate buffered saline soaked fiber mats showing a young's modulus of 0.15 MPa, failure strain of 75 % and a tensile strength of 0.38 MPa. Interestingly, the use of higher weight/volume ratios of spinning solution results in ribbon-like instead of cylindrical fiber morphology for recombinant tropoelastin (rTE) also seen in electrospun ELPs.[86,87] The phenomenon of ribbon-formation with rTE and ELP may result from coacervation interactions that are enhanced in elastin solutions with higher concentrations.[87] Similar to electropun ribbons of poly(ether imide), the rTE/ELP may quickly form a thin skin around the spinning jet and the remaining solvent diffuses out of the skin instead of quick evaporation.[88] Since the elastin skin is soft, the fiber collapses into ribbons as observed with rTE and ELP electrospun fabrics.[82,87,88] Another example of rTE-based tissue engineering scaffold is a photocrosslinkable compliant hydrogel.[89] Annabi *et al*. synthesized methacrylated tropoelastin (MeTro) by reacting rTE with methacrylate anhydride. MeTro can then be mixed with the photoinitiator 2-hydroxy-1-(4-(hydroxyethoxy) phenyl)-2-methyl-1-propanone and crosslinked under UV to create both 2D cell culture substrates and 3D cell encapsulating gels.[89] Microgrooved compliant MeTro gels that allow for cell alignment have also been used for cardiac tissue engineering with control over cell orientation.[90] These gels have

variable young's modulus from 2 to 14 kPa and can undergo up to 400% strain with low energy loss.[89,90] Porous tropoelastin hydrogels have also been produced by chemical crosslinking using disuccinimidyl suberate as described by Tu *et al*.[91] In addition to the direct utilization of rTE, many researchers have also explored its use in improving and tuning properties of materials made of polymers such as polycaprolactone,[92] natural polysaccharides such as heparin and dermatan sulfate[93] and proteins such as collagen[94] and silk.[95-97]

Although recombinantly expressed tropoelastin is a homogeneous polypeptide able to mimic natural elastin, only fully synthetic ELPs give the user freedom over sequence design that could be advantageous for developing diverse biomaterials. ELP is also highly biocompatible and therefore has already been used in applications such as cartilage, ocular and liver tissue engineering.[14] A common type of scaffold useful for such applications is a compliant hydrogel, which is achievable for a soft protein such as ELP.[42] An important aspect of hydrogel formation using ELP has been the use of lysine for chemical crosslinking. Succinimidyl derivatives such as tris-succinimidyl aminotriacetate,[98] and N-hydroxysuccinimide functional 4-arm PEG[99] have been used for ELP hydrogel formation. The use of organic solvents to avoid hydrolysis of succinimide derivatives has an additional advantage of preventing ELP temperature-transition during crosslinking and thus allowing the formation of optically clear gels with constant gel crosslinking.[98,99] ELP hydrogels are also thermoresponsive due to the ITT property of ELP; coacervation of ELP with increasing temperatures results in gel dehydration and a decrease in gel volume as a consequence.[98,99] This reversible property also affects gel mechanical properties as seen with TSAT crosslinked gels that show a softer range of young's modulus of 0.24 to 3.7 kPa at 7°C, while relatively dehydrated gels show a range of 1.6 to 15 kPa at 37°C.[98]

Many researchers have also sought cell encapsulation using ELP hydrogels to mimic extracellular matrix like 3D environments for tissue engineering.[100] For example, lysine containing ELPs were enzymatically crosslinked using transglutaminase.[101] The resulting hydrogels could encapsulate chondrocytes and induce formation of hyaline cartilage-like substrate rich in collagen-II.[101] Non-enzymatic alternative that also use amines for crosslinking in mild aqueous conditions is the use of (hydroxymethyl) phosphine derivatives such as [tris(hydroxymethyl)phosphino]propionic acid (THPP)[102,103] and tetrakis(hydroxymethyl) phosphonium chloride (THPC).[104] The fast reaction between phosphines and amines enables rapid crosslinking that can also be done *in situ*.[103,104] THPP crosslinked gels with an elastic modulus of about 11 kPa have been used for cartilage engineering,[103] while the more recent THPC crosslinked soft gels with an elastic modulus of about 810 Pa (estimated from shear modulus assuming $\nu = 0.5$) have been combined with vascular endothelial growth factor (VEGF) derived QK motif to stimulate human umbilical vein endothelial cell (hUVEC) behavior[105] as well as to study neurite growth in 3D environments.[106] The THPP crosslinked gels also show a sequence dependent elasticity tuning with an increasing distance between crosslinking lysine domains resulting in softer gels.[103] *In situ* crosslinkable ELP hydrogels using cysteine based disulfide bridge crosslinks have also been engineered by Chilkoti and coworkers.[107,108] These soft gels with an estimated elastic modulus as high as 450 Pa

undergo crosslinking in oxidizing conditions in the presence of H_2O_2 with gelation rate and gel stiffness controlled by amounts of H_2O_2 and protein concentration, respectively.[107,108] The mild concentration of H_2O_2 enables cell encapsulation and *in situ* formation of these soft gels useful in tissue engineering.[107]

The cell encapsulating ELP hydrogels mentioned so far use natural amino acids as reactive groups and mild reaction conditions; however, residues such as lysine are an integral part of other biomolecules and the side-reactions with crosslinkers can result unwanted modifications. Ways to avoid this include: using bio-orthogonal chemistry or using physical crosslinking. Bio-orthogonal chemistry involves the use of reactants that do not interact with biological molecules like the catalyst-free click reaction between azide and cyclooctyne developed by Bertozzi and coworkers.[109] In a recent report, Torre *et al*. functionalized ELP with either azide or cyclooctyne; the copper-free click reaction spontaneously occurs when the two ELPs are mixed to create hydrogels with elastic moduli between 1.8 and 7.5 kPa at 37°C.[110] The advantage of these gels over the azide-alkyne "clickable" gels developed by Teeuwen *et al*. is that they do not require the cytotoxic copper catalyst and can safely be used for *in situ* gel formation.[110,111] A major disadvantage for the clickable gels is that ELP functionalization with azides and cyclooctayenes requires complex chemical processing compared to other methods and especially compared to physical crosslinking. Physical crosslinking can be accomplished using two elastin-derived plastic, self-associating sequences: 'VGGVG' and 'I/V-PAVG'.[112-115] Although not used for gel formation, a tri-block elastin-mimic polypeptide with self-associating 'VGGVG' end-block sequences and hydrophilic 'VPG(V/F)G' mid-block have been shown to self-assemble into beaded fibrils.[112] This is expected as 'VGGVG' is known to form amyloid-like fiber aggregates.[116] Similarly, tri-block polypeptides using plastic-like 'I/V-PAVG' repeats can form hydrogels as shown in several studies.[114,117,118] The gels can assemble thermoresponsively with the plastic 'IPAVG' blocks self-associating into physical crosslinks.[114,117,118]

Interestingly the physically forming gels of elastic/plastic tri-block ELPs have also been cast into elastic films. Upon film formation, the film crosslinking can be further enhanced by introducing chemical crosslinks between lysine via GTA[118] or by introducing hydrazone crosslinking between tri-block ELPs functionalized with hydrazide and aldehyde groups.[117] The tough physically crosslinked films result in a young's modulus (E) of 0.74 MPa and failure strain of 437 % and the films increase in stiffness to E = 1.53 MPa and E = 3.16 MPa for chemical crosslinking with hydrazone and GTA, respectively.[117] Several other types of films have been synthesized with a focus on the use of ELPs fused with 'RGD' and related functional modules. Similar to hydrogels, film crosslinking strategies have relied on lysine residues linking using chemicals such as bis(sulfosuccinimidyl) suberate,[119,120] disuccinimidyl suberate,[119] and hexamethylene diisocyanate.[121,122] ELPs with cell adhesive motifs such as 'RGD' and CS5 domain have also been used as simple surface coatings to study their biochemical effects on cells.[123,124] Some recent film/coating work includes ELP membranes for maintenance of retinal pigment epithelial cells,[121] fibronectin mimicking ELP surface coatings to grow and stimulate fibroblasts and neuroblasts,[125,126] and in general to improve cell-interactive properties of synthetic polymer scaffold surfaces such as

poly(lactic) acid surfaces.[127] Improved osteogenic differentiation of hMSCs in the absence of osteogenic medium has also been shown on microtextured ELP membranes fused with 'RGDS' and 'REDV' motifs along with hydroxyapatite mineralizing motif.[128] A final type of ELP scaffold is electrospun fibrous mats as mentioned previously.[86,87,129] It is suggested that the higher surface area of the characteristic ribbon-like fibers of ELP resulting from the use of concentrated spinning solutions may allow for a better display of cell signaling modules to the interacting cells.[86]

1.3.2 Collagen & Collagen-like polypeptides

Collagen has been one of the most effective biomaterials in tissue engineering applications as it makes up a hefty 30 % of all proteins in our body.[50] Scaffolds used as grafts made of naturally-derived collagen from bovine, porcine and human cadaveric sources have already been commercialized.[130-132] Moreover, collagen-based products such as Matrigel are also used as standards for 3D cell culture.[133] However, as the sources of these materials change, there is biochemical and biophysical variability, possibility of disease transfer and of immunogenic responses to the material.[134,135] In order to overcome these issues, recombinant collagen has been expressed in different host systems. Homologous proteins with specifically designed functionalities can be synthesized each time, thus enabling tuning of collagen properties.

Commercially available recombinant human collagen expressed in yeast or transgenic tobacco plants has been used for tissue engineering by several researchers.[134,135] For example, Shilo *et al*. recently used tobacco plant derived recombinant human collagen-I based 'flowable gels' for wound healing. The flowable recombinant collagen gels were shown to promote faster wound healing compared to those consisting of solubilized collagen from bovine and human cadaver sources.[136] Recombinant human collagen -I and -III expressed in yeast (*Pichia pastoris*) have also been used to develop corneal substitutes by Griffith and coworkers.[137,138] The researchers chemically crosslinked the proteins using 1-ethyl-3-(3-dimethylaminopropyl)carbodiimide and N-hydroxysuccinimide to form hydrogels. The synthesized hydrogels have a water content of about 90 %, elastic modulus of 16.7 MPa for collagen-I and 20.3 MPa for collagen-III, and refractive index comparable to natural cornea, but only the gels composed of collagen-III showed high enough light transmission.[138] The gels were shown to be non-cytotoxic and successfully tested in an animal trial. Fagerholm *et al*. also used these optically clear gels in a Phase I clinical study and showed successful results in human patients for the collagen-III corneal implants.[139,140] The implants were successfully integrated into the cornea and remained avascular in all patients 24 months after surgery.[139,140] Similarly, yeast-derived recombinant human collagen-II was used by Pulkkinen *et al*. to synthesize gels with potential for cartilage tissue engineering.[141] Similar to natural collagen, the recombinant collagen also forms physical gels used by the researchers to encapsulate chondrocytes.[141] The cell laden gels have been shown to be safe and perform better than untreated cartilage injury sites in mouse and rabbit models. Although the material by itself shows only modest improvements in wound healing, this recombinant protein scaffold is free of any contaminants lowering chances of adverse effects and may prove to be more advantageous in the future.[142,143]

In contrast to the recombinant expression of unmodified human collagen sequences, de Wolf and coworkers have used the *P. pastoris* expression system to develop polypeptides with fully synthetic genes to form a triblock PBP with CLP end-blocks containing the characteristic 'PGP' sequence and a random coil mid-block.[144] The CLP end-blocks undergo physical crosslinking as they self-associate to form the collagen-like triple helix while the random mid-block remains hydrated. These gels have tunable melting temperature based on the length of the CLP end-blocks[145] and can be used to encapsulate cells just like natural collagen. The mid-block can also be replaced by other polypeptides such as flexible ELP or RLP sequences to produce a chimeric protein with unique properties.

Most recombinantly produced collagen is expressed in yeast- or plant-based expression systems that can also produce prolyl 4-hydroxylase for post-translational modification of proline to hydroxyproline.[134,135] As an alternative to these rather complex and difficult to use expression systems, researchers have explored the use of bacteria derived collagen mimics such as those from *S. pyogenes* among several other sources.[58,59] *S. pyogenes* naturally express triple helix forming CLP on their surface and use it to adhere to and enter mammalian cells upon infection. The polypeptides do not require post-translational modifications as charge-charge interactions between positively and negatively charged amino acids is enough to from triple helical structures.[56,59] Additionally, the bacterial origin of the proteins makes them easy to express in *E. coli* in concentrations as high as 19 g/L of culture.[146] Additionally, the *S. pyogenes* derived CLP has been shown to be completely biocompatible and can be easily processed into cell-supporting sheets and porous 3D scaffolds stabilized with glutaraldehyde mediated crosslinking.[147] Bioactivity has also been incorporated in these bacterial CLP with the incorporation of heparin binding sequence, 'GRPGKRGKQGQK', from acetylcholine esterase and integrin binding sequence, 'GERGFPGERGVE' from collagen-I.[148] This easy to express alternative to mammalian collagen will like find success as our understanding of collagen stability and hierarchical organization increases.

1.3.3 Silk & Silk-like polypeptides

Silk and silk-like polypeptides have been used extensively in tissue engineering studies. Naturally derived silk fibroin from silkworms is a readily available source of these proteins. It has been processed to form hydrogels, films, electrospun nanofibers as well as porous scaffolds.[149] The tough silk fibroin can even be processed into devices such as biodegradable screws and plates useful for craniofacial bone fixing applications as shown recently by Perrone *et al*.[150] Spider silks have also used in applications that require durable materials.[151,152] For example, dragline spider silk harvested from *Nephila spp* was used to fabricate woven scaffolds as artificial skin able to support fibroblasts and keratinocytes.[152] A major advantage of silk, especially spider silk, is its toughness derived from a combination of crystalline, flexible and amorphous domains that make up the protein. However, harvesting mechanically robust silk spidroin is impractical and a limitation of natural silk from spiders and silkworms is that they lack intrinsic bioactivity and cannot be genetically modified like recombinant proteins.[21,64]

Researchers using recombinantly expressed silk-like polypeptides or SLPs has focused on the spider silk derived consensus sequences from spiders such as *N. clavipes* and *A. diadematus*.[153-155] The mechanical robustness of native spider silks has kept researchers motivated to improve SLPs to fabricate tough structures like fibers, films and coatings.[67,153-155] Such structures would be useful to replace skeletal tissues and skin as well as for many non-biological uses.[156] Until recently, however, SLPs lacked the remarkable properties of natural silk because of the difficulty in recombinant expression of full-length proteins. The hurdle was overcome by Xia *et al*. when they expressed full length, 284.8 kDa, MaSp1 protein from *N. clavipes* in *E. coli*.[68] Fibers extruded using the full length recombinant spidroin have a young's modulus of 21 GPa, breaking strain of 15 % and tenacity of 508 MPa in dry conditions comparable to natural *N. clavipes* dragline silk (11-14 GPa; 18-27 %; 740-1200 MPa, respectively).[68] Another type of SLP with remarkable strength was synthesized in transgenic silkworms that contained chimeric silkworm/spider silk genes.[157] Fibers spun from this chimeric silk were shown to have a young's modulus as high as 5.5 GPa, breaking strain of 31.1% and ultimate stress of 338 MPa along with toughness of 77.2 MJ/m^3 which is comparable to dragline spider silk.[157] In addition to the production of robust SLP fibers, these two studies also present strategies useful for scaling up the production of high strength artificial silk. Additionally, gaining a full understanding of and replicating silk spinning process as performed by spiders will greatly enhance the robustness of SLP fibers that can be produced.[29,69]

Parallel to the development of tough silk fibers, the bio-applications of SLP have mainly focused on exploring biocompatibility of the proteins, ways to impart bioactivity and synthesizing different forms of scaffolds rather than using the strongest versions of SLP fibers. For example, porous scaffolds fabricated using *N. clavipes* MaSp1 sequence derived SLP expressed in *E. coli* have been shown to not only be biocompatible, but the scaffolds also show vascularization and tissue ingrowth during subcutaneous implantation in Balb/c mice.[158,159] Moisenovich *et al*. also conclude that the porous scaffolds show bone healing after defect repair with these scaffolds compared to the control in Wistar rats.[159] Kaplan and coworkers have also used the *N. clavipes* derived sequence to synthesize SLPs with various functionalities including RGD functionalized SLP to improve cell adhesion, silaffin derived R5 sequence to mineralize silica,[160] and dentin matrix protein 1 sequence to mineralize calcium phosphate.[161]

Tissue engineering substrates have also been synthesized using the major ampule ADF4 protein from *Araneus diadematus*. Fibers are commonly produced using self-assembling SLP with post-spinning treatments such as soaking in ethanol/methanol to change protein crystallinity in fibers.[162] A different structure using the ADF4 derived SLP is a hydrogel. SLPs with 4 repeat units of ADF4 have been chemically crosslinked under visible light in the presence of ammonium peroxodisulfate and tris(2,2'-bipyridyl)dichlororuthenium(II) to form soft gels with a young's modulus of 8.4 kPa.[163] Interestingly, unlike other hydrogels, these SLP hydrogels are composed of a loosely interconnected network of amyloid-like nanofibrils as shown by AFM scanning of dried gels and X-ray diffraction.[163,164] Further characterization of gel formation was studied using the eADF4(C16) protein with respect to concentration and chemical

functionalization of the SLP besides gel crosslinking.[165] A consistent way of forming gels using eADF4(C16) is to remove water via dialysis, thus concentrating the protein that leads to spontaneous gel formation. Chemical crosslinking of these physical gels leads to gel stiffening, whereas functionalization of the protein with a molecule such as fluorescein hinders its self-assembly making the gels softer.[165] Unfortunately, these tunable hydrogels have little cell interaction property on their own due to a lack of features.[166] eADF4(C16) films also do not show proper cell activity without the presence of integrin binding 'RGD' sequences due to a similar lack of micron-scale structures.[17,166] An eADF4(C16) structure that does promote cell adhesion and proliferation even in the absence of 'RGD' motifs is electrospun fibers.[166] A recent report also revealed that a micropatterned film surface with 20 μm wide and 1 μm deep grooves shows similar cell adhesion with or without the presence of RGD.[17,167] Thus, eADF4(C16) based substrates show surface topography based cell interactive properties possibly similar to cell adhesion on textured surfaces composed of nonadhesive poly(ethylene glycol).[168]

An alternative type of SLP that has also been used to develop cell interactive substrates is the *Euprosthenops australis* derived 4RepCT. 4RepCT has been used to prepare films, foams, fibers, and meshes that were tested for interactions with human primary fibroblasts.[169] Widhe *et al*. show that all the substrates were compatible with the fibroblasts and sustained similar cell properties such as collagen formation even after 14 days of culture.[169] Similarly, Lewicka *et al*. showed that 4RepCT films are compatible with neural stem cell culture and comparable to plates coated with poly-L-ornithine and fibronectin from bovine plasma.[170] Recently, 4RepCT fused with cell adhesion motifs such as RGD, IKVAV, and YIGSR were shown to promote better cell adhesion than controls especially for Schwann cells on IKVAV functional 4RepCT compared to laminin coated control.[171] Furthermore, 4RepCT fusions with different biomolecule binding domains like IgG binding, biotin binding, and albumin binding have also been prepared.[172] Site-specific immobilization of different biomolecules can be a powerful method to impart extracellular matrix-like activity to SLP or any other PBP used for cell interaction and tissue engineering.

1.3.4 Resilin & Resilin-like polypeptides

Resilin-like polypeptides (RLPs) are relatively unexplored in the field of biomaterials. Researchers who use RLP have focused on developing hydrogels for tissue engineering. As described in section 1.2.4, RLP gene from *D. melanogaster* resilin has three exons, each with a different purpose.[78] Qin *et al*. synthesized full length resilin from *D. melanogaster* resilin genes to synthesize hydrogels.[173,174] The expressed resilin was crosslinked by forming di-tyrosine bridges in two ways: enzymatically, using horseradish peroxidase; and photo-Fenton reaction, using $FeSO_4$ and H_2O_2 followed by UV-exposure.[174] The researchers showed that among the three exons, hydrogels from exon 1 showed 90 % resilience, while those from exon 3 were show only 60 % resilience.[173,174] These studies paved the way to the mechanism of resilin function proposed by Qin *et al.*,[78] explained in section 1.2.4.

Studies such as those by Kiick and coworkers have further revealed the excellent properties of the elastomeric 'GGRPSDSYGAPGGGN' sequence derived from exon 1 of

D. melanogaster resilin. The RLP12 containing 12 consensus sequence repeats have been crosslinked in mild conditions using [tris(hydroxymethyl)phosphino]propionic acid[175] or tris(hydroxymethyl)phosphine[19] crosslinkers in coordination with primary amines on the RLP12. Charati *et al*. engineered RLP12 to contain cell binding motifs, MMP degradation sites, and heparin binding sites spread throughout the polypeptide.[175] These gels have a storage modulus of about 10 kPa and were observed to withstand up to 450 % strain. On the other hand, Li *et al*. developed tunable hydrogels using 4 different RLPs: one each with a cell binding site, a MMP site, a heparin binding site or non-functional RLP.[19] These hydrogels were shown to have an RLP- and crosslinker- density dependent storage moduli in the range of 1 kPa to 25 kPa.[19,176] Due to their intrinsic high resilience and a simple ratio-dependent tuning of functional motif content, these hydrogels were indicated for use in vocal fold engineering and many other tissue engineering applications.[19] Slightly modified RLP hydrogels for vocal fold tissue engineering with RLP containing lysine and glycine rich crosslinking motifs have been further shown to have a resilience of up to 98% by Li *et al*.[177] These gels show better energy storage and recovery than synthetic polymer gel controls and their tensile properties were comparable to vocal fold tissue.[177] An additional type of RLP hydrogel produced by McGann *et al*. was made using cysteine (for sulfhydryl-based crosslinking) containing RLPs of different lengths: 12, 24, 36, and 48 monomer repeats.[178] Interestingly, the gels were measured to have the similar storage moduli (7 – 9 kPa) using 1:1 RLP:crosslinker ratio (crosslinker: vinyl sulfone functional 4-armed PEG) since the RLP molecular weight between each pair of cysteine residues was kept the same. The mild crosslinking chemistry allows for cell encapsulation and the range of measured storage moduli make the gels ideal for cardiovascular tissue engineering.[178] Another type of RLP with the consensus sequence from *A. gambiae* resilin, 'AQTPSSQYGAP', has also been used to create hydrogels. Renner *et al*. synthesized RZ10, an RLP with 10 repeats of the *A. gambiae* resilin derived sequence. The RZ10 hydrogels were shown to have a dynamic modulus of 22 kPa and surfaces coated with RZ10 fused with RGD showed proper cell spreading.[179] Additionally, similar to the development of bioactive ELP in section 1.3.1, control of stem cell differentiation such as human mesenchymal stem cells into osteoblasts has also been shown on surfaces coated with RZ10 fused with bioactive motif from bone morphogenic protein-2.[180]

1.4 Tackling materials challenges: A case for ELP

Elastin-like polypeptides have been used for a variety of applications as mentioned in section 1.3.1. My goal has been to exploit the core properties of ELP -- stimuli-responsiveness and flexibility-- to address a variety of challenges in materials science and bioengineering.

My work spans a broad range of topics including recombinant protein engineering, materials science, biology and optics. The unique combination of properties of ELP, and our synthesis and design strategies enable us to explore and generate solutions using the same family of materials. The use of ELP in hydrogel development is an established idea with numerous synthesis strategies.[11] However, a common theme that emerges among the

employed strategies is the presence of numerous crosslink points throughout the ELP chains. In many cases, the goal is to mimic mature elastin using 'Ala-Lys' repeats or simply 'Lys' dispersed through the designed polypeptides.[90,106] Although this is a great starting point, the high crosslink densities limit the potential of these unstructured spring-like polymers to stretch. Thus, for our first challenge, we pursue the design of mechanically robust hydrogels.[181] We hypothesized that since ELP deswells and coils at high temperature, we can exceed the extensibility of all previous ELP hydrogels by minimizing the crosslink density and maximizing the ability of the chains to stretch fully.

Next, we focus on the applicability of ELP hydrogels as flexible adhesives, which will be valuable for surgical sealing of soft tissues. Surgical adhesives are advantageous compared to sutures due to faster healing and lower risk of complications. However, commonly used cyanoacrylate glues and hydrogel-based adhesives can cause inflammatory responses and toxicity.[182,183] Furthermore, protein-based adhesives such as fibrin, gelatin and collagen are risky due to poor adhesion on wet surfaces, swelling and disease transfer.[184] Our strategy of using recombinant proteins gives us a monodispersed raw material that inherently deswells at high temperatures and shows great biocompatibility. In addition, we can use the knowledge we gained from creating rubber-like hydrogels to create a truly unique flexible adhesive. Through our work, we create a path to achieve materials that were previously inconceivable.

In our work, we also aimed to develop an *in situ* forming and self-healing material that will be useful for wound healing and regenerative medicine.[185] The inorganic ceramic, bioglass, has been used to develop many composites useful for regenerative medicine.[186,187] Bioglass can promote bone growth and accelerate wound healing, has anti-bacterial properties, while showing excellent biocompatibility.[186] Since bioglass increases alkalinity of its local environment, we designed ELPs that can crosslink via pH-driven reversible aldimine bonds. The end result is a material that can reinstitute its bonding after being severed.[185] In addition, transition of ELP upon crosslinking promotes rapid aggregation and crosslinking of the hydrogels into a stable structure.

Finally, we dive into the development of protein-based biolasers.[188,189] Unlike chemical and biological fluorophore based probes, biolasers can yield dramatically greater sensitivity to changes.[188] They can therefore be used to develop optically active sensors for applications in biosensing. With our experience and knowledge, we propose and synthesize protein-based hydrogel devices capable of stimuli-responsive property changes.[181,190] Through testing and optimization, we hope to yield a successful sensing system in the near future.

In the remainder of this dissertation, I will describe our journey and provide the insights we gained through our use of ELP. Through this manuscript, I hope to convey the truly protean characteristics of ELP and inspire future research in the creation of previously unimaginable materials to address real-world problems.

Chapter 2 ELP engineering

2.1 Introduction

Elastin-like polypeptides are synthesized through recombinant expression in *E. coli*. Unlike solid phase peptide synthesis, recombinant expression allows for the synthesis of long polypeptides with narrow dispersity. This allows us to engineer our polymeric material with high precision. Engineering ELP begins with the design of the core pentapeptide sequence – 'Val-Pro-Gly-Xaa-Gly.' The guest residue 'Xaa' (cannot be 'Pro') can be used to tune ELP transition properties in addition to charge and functional groups for modification and crosslinking. In our strategy, the ELP gene is constructed to the desired lengths using a routine cloning vector. Separately, the expression vector is modified with a gene cassette containing the N-terminal and C-terminal sequences along with a site for ELP insertion. This modular design allows us to rapidly combine and synthesize ELP with different sizes.

In this chapter, I will describe our genetic engineering scheme, originally developed by Dr. Eddie Wang and ELP synthesis procedure.[18,99]

2.2 Strategy for seamless cloning of ELP

2.2.1 Genetic engineering scheme

Since ELPs are composed of a repetitive sequence, we synthesize the genes iteratively by concatemerization of a short ELP gene to achieve desired lengths.[18,99] We use a customized pJ54 vector from DNA 2.0 Inc with a specific combination of restriction endonucleases (REs) for cloning using the scheme shown in Figure 2.1. Among the two types of REs used, type IIS have an asymmetric recognition site and cleave DNA at a fixed distance from it, while type IIP Res have a palindromic recognition site and cleave at the site in or adjacent to it. Specifically, the vector contains two type IIS RE sites – REIIs-A (BpiI) and REIIs-B (Eco31I) – that surround the ELP gene and two type IIP RE sites – RE1 (BamHI) and RE2 (XhoI) – upstream and downstream of the type IIS sites. The strategy described in Figure 2.1 can be employed in any standard cloning vector that does not contain the four restriction sites.

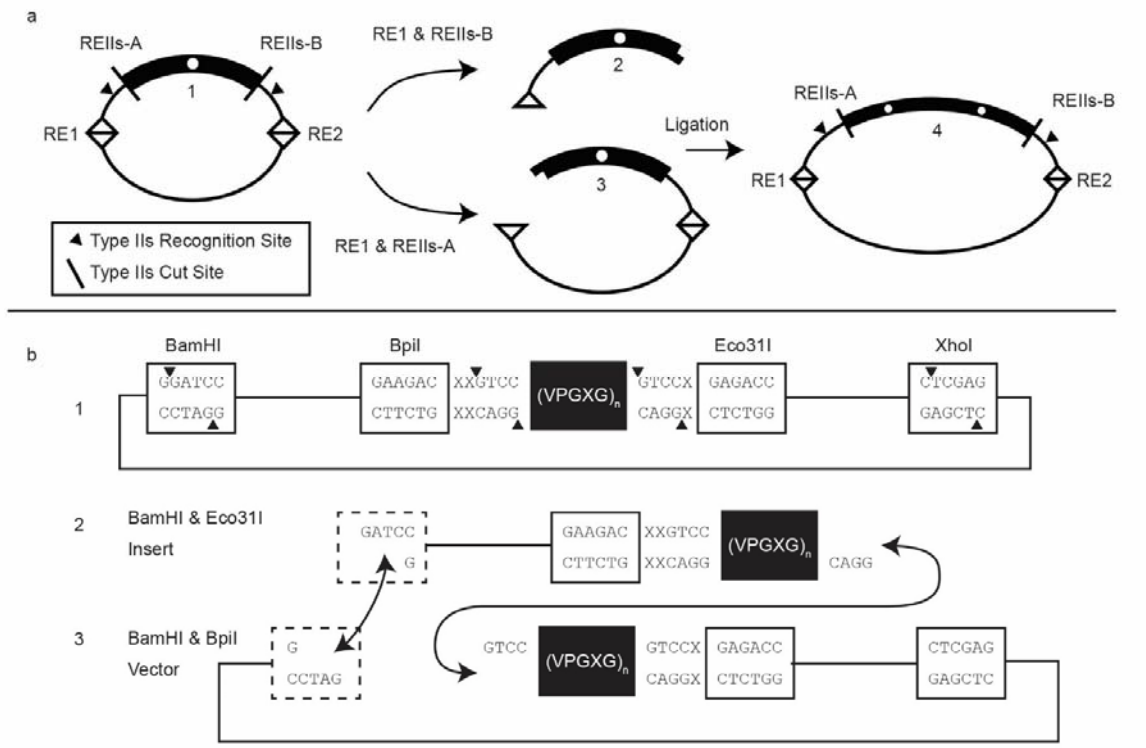

Figure 2.1 ELP gene construction scheme *a. Plasmid (1) contains four restriction endonuclease sites. Insert (2) is created by digesting the plasmid using RE1 and REIIs-B, and vector (3) is created by digesting the plasmid using RE1 and REIIs-A. Ligation of the insert and vector yields a larger ELP gene (4) that can be used for further cloning. Through the use of type IIs restriction endonucleases that cut downstream of their recognition sites, this method allows for seamless concatemerization of ELP genes; b. Detailed scheme showing the relevant sequences for the restriction endonuclease recognition and digestion sites. (Reproduced with permission from Dr. Eddie E. Wang from dissertation titled "Development of Stimuli-Responsive Elastin-like Polypeptide-based Nanocomposite Biomaterials." Copyright 2012 Eddie Eugene Wang)*

2.2.2 Method for cloning ELP genes

Routine cloning can be done with standard *E. coli* strains such as XL-1 Blue and DH5-alpha cells. We use XL-1 Blue cells for cloning. Our method uses ampicillin resistance gene for selection, which must be taken into account for strain selection.

1. Insert oligos encoding the ELP, $[VPGVG]_5$, into the pJ54 plasmid (Table 2.1). Prepare pJ54 vector by double digesting it with RE1 and REIIs-A. Prepare inserts from oligos shown in Table 1 by first phosphorylating them using T4 polynucleotide kinase in the presence of ATP. Anneal the complementary DNA pairs by mixing each pair in a separate tube, fully denaturing the strands at 95˚C and slowly cooling to 5˚C. Ligate the annealed fragments with the pJ54 vector using T4 ligase and transform the ligation reaction into electrocompetent XL1-Blue cells. Select and verify three colonies. Freeze and store a successful colony in 15% glycerol at -80˚C for further use.

2. Prepare vector and insert from ELP modified pJ54 as shown in Figure 3. Liberate the ELP insert by double digesting the plasmid with enzymes RE1 and REIIs-B. Prepare the ELP vector by double digesting the plasmid with enzymes RE1 and REIIs-A. Purify insert and vector using agarose gel electrophoresis and gel column purification.
3. Ligate insert and vector using T4 ligase. Transform 40 μL of XL1-Blue electrocompetent cells with 1 uL of ligation reaction. Culture cells on agar plates with appropriate antibiotic for selection. Pick three colonies, and verify the sequence and gene size. Freeze and store one successful colony.
4. Repeat steps 2 and 3 to double ELP gene sizes or use a combination of two ELP gene sizes to construct the desired gene lengths. For our work, we constructed V50, V75, and V100 to test the effects of ELP size on material properties.
5. Once ELP genes are constructed, synthesize an insert for each gene by double digesting it with REIIs-A and REIIs-B. Purify the insert with agarose gel electrophoresis and gel purification column. These inserts contain the ELP genes that can be seamlessly integrated with terminal modification sequences prior to protein expression.

Table 2.1 Oligo sequences for ELP gene. Each segment encodes half of the desired sequence.

Segment	Name	DNA	Peptide
Left	V5L1	GATCCTTCACATATGCGAAGACAAGTCCCAGG TGTGGGCGTACCG	$[VPGVG]_5$
	V5L2	CACCAACGCCCGGTACGCCCACACCTGGGACT TGTCTTCGCATATGTGAAG	
Right	V5R1	GGCGTTGGTGTTCCTGGTGTCGGCGTGCCGGG CGTGGGTGTTCCGGGCGTAGGT	
	V5R2	GGACACCTACGCCCGGAACACCCACGCCCGG CACGCCGACACCAGGAA	

2.2.3 Method for construction the expression vector

Once we synthesize an ELP gene of desired length, we prepare a pet28b expression vector with the desired N and C terminal modifications, restriction sites, and a stop codon for ELP gene insertion. The restriction site in the center consists of REIIs-B enzyme recognition sequences such that the digestion site produces a vector with ELP insert compatible sticky ends. This approach gives us a modular system in which we can insert the desired ELP gene to rapidly engineer a series of proteins with the same terminals. We use the *E. coli* strains XL1-blue for routine cloning and insert the completed plasmid into BLR(DE3) for expression.

1. Prepare the pet28b expression vector for modification with a gene cassette containing ELP terminal sequences and insert site (Table 2.2) by double digesting it with NcoI and BamHI. Purify the vector using agarose gel electrophoresis and a gel purification column.

2. Ligate the gene cassette with compatible sticky ends into the pet28b vector. Prior to ligation, the synthetic single stranded DNA fragments should be phosphorylated and annealed. Ligate the annealed fragments with pet28b vector using T4 ligase and transform the ligation reaction into electrocompetent XL1-Blue cells. Select and verify three colonies. Freeze and store a successful colony in 15% glycerol at -80˚C for further use.
3. Prepare modified pet28b vector for ELP gene insertion. Digest the modified plasmid with REIIs-B to create a vector containing sticky ends compatible with ELP inserts. Purify the vector using agarose gel electrophoresis and a gel purification column.
4. In separate reactions for each ELP insert, ligate the insert with modified pet28b vector using T4 ligase. Transform the ligation reaction into electrocompetent XL1-Blue cells. Select and verify three or more colonies for plasmid sequence and size of the ELP gene. Freeze a successful colony for each ELP type in 15% glycerol at -80˚C for further use. (*Note: This step can be challenging as all the sticky ends are identical. This can lead to vector self-ligation and/or concatemerization of inserts. Therefore, it is especially important to verify the size of the region of interest.*)
5. Once the expression plasmids are fully constructed, they can be transformed into BLR(DE3) competent cells. After transformation, it is good practice to verify the sequence of the plasmid and gene size once again. Freeze the successful expression colony for each ELP type in 15% glycerol at -80˚C for use in protein expression.

Table 2.2 Oligo sequences used to modify pet28b prior to ELP gene insertion

Location	Name	DNA	Peptide
N-terminus	N-F	CATGAGCGGCGTTGGCGTCCTGAGACC	MSGVG
	N-R	GTGACCAGTGGGTCTCAGGACGCCAACGCCG CT	
C-terminus	CK1-F	CACTGGTCACGGTCTCGGTCCCGGGTAAAGG CTAATAA	VPGKG
	CK1-R	GATCTTATTAGCCTTTACCCGGGACCGAGAC C	

2.2.4 ELP Expression and Purification

Using this method, ELPs can be expressed without IPTG induction. Overexpression is accomplished by culturing the cells overnight in high nutrition TB media in the presence of glycerol [18,99,181,191]. Furthermore, due to their thermo-responsive property, ELPs can be purified without the need for purification columns as described below.

1. Prepare 60 mL of LB media with kanamycin in a 250 mL baffle flask for each protein to be expressed. Use a sterile pipette to scrape engineered *E. coli* from the frozen cell stock and dip it into the media to inoculate. Transfer the flask(s) to a shaker incubator and incubate for 16 hours at 37˚C and 220 RPM.

2. Prepare 4 L baffle flasks with 900 mL TB media and kanamycin. Use a pipette to add the starter culture. Transfer the flask(s) to a shaker incubator and incubate for 20 to 24 hours at 37˚C and 220 RPM.
3. Pellet E. coli cells from the culture media and resuspend the cells in resuspension buffer to begin protein purification. Remove flask(s) from the incubator and transfer the contents into 1 L centrifuge bottles. Centrifuge the culture at 4˚C and 6000 RCF for 30 minutes to form a stable cell pellet. Decant the supernatant and follow local regulations for proper disposal. Resuspend the pellet in 40 mL chilled resuspension buffer per centrifuge bottle. (*Note: Once the cell culture is removed from the incubator, the suspensions in all subsequent steps should be kept at a lower temperature to prevent protein degradation.*)
4. Lyse resuspended *E. coli* by ultrasonication in the presence of a protease inhibitor. Combine two samples of resuspended cell solution, approximately 100 mL, into a 200 mL beaker. Place the beaker in an ice bath, add 1 mL of PMSF solution and sonicate the solution using a standard probe-tip sonicator operating at 7.5 W. Pulse for 10 seconds followed by cool-down time of 30 seconds with a cumulative "ON" time of 3 minutes and 30 seconds.
5. Centrifuge cell debris from the cell lysate. Distribute the lysate solution into centrifuge tubes and incubate on ice for 15 minutes. Centrifuge cell lysate at 4˚C and 30,000 RCF for 30 minutes. Decant the supernatant into fresh tubes and dispose the pellet containing cell debris.
6. Precipitate DNA using polyethylene imine and centrifuge the lysate solution. Add 10% polyethylene imine solution to a final concentration of 0.5% and mix to precipitate DNA. Incubate solution on ice for 15 minutes. Centrifuge lysate at 4˚C and 20,000 RCF for 15 minutes. Decant the supernatant into fresh tubes and dispose the pellet containing DNA.
7. Inverse temperature cycling is used to remove the remaining contaminants and purify ELP (Figure 2.2). It involves sequential centrifugation steps at high and low temperatures to isolate thermo-responsive ELP. If frozen, thaw lysate solution to room temperature and distribute into clean centrifuge tubes.
    a. Add 2 M ammonium sulfate solution to a final concentration of 0.6 M.
    b. Incubate tubes at 45 ˚C for at least 45 minutes to allow ELP to phase separate.
    c. Centrifuge tubes at 35˚C and 18,000 RCF for 20 minutes and discard the supernatant.
    d. Add 10 mL of chilled resuspension buffer and gently disrupt the pellet, while keeping the tubes chilled.
    e. Incubate tubes on ice for 15 minutes once the pellet is fully dissolved.
    f. Centrifuge tubes at 4˚C and 20,000 RCF for 15 minutes and decant the supernatant into fresh tubes. Combine supernatant from two tubes into one in order to concentrate the protein solution.
    g. Repeat steps a-f once to complete the second cycle. However, this time use a 0.5 M final concentration of ammonium sulfate in step a.

h. Repeat steps a-f to complete the third cycle. However, this time use a 0.4 M final concentration of ammonium sulfate in step a and use diH_2O for resuspension in step d.

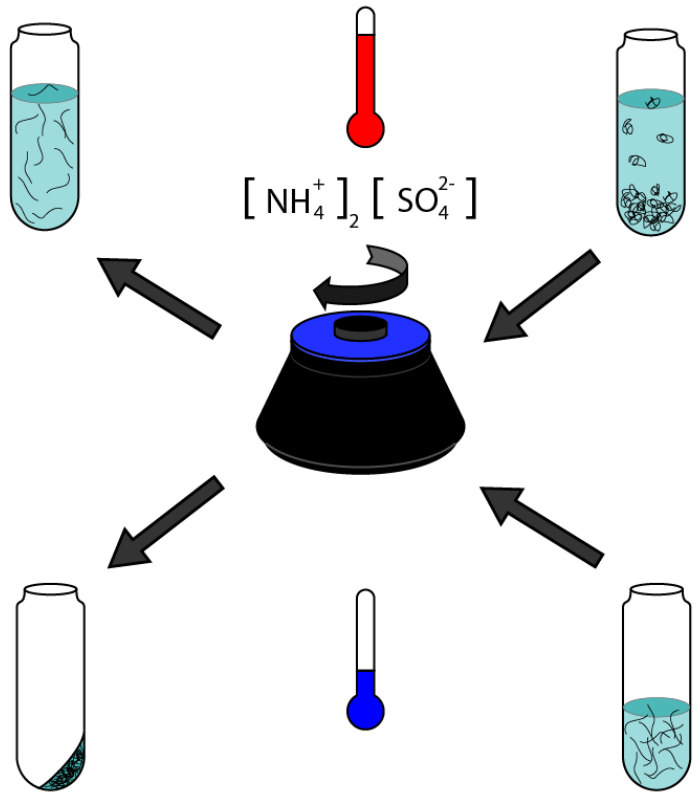

Figure 2.2 Schematic showing temperature cycling process to purify ELP. *Inverse temperature cycling can be used to purify ELP due to its thermo-responsive behavior.*

8. Dialyze the purified protein solution to remove salt and debris. Transfer purified solution into regenerated cellulose dialysis tubing with 6-8 kDa cutoff. Dialyze the sample in a 4 L beaker against diH_2O with constant stirring. Change water six times over two days. (*Note: There may be impurities that precipitate into white aggregates as the remaining salts and soluble small molecules leave the protein solution. These aggregates can be removed after dialysis by centrifuging the solution at 20k RCF for 15 minutes prior to filtration.*)
9. Prepare the purified ELP solution for lyophilization by filtration and freezing. Remove any precipitated debris by filtering it using a syringe with 0.45 μm filter. Filter into a clean beaker and cover the mouth of the beaker with parafilm. Puncture the parafilm using a sharp tool prior to freezing. Freeze the sample for at least 1 hour at -80˚C.
10. Lyophilize the frozen proteins. Place the frozen sample into a lyophilizer and allow the sample to completely dry for at least 2 days.
11. After lyophilization, the dried protein can be stored in an air-tight tube at room temperature. Protein mass should be verified using MALDI-TOF mass

spectrometer and the transition temperatures of ELPs can be determined by measuring their solution turbidity using a visible light spectrometer.

Chapter 3 Rubber-like hydrogels

3.1 Introduction

Hydrogels with diverse chemical, biological and mechanical properties are needed in many fields, including biomedicine.[192,193] They are ideal for biomaterial development due to the high water content that is needed for cells to exchange nutrients, communicate and perform the required tasks for survival. On the other hand, if it is for use as an implant scaffold, the same hydrogel must also be able to physically support the biological tissues and organs, and maintain its shape after being constantly deformed from our daily activities. However, typical hydrogels are soft and have limited capacity to retain shape when deformed. Hydrogels are commonly synthesized by polymerization of a monomer or by crosslinking a polymer chain into a connected network. Their mechanical properties depend on factors such as the type and density of polymers, and the type and density of crosslinks. Stiff hydrogels can be synthesized by increasing the density of the polymer and crosslinks. However, high stiffness tends to be achieved at the cost of flexibility. In general, short, uneven inter-crosslink distances and poor polymer chain extensibility limit the ability of the hydrogels to stretch.

Various strategies have been used to improve hydrogel properties such as extensibility and toughness through physical bonds.[1,193-196] Among these, hydrogels based on double networks,[197-199] nanocomposites [200-202] and slide-ring networks [203,204] can exhibit good toughness and high extensibility due to physical bonds that break and regenerate.[193] More specifically, the properties of these hydrogels arises from their ability to dissipate energy. As a material is stretched or compressed within its elastic region, it stores the energy, which is released either when the material comes back to its original position or when it ruptures and creates new surfaces. In the case of tough hydrogels, the physical bonds can rupture and release energy being stored during the mechanical deformation. This prevents the chemically bound polymer network from rupturing, and slows crack formation and propagation. Now, although the physical crosslinks can recover with time, the process can be extremely slow. Prior to the recovery of the physical network, the hydrogels show high hysteresis and stress softening that leads to a loss of performance under repeated deformations.[205,206] Furthermore, such a material remains in the deformed state for a prolonged time, the physical bonds can re-form prematurely alter material properties, decreasing its practicality. Therefore, there are continued efforts to develop robust, elastomeric hydrogels that have the durability to undergo reversible extensions.[89,176,207] Applications requiring large and repeated deformations can certainly benefit from rubber-like elastomeric hydrogels.

Creating a rubber-like elastomeric hydrogel requires control over the architecture of the crosslinked network and a judicious choice of polymer. The architecture of the hydrogel should be homogeneous. Specifically, the chain length between crosslinks should be constant to avoid local concentrations of stress that would lead to premature fracture. Furthermore, the crosslinking scheme should ensure proper chain incorporation

to avoid dangling chains that do not participate in the elastic network. Meanwhile, the polymer should ideally behave like an entropic spring that recoils once unloaded. Unlike energy storage in bonds, the driving force restoring an entropic spring is an increase in entropy as the chain goes from a stretched state with limited movements to a coiled state. Using these principles, we can develop elastomeric hydrogels that can reversibly extend to large deformations.

3.2 Strategy for improved flexibility

When it comes to the history of ELP-based hydrogel development, the major design theme revolves around the idea of mimicking mature elastin. Mature elastin is a highly crosslinked and insoluble protein network consisting of the repetitive elastic sequences and 'Ala-Lys' containing crosslinking regions. Therefore, beginning with the use of organic solvents and quickly moving to aqueous crosslinking schemes, majority of ELP hydrogels have the common design consisting of evenly distributed crosslinking sites. A large number of crosslink points along the chain is especially important in the case of aqueous reactions involving primary amines due to a lower reaction yield. Although aqueous crosslinking schemes are useful for cell encapsulation, it generally results in opaque hydrogels because as ELP reacts with the crosslinker, it turns more hydrophobic and aggregates. Random aggregations lead to light scattering and opaque hydrogels. We further hypothesized that the uneven distribution of crosslinks and an overall high density of crosslinks lead to materials that fail at relatively small strains.

Protein-based polymers are genetically encoded and recombinantly expressed materials that provide unique opportunities for engineering hydrogels with the aforementioned network and polymer properties. We can finely control their sequence and length to the extent that the distance between the available crosslinking sites would be theoretically monodisperse. Moreover, we can access a library of peptide domain sequences with different mechanical behaviors to synthesize the desired polymers.[11] For creating elastomers, elastin-like polypeptide (ELP) sequences are one natural choice because they have been characterized as entropic springs.[41] ELPs are built on a repetition of the pentapeptide Val-Pro-Gly-X-Gly with a guest residue 'X' that cannot be proline. ELPs are also thermo-responsive and undergo a process known as the inverse temperature transition (ITT) at a characteristic transition temperature (T_t). The ELPs reversibly transition from a hydrophilic to a hydrophobic state and phase separate around their T_t.[39-41,208-211] Specifically, during ITT, the hydrogen bonding between ELP backbone and water molecules breaks and the ELPs collapse. Thermodynamic factors including the hydrophobic interactions within the chains keep the polypeptides in an unstructured coil form after the transition and play a role in the elastomeric nature of the polypeptides.[212] In general, crosslinked ELP networks maintain the properties of elasticity and thermo-responsiveness.[98,99,102] Although chemically crosslinked ELP networks have excellent elastomeric properties, even the best hydrogels developed so far only stretch to a strain of 400% due to limited control over crosslinking that led to random chain tethering.[89,213] In this work, we created simple hydrogels that combine the inherent properties of ELPs with controlled crosslinking to create near ideal networks with end-to-end tethered chains

using the two components shown in Figure 3.1. The resulting rubber-like elastic hydrogels attain failure strains up to 1500%, significantly exceeding previous examples.[89,213] The properties of failure strain and high resilience even at large deformations were tuned by precisely varying the lengths of the monodispersed peptide chains. We attribute the robustness of these hydrogels to polymer architectures embedding entropic springs and their thermo-responsive deswelling at physiological temperature of 37°C (Figure 3.2).

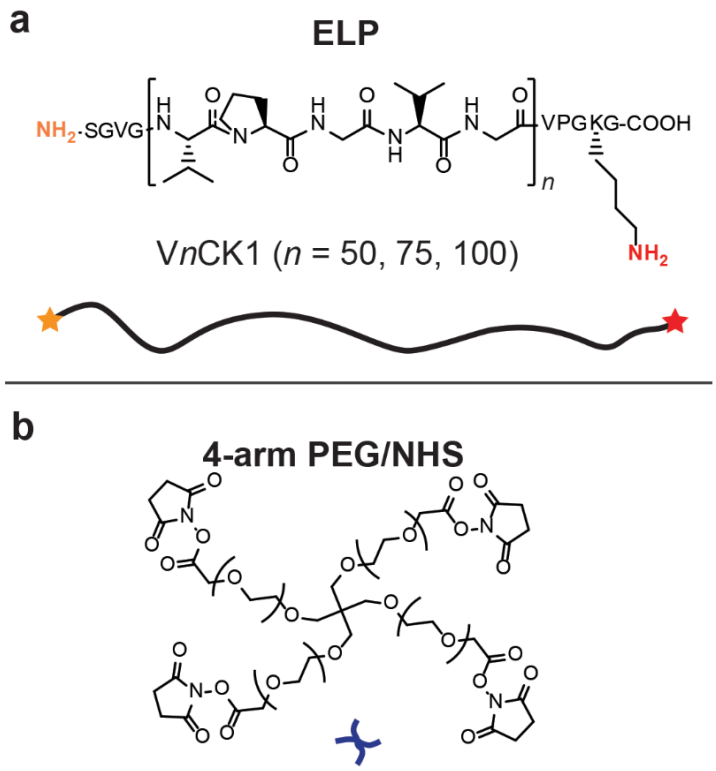

Figure 3.1 Schematic showing ELP design and the 4-arm PEG crosslinker. *a) ELP is designed with the core pentapeptide 'VPGVG,' which is repeated 50, 75, and 100 times. N-terminal amine and C-terminal lysine provide the reactive groups used for crosslinking; b) N-hydroxysuccinimide terminal groups on the 4-arm PEG linker can efficiently react with amines to form crosslinked networks.*

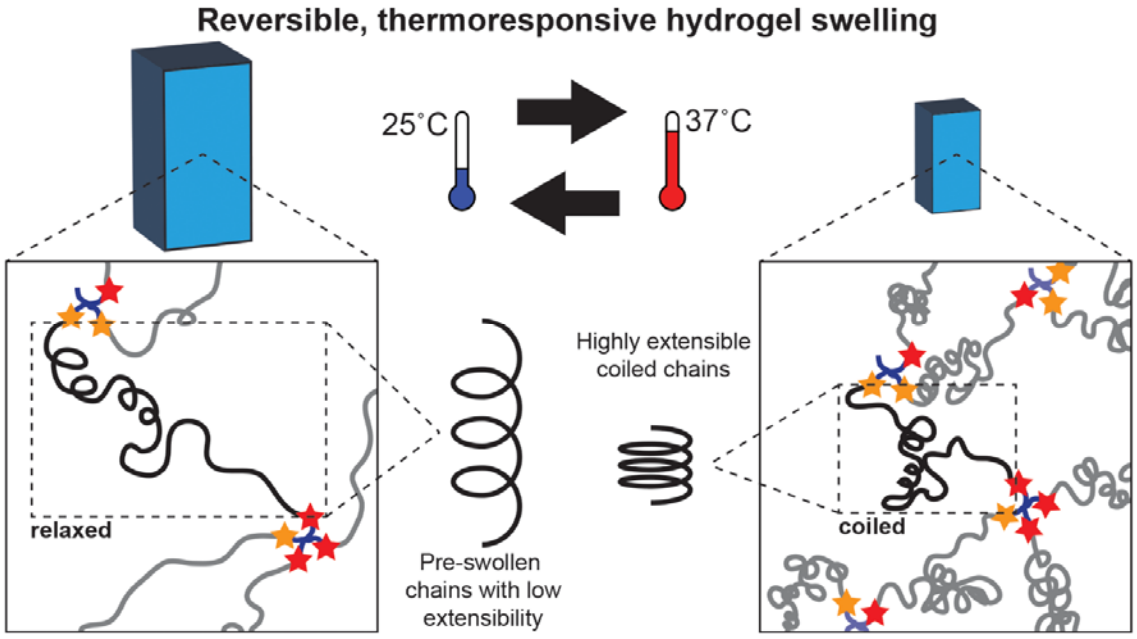

Figure 3.2 ELP hydrogel scheme includes a telechelic polypeptide and a four-arm crosslinker to from the network. *Due to the thermo-responsive property of ELP, the hydrogels can be synthesized at low polymer concentration. We expect the materials to have a high water content at lower temperatures and a gradual decrease in water content as they deswell with an increase in temperature. The greater coiling of ELP will allow the hydrogels to stretch to large extensions similar to a dense spring.*

3.3 ELP design and characterization

We used genetic engineering and recombinant expression to synthesize three different ELPs to fabricate the elastomeric hydrogels (Table 3.1). The target proteins were designed to contain a single primary amine on the C-terminal lysine and a second amine provided by the N-terminal for crosslinking. The core pentapeptide repeat unit is composed of 'Val-Pro-Gly-Val-Gly,' while the C-terminal contain a single pentapeptide with the sequence 'Val-Pro-Gly-Lys-Gly'. Based on this sequence design, we designate ELP name with the general from of 'V*n*CK1' for SGVG[VPGVG]$_n$VPGKG. The core pentapeptide is repeated 50, 75 and 100 times to create V50CK1, V75CK1 and V100CK1.

Genetic engineering was performed using the methods provided in Chapter 2. After expressing and purifying the final proteins, they were characterized for their size using a MALDI-TOF mass spectrometer. As expected, we observed sharp peaks for each synthesized protein with molecular weights of 21.2, 31.4 and 41.7 kDa for V50CK1, V75CK1, and V100CK1, respectively, matching their theoretical weight (Figure 3.3, Table 3.2). Our monodisperse ELPs engineered with only terminal reactive sites serve as well-defined components for the synthesis of our near ideal networks.

Table 3.1 ELP nomenclature and sequence

Name	N-terminal	Backbone	C-terminal
V50CK1	SGVG	$[VPGVG]_{50}$	VPG
V75CK1	SGVG	$[VPGVG]_{75}$	VPG
V100CK1	SGVGG	$[VPGVG]_{100}$	VPG

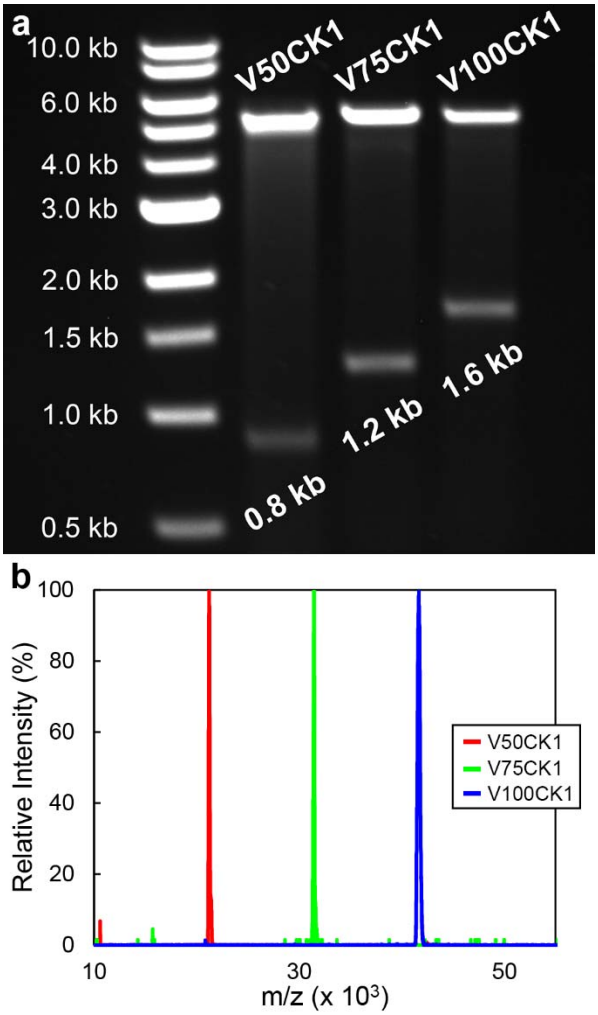

Figure 3.3 ELP genetic engineering and recombinant expression *a. Double digest of plasmids with XbaI and HindIII shows vectors at 5 kb and ELP genes at 0.8 kb, 1.2 kb and 1.6 kb for V50CK1, V75CK1 and V100CK1, respectively. b. Mass spectrometer data shows a single peak for each type of ELP. Measured masses: V50CK1 = 21.2 kDa, V75CK1 = 31.4 kDa, V100CK1 = 41.7 kDa).*

3.3.1 ELP transition temperature

Another basic characteristic we determine is the ITT of each ELP. ELP show their temperature transition properties when they are in an aqueous solution. The transition temperature of an ELP depends greatly on intrinsic properties of the protein such as the molecular weight and chemical composition. We determined the property using solutions

of each ELP and measuring the solution turbidity with increasing temperature. With an increase in molecular weight, the transition temperature (T_t) of ELPs decreases from 40 °C for V50CK1 to 34 °C and 31 °C for V75CK1 and V100CK1, respectively (Figure 3.4, Table 3.2). As is typical for ELP, T_t depends on many factors including the peptide molecular weight.[11,39] As hypothesized in previous studies, longer ELP likely has lower T_t due to increased and more stable hydrophobic interactions that disrupt peptide backbone hydrogen bonding with water.[39] We also took advantage of the ITT process to synthesize the hydrogels at a low initial protein concentration at which the lower viscosity helps create homogeneous ELP mixtures.

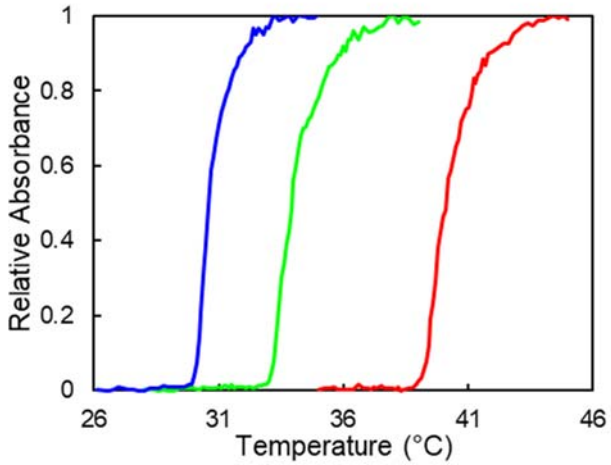

Figure 3.4 ITT of ELP measured by turbidity tests. *V50CK1 has a high Tt of 40°C followed by V75CK1 with 34°C and V100CK1 with 31°C.*

Table 3.2 Basic characteristics of ELP

ELP	Molecular weight (kDa)	Transition temperature (°C)
V50CK1	21.2	40
V75CK1	31.4	34
V100CK1	41.7	31

3.4 Thermo-responsive behavior of ELP hydrogels

We synthesized stimuli-responsive hydrogels with well-defined networks by end-linking our ELPs with four-arm crosslinkers (Figure 3.2). Specifically, the ELPs' N-terminal amine and C-terminal amine (lysine) groups react with the N-hydroxysuccinimide (NHS) esters on the end of each arm of a 4-armed polyethylene glycol (PEG) molecule (2 kDa). We performed crosslinking in a mixture of dimethyl sulfoxide (DMSO) and dimethylformamide (DMF) rather than in water to prevent any ITT-induced phase separation during crosslinking. This prevents regions of non-uniform ELP concentration and undesired hydrolysis of NHS-esters. In addition, the low viscosity of the 14% weight/volume (w/v) ELP solutions used for crosslinking permits easy mixing of reactants. These factors result in isotropic, homogeneous and optically transparent hydrogels.

The thermo-responsiveness of ELP is conserved after crosslinking into hydrogel. However, there is a difference between the thermal response of ELP in solution and crosslinked states. This likely relates to the concentration of ELP. It is known that the transition temperature of ELP increases with an increase in protein concentration up to a certain extent, beyond which the behavior of the proteins changes. Through our characterization we learned that at room temperature, in physiological ionic strength solutions, the equilibrium water content of the hydrogels ranged from 74% to 84%. At 37 °C, the collapse of ELP causes the gels to deswell and thus reducing the water content to 60% (Figure 3b). We further learned that at least at low temperatures, the hydrogel swelling behavior also depends on the molecular weight of ELP. For example, at 26°C, the equilibrium swelling for V50CK1 (21 kDa) hydrogels is 74% compared to hydrogels composed of the larger V100CK1 (42 kDa) that has a water content of 84%. The three gels were observed to approach similar water content at 37°C with only V50CK1 and V100CK1 being significantly different likely due to the limit to which the chains can contract. We hypothesized that the gradual temperature-induced collapse of ELP chains into unstructured coils with only weak inter- and intra-chain interactions in combination with the uniform chain length between crosslinks as well as the low crosslink density would allow our hydrogels to be highly resilient and extensible.

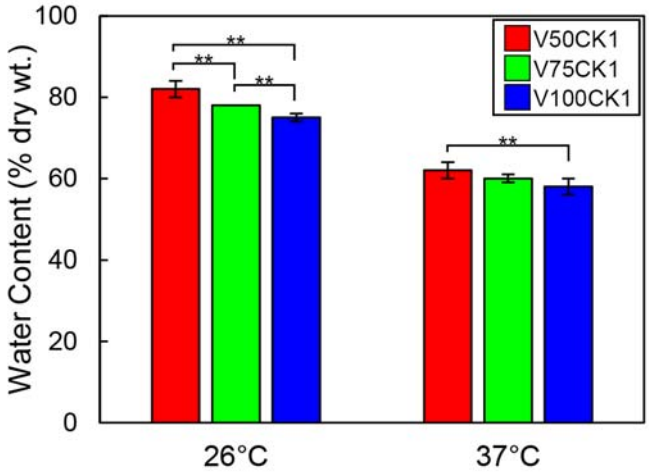

Figure 3.5 Figure 10 Comparison of ELP hydrogel water content in different conditions. *Water content decreases with higher temperatures and greater ELP size. (n = 5, except for V75CK1 with n = 6; statistically significant differences noted with '**' for p < 0.01)*

3.5 Uniaxial tensile testing of ELP hydrogels

The ELP hydrogels stretched to large magnitudes under uniaxial tensile testing. We conducted the tests using rectangular hydrogels of each ELP equilibrated at 37 °C in PBS. Failure strains increased significantly with increase in chain lengths. V50CK1, V75CK1, and V100CK1 achieved average strains of 1030%, 1210%, and 1440% (Figure 3.7 & Figure 3.6). Moreover, V100CK1s gel reached failure strain as high as 1530%,

which is considerably more than the previous best ELP value of 400% and the largest observed for a chemically crosslinked protein-based hydrogel to our knowledge.[89,213] Although we measured statistically significant differences between failure strains among the three hydrogels, their elastic moduli were practically the same at 19 kPa (Figure 3.6). Similarly, there was no difference between their ultimate tensile stresses (average of 100 kPa) (Figure 3.7 & Figure 3.6). We hypothesize that the hydrogel moduli are indistinguishable because at low strains the coiled chains are unraveling and the stress is mainly borne by entanglements and intra-/inter- chain interactions that should both be similar for all of the hydrogels. In addition, all the hydrogels have very low crosslink densities, which would be expected to contribute to greater stiffness. At higher strains, once the chains are uncoiled, the load starts to fall directly on the chains and crosslinks and there is a drastic increase in stress with plastic deformation. The onset of this behavior is reached by V50CK1 first, followed by V75CK1 and V100CK1 due to their greater chain lengths.

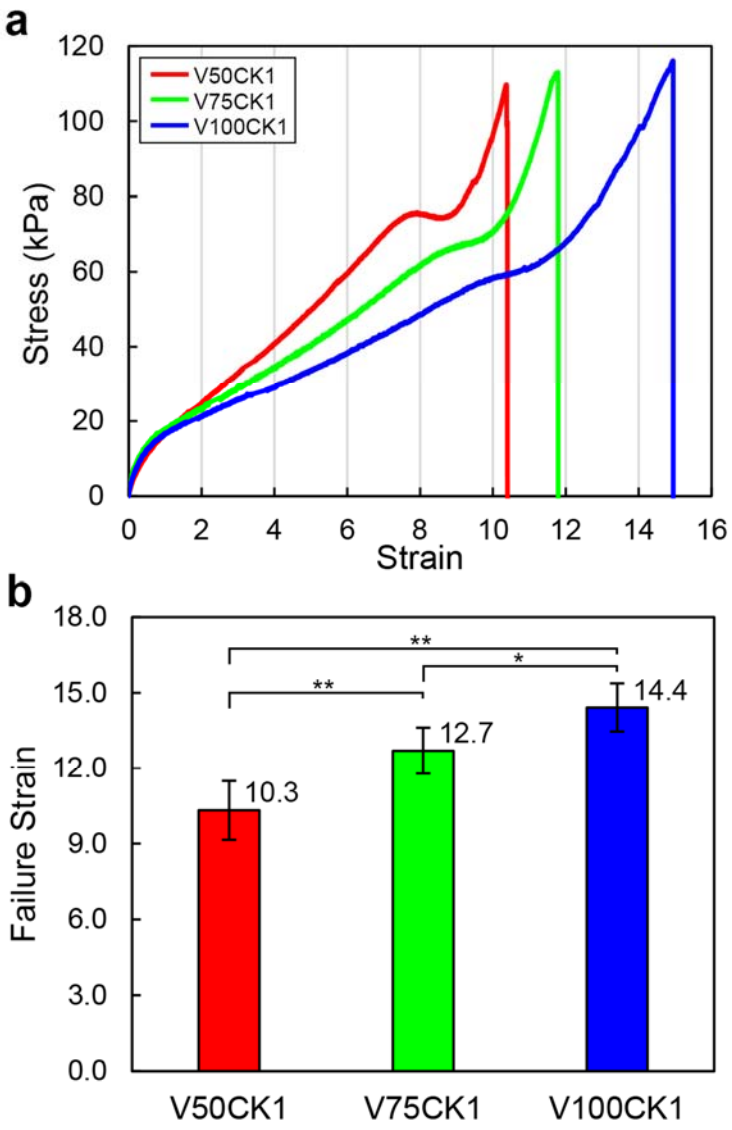

Figure 3.6 Tensile tests to failure *a) Representative plots for tensile test to failure (red: V50CK1, green: V75CK1, blue: V100CK1); b) Extremely high failure strains were observed with strains as high as 1530% for ideal-network ELP hydrogels. Failure strains directly depend on ELP size. (n = 5; statistically significant differences noted with '*' for $p < 0.05$ and '**' for $p < 0.01$)*

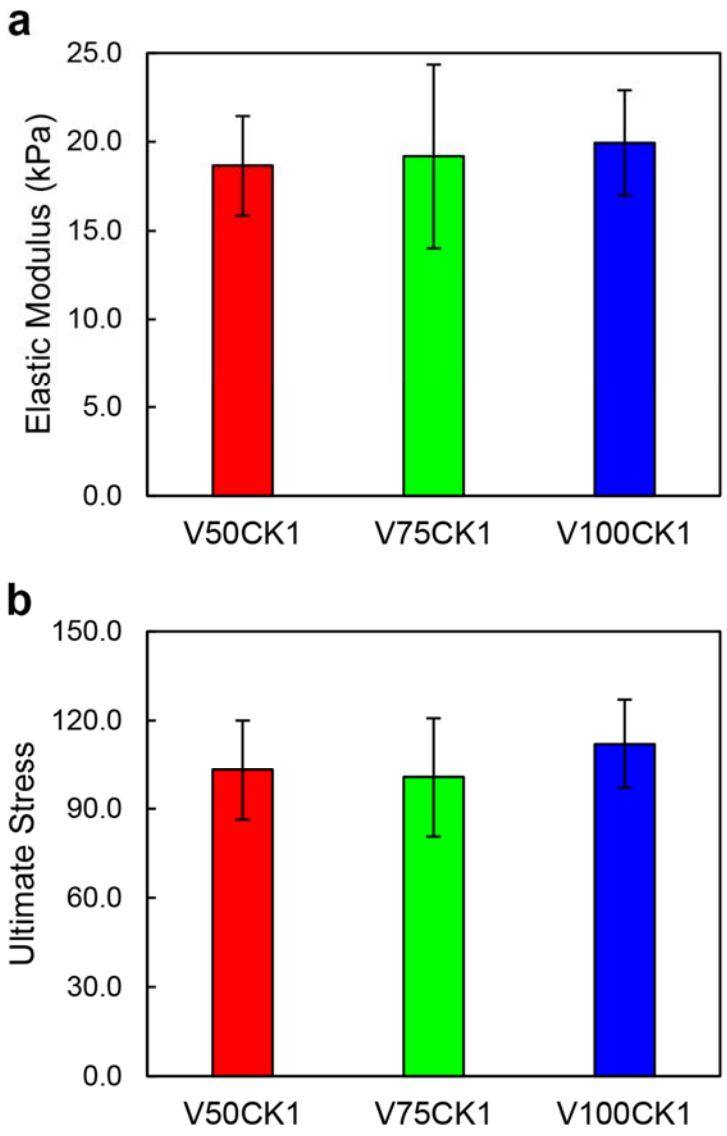

Figure 3.7 Tensile test modulus and ultimate stress *a) Elastic modulus of ELP hydrogels shows that between strains of 15% and 30%, all three types of proteins generate a similar modulus of about 19 kPa; b) Ultimate tensile stress measured prior to failure shows that regardless of ELP type, the hydrogels can handle about 105 kPa of stress before failure. (n = 5; no statistically significant differences were observed)*

3.6 Cyclic tensile testing of ELP hydrogels for resilience

We further characterize the elastomeric properties of our ELP hydrogels by performing cyclic tensile tests and show high resilience and low stress softening. We hypothesized that the protein size should influence potential hysteresis among hydrogels due to differences in ELP interactions. The cyclic tensile tests were performed by stretching the hydrogel to a strain of 600% at a strain rate of 100%/minute for 6 cycles to clearly show their resilience (Figure 3.8). We chose 600% strain in order to stay within the elastic limit of the shortest ELP, V50CK1, as determined from cyclic tests with

increasing strains as described in the next section. Cyclic tests show that V50CK1 hydrogels have the lowest hysteresis with an energy recovery of 94%, while V75CK1 and V100CK1 recover 88% and 83%, respectively (Figure 3.8b). The values are averaged over the last five cycles and statistically significant differences among the three hydrogel groups clearly indicates the influence of polymer type on hydrogel performance.

As is typical for hydrogel materials, our hydrogels also show viscoelastic behavior. The size of ELP contained within the hydrogel dictates the influence of elastic and viscous components. We attribute the rubber-like elastic behavior in our hydrogels to the random coiling based on weak hydrophobic interactions typical for ELP. The viscous behavior likely arises from the entanglements in the dense hydrogels and the inter-/intra-chain interactions of ELPs. As shown earlier, larger ELPs have lower T_t due to a greater amount of hydrophobic interactions that stabilize them in a coiled state at lower temperatures compared to small ELP. Thus, increased interactions can increase hysteresis in V100CK1 gels compared to V50CK1. In general, the first cycle shows higher hysteresis (Figure 3.11) because of the unraveling of knotted and entangled polymer chains as well as permanent damage from rupturing of some chains. Observation of hydrogel stress softening during the first couple of cycles supports the argument of permanent structural changes that taper off upon repeated deformations (Figure 3.8 & Figure 3.9). Majority of hysteresis (viscous component) observed beyond the first cycle is likely due to the weak hydrophobic interactions that ELP chains can undergo. Repeated coiling and uncoiling results in constant restructuring of chains and the consequential changes in inter-/intra- chain interactions would increase hysteresis (Figure 3.9).

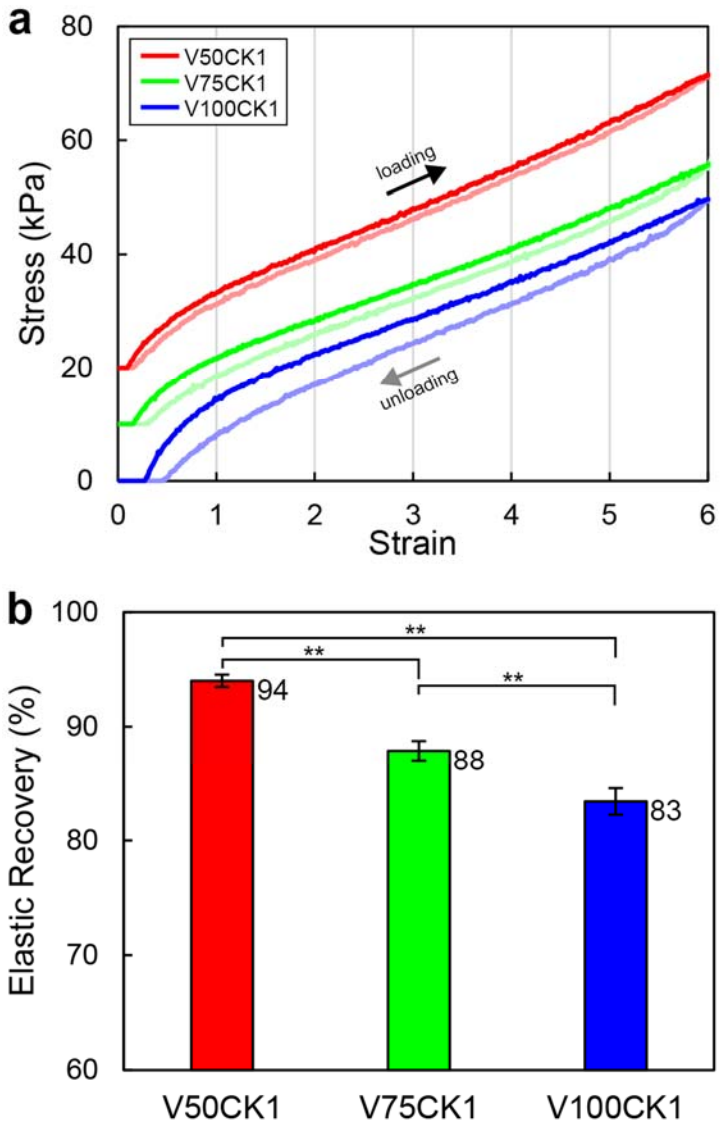

Figure 3.8 Cyclic tensile tests *a. Representative plots for the second cycle of a cyclic tensile test (V75CK1 is shifted up by 10 kPa and V50CK1 by 20 kPa for clarity) (red: V50CK1, green: V75CK1, blue: V100CK1).* ***b.*** *Cyclic tests show an increase in energy recovery with a decrease in ELP size. The increase in energy loss for longer ELPs is likely due to an increase in ELP interactions with an increase in size. (n = 5; statistically significant differences noted with '**' for $p < 0.01$)*

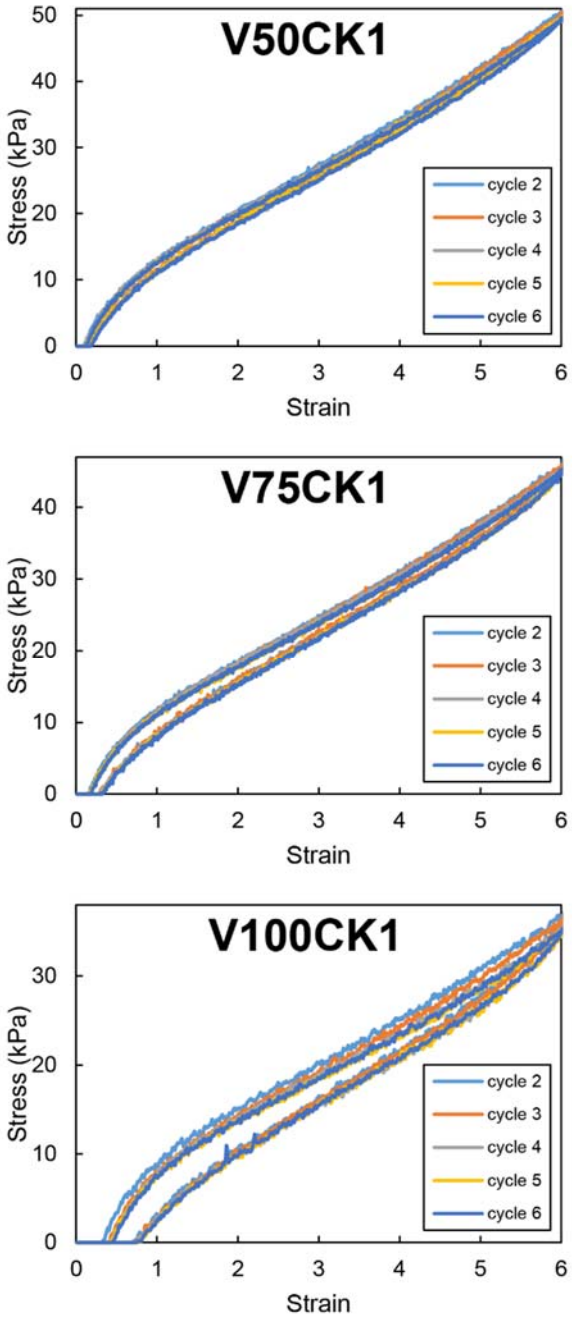

Figure 3.9 Representative cyclic tests showing cycles 2 to 6. *Majority of the plots overlap due to the elastic nature of ELP hydrogels.*

3.7 Cyclic tensile tests to determine the extent of elasticity

In order to explore the hyper-elastic nature of our hydrogels, we cyclically strain them over a series of increasing strains. Unlike other protein based hydrogels, these ELP hydrogels remain elastic even at high strains. We hypothesized that similar to failure strain, the extent of the elastic region also depends on the length of the ELP. Figure 3.8a

shows the stress strain cycles for each type of hydrogel. When the hydrogel is in its elastic region, the unloading curve shows some hysteresis depending on the type of ELP. Once the strain reaches plastic deformation, we see a drastic drop in stress during unloading phase. Figure 3.10 shows elastic recovery during these tests. The high hysteresis at initial low strains is likely due to the large amounts of chain untangling that occurs in the end-to-end tethered hydrogels. Once the untangling is already complete at lower strains, it has a smaller and smaller influence on the hydrogel hysteresis. Similarly, Figure 3.8 shows the second cycle with low hysteresis for each ELP hydrogel during repeated cycling. This should be similar for the hydrogels at other strains below the plastic deformation regime. Once the hydrogels undergo plastic deformation, hysteresis increases to high levels until the hydrogels break. Correlating the shape of stress v. strain curves in Figure 3.10 with Figure 3.6, we hypothesize that the distinct region in the curves where the stress stagnates even as strain increases is the beginning of plastic deformation. As can be seen in Figure 3.10, V50CK1 gels can remain elastic up to a strain of 700%, V75CK1 up to 900% and V100CK1 up to 1100%. This can be attributed to the coiling of polymer chains and thought of as longer springs that remain elastic at large deformations.

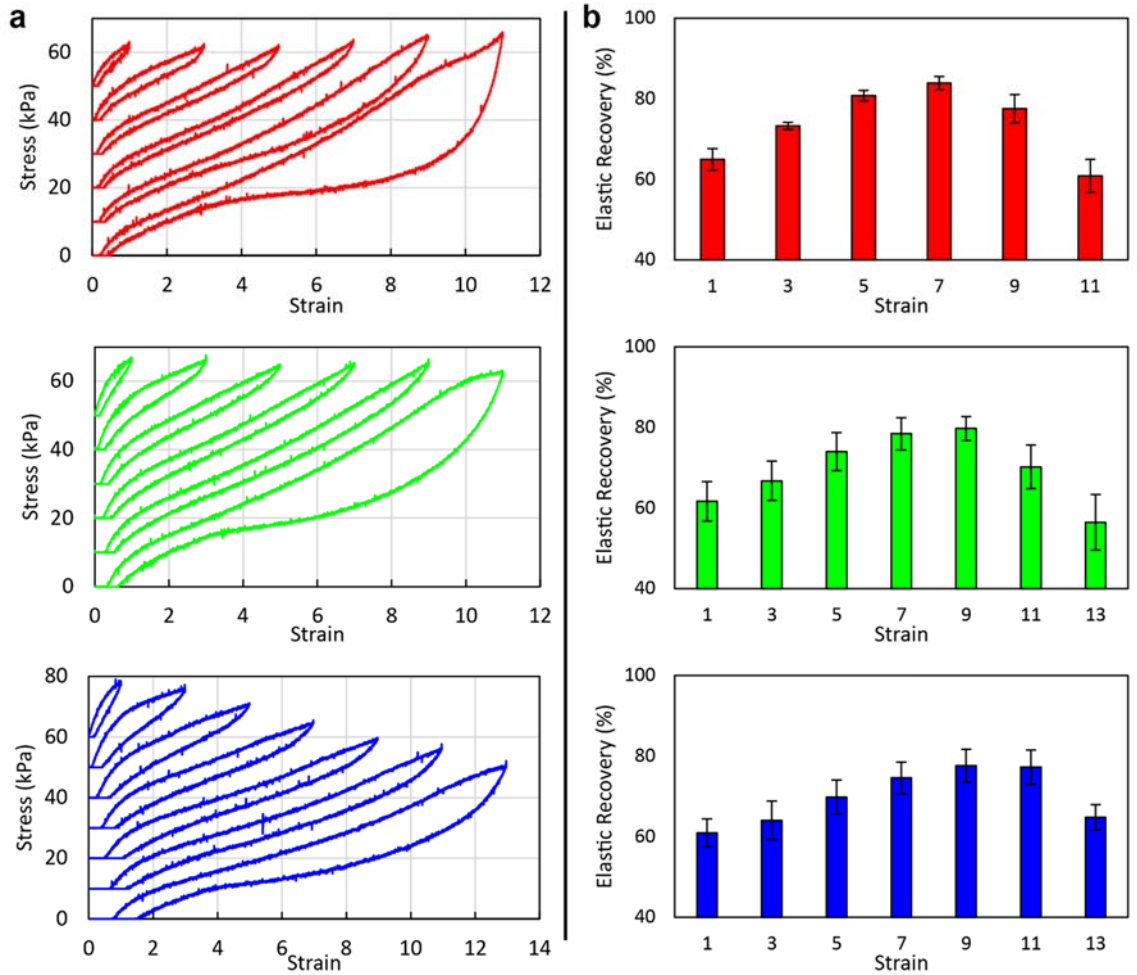

Figure 3.10 Cyclic tests with increasing strain. *Rubber-like elastic nature of ELP hydrogels can be seen through cyclic tensile tests with increasing strain (red: V50CK1,*

green: V75CK1, blue: V100CK1); a) Representative tensile cycles with each loop shifted up by 10 kPa for clarity. Hysteresis increases drastically once hydrogels undergo plastic deformations and this depends on ELP type; b) Elastic recovery over subsequent tensile cycles shows how untangling at low strains affects elastic recovery as well as strains at which hydrogels appear to undergo plastic deformations: >7 for V50CK1, >9 for V75CK1 and >11 for V100CK1.

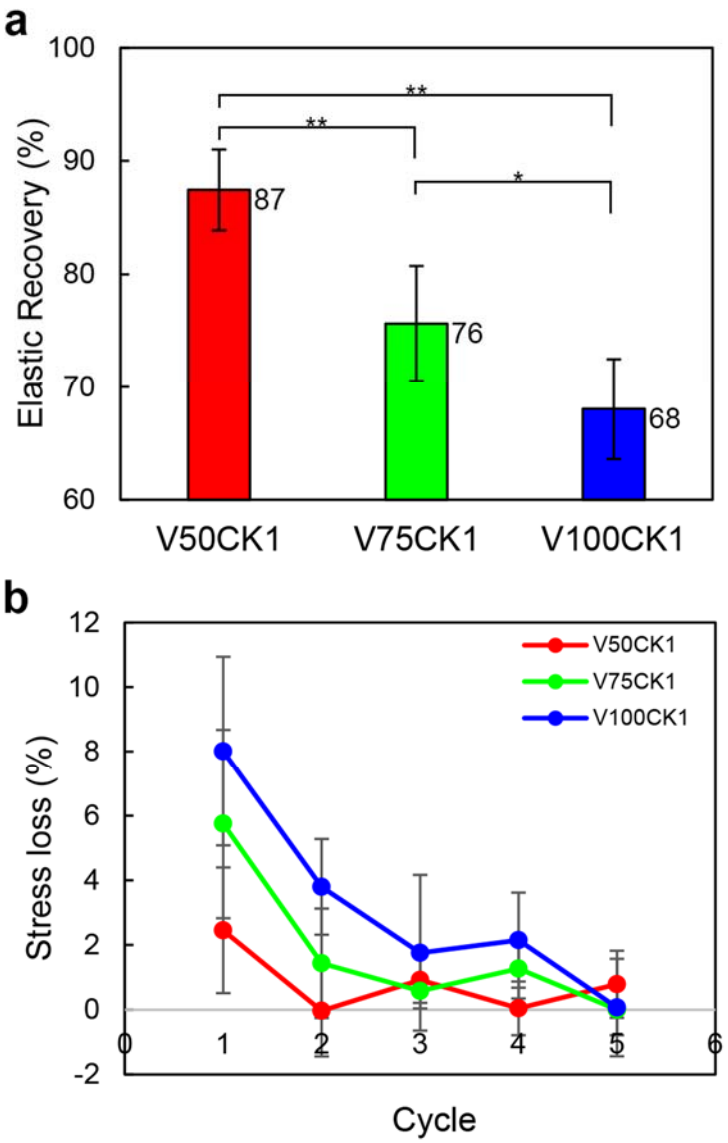

Figure 3.11 Elastic recovery in cycle 1 and hysteresis *a) Lower resilience is observed during the first cycle likely due to the unraveling and rupture of highly entangled and collapsed chains. Trend is similar to that of the remaining cycles; b) Stress loss of a cycle compared to previous cycle at the strain of 600%. Initially, V100CK1 incurs significant amount of stress loss due to disentanglements of the highly coiled and intertwined chains as well as chain rupture. After the first couple of cycles, stress loss is minimal for all*

three types of hydrogels. (Statistically significant differences noted with '' for $p < 0.05$; '**' for $p < 0.01$)*

3.8 ELP hydrogel resilience is potentially influenced by ELP size

Intrigued by the trends we observed for the series of hydrogels tested, we delve further to study the causes of the hydrogel properties. In particular, we investigate a hypothesis that the ELP-ELP interactions in addition to entanglements play a role in altering hydrogel hysteresis. In layman's terms, as a stretched hydrogel begins to return to its normal shape after extension, the extended polymer chains begin to coil. The hysteresis is caused by the sliding of chains against one another, which results in resistance due to interactions between the chains (Figure 3.12). Earlier cyclic tests showed a clear trend for hysteresis in which shorter ELPs have higher energy recovery, however it is difficult to determine the mechanism through the presented data. In order to investigate, we must alter the interactions between ELPs to decrease hydrogel hysteresis. We accomplish this by showing a specific example by matching the cyclic characteristics of V75CK1 hydrogels to the highly resilient V50CK1 gels. We use guanidinium hydrochloride (GuHCl), a well-known chaotropic protein denaturant to influence ELP thermo-responsive behavior. GuHCl increases ELP chain hydration by impeding chain interactions and thus preventing ELP hydrophobic collapse and increasing their T_t. Through our studies, we found a linear relationship between the concentration of GuHCl and the ELP T_t for both V75CK1 and V100CK1 (Figure 3.13). We used this data to rationalize a concentration of GuHCl that would be enough to affect hydrogel properties assuming that if the ELP transition temperatures are matched, their interactions will be similar. We observed that T_t of V75CK1 (Figure 3.13, *green*) matches that of V50CK1 (Figure 3.13, *red arrow*) at close to 0.5 M GuHCl concentration. Using linear regression, we determined that 0.49 M GuHCl in PBS should be optimal for showing a significant change in hysteresis during the cyclic tests. We also confirmed that PBS maintains its pH after the addition of GuHCl to avoid potential effects of pH on ELP prior to testing. Similar to the previous cyclic tests, these hydrogels were equilibrated at 37°C in PBS with 0.49M GuHCl to ensure homogeneous swelling pre-test and stretched cyclically over 6 cycles using the same test parameters. Figure 7b shows the second loop for V75CK1 with and without GuHCl. We can observe a distinct change in the hydrogel hysteresis with a statistically significant increase in V75CK1 energy recovery in the presence of GuHCl. In fact, the energy recovery for V75CK1 with GuHCl closely matches V50CK1 with a 1% difference (Figure 3.14). Thus, with the help of the chaotropic agent, we showed how the mitigation of inter-/intra- chain hydrophobic interactions allows V75CK1 chains to slide past each other with similar ease to V50CK1 and lower hysteresis in our rubber-like elastomeric hydrogels.

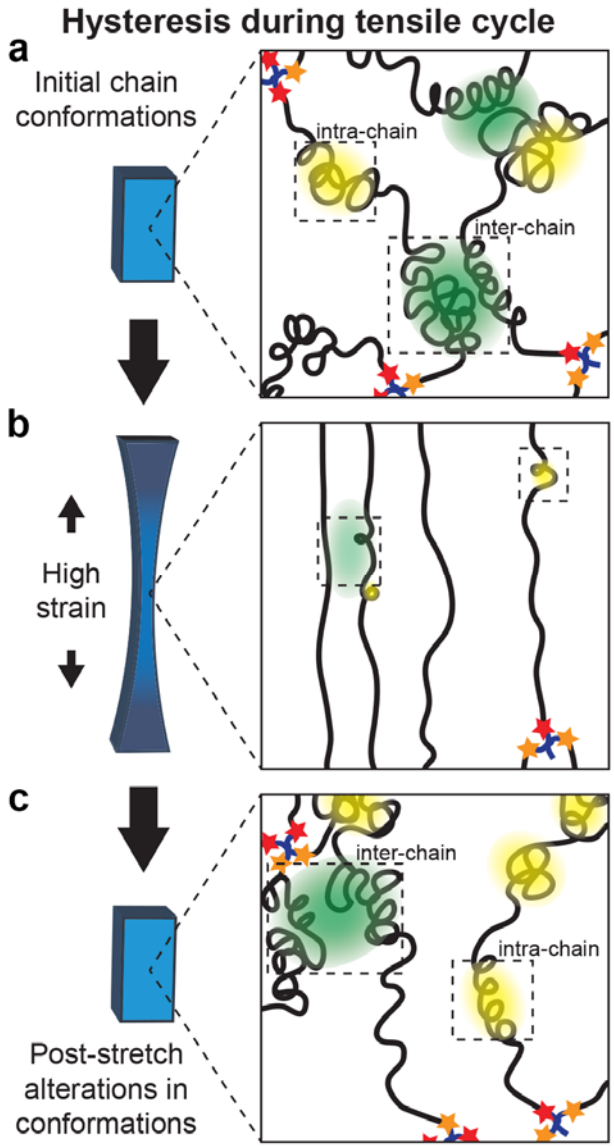

Figure 3.12 Hysteresis during cyclic tensile tests is caused by chain interactions *a. Initially, ELP chains are coiled and entangled.* **b.** *Once the entanglements are unraveled in the first cycle, hydrophobic interactions dominate hysteresis seen during the subsequent cycles.* **c.** *Specifically, ELP-ELP chain interactions cause changes in conformations of relaxed ELP chains after each cycle leading to hysteresis.*

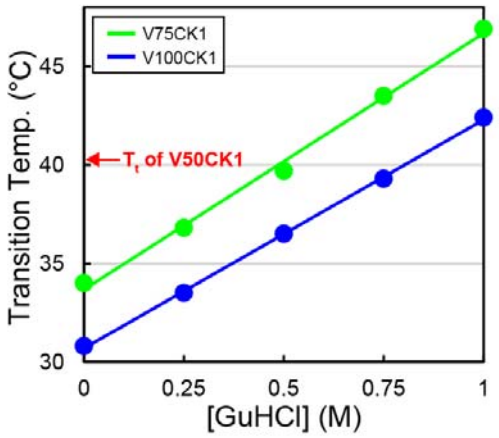

Figure 3.13 Increasing concentration of GuHCl raises ELP T_t. *V75CK1 (green) with 0.49M and V100CK1 (blue) with 0.81M GuHCl have T_t similar to V50CK1 at approximately 40°C.*

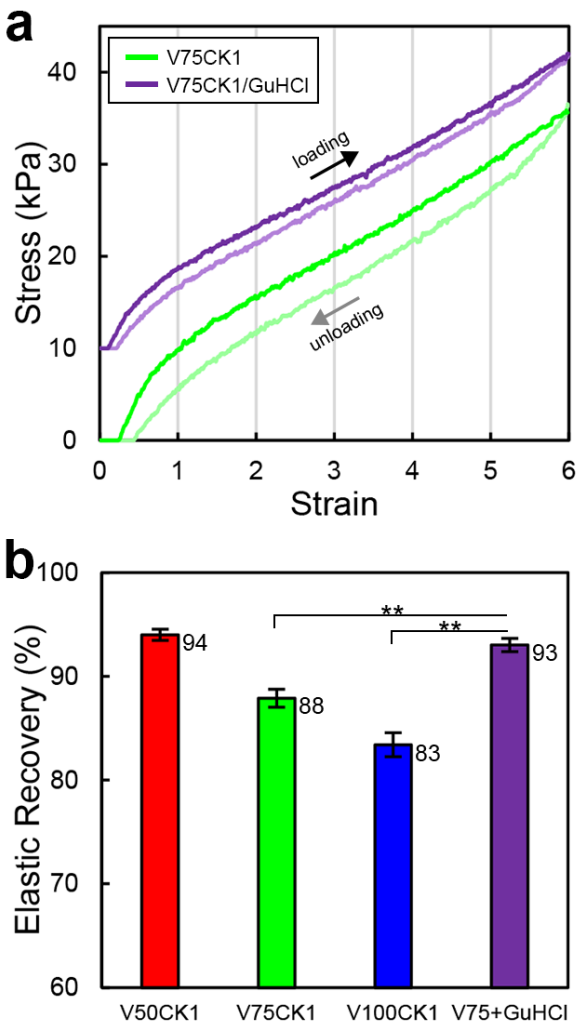

Figure 3.14 ELP chain interaction based hysteresis *a) Representative plots for V75CK1 hydrogels with and without GuHCl showing a clear decrease in hysteresis in the presence of the chaotropic agent (green: V75CK1, violet: V75CK1 with GuHCl); b) In the presence of GuHCl, V75CK1 hydrogels show a statistically significant increase in elastic recovery to match that of V50CK1 in PBS. (n = 5 except for V75CK1 gels in GuHCl with n = 3; statistically significant differences noted with '**' for p < 0.01)*

3.9 Conclusion

In this project, we used ELP to create protein-based mechanically robust hydrogels with rubber-like extensibility. End-to-end tethered coiled chains enabled our hydrogels to extend to strains as high as 1500% and maintain high resilience. In order to design such mechanically robust hydrogels, we exploited ELP for its entropic spring nature as well as genetic engineering to conduct precise polymer design and synthesis. Control over ELP sizes and sequence along with crosslinking using 4-arm NHS/PEG helped regulate inter-crosslink distances. Our strategy led to observations of clear

correlations between the molecular architectures of polymer networks and hydrogel extensibility as well as reversibility. Moreover, ELP's unique ITT property and resulting chain interactions along with the capability of guanidinium to affect these interactions helped us examine how the polymer chain interactions influence hydrogel hysteresis. An important conclusion from this work is that the selection of polymer length is critical to achieve the right properties. For example, because V50CK1 shows low hysteresis, it will be ideal for situations that require repetitive deformations, compared to the longer ELPs that show higher stress softening.

In addition to the exceptional properties described, the ELP hydrogels also have a biologically relevant elastic modulus matching soft tissues and numerous studies have already shown its excellent biocompatibility.[14] Unlike many other hydrogels that lack the ability to deform reversibly, these ELP hydrogels can be used as tissue engineering materials to develop extraordinarily robust scaffolds. Through further incorporation of cell-stimulating motifs by genetic engineering, our rubber-like hydrogel scaffolds will be useful for regenerating diseased tissues such as skeletal and cardiac muscles, blood vessels, dermal tissues, etc. that undergo repetitive deformations.[1,7,14,15,195]

3.10 Methods

3.10.1 Swelling Tests

In order to characterize the hydrogel swelling properties, we measured the weight of each hydrogel at 26 and 37 °C. Specifically, each hydrogel was first placed on a preweighed clean glass slide and excess water was removed using a tissue paper. The slide with hydrogel was then weighed, and the hydrogel was placed back in its container. Each hydrogel was weighed 2 more times with at least 30 min of incubation between each measurement in order to minimize measurement errors. Once the weights were recorded, the same hydrogels were incubated overnight at the next temperature, and the measurements were repeated in the same manner. After recording hydrogel weights in wet conditions, they were incubated in 15 mL of deionized water at room temperature and the water was exchanged at least 3 times over 2 days to remove salt. After 2 days, most of the water was aspirated from the glass vial and the hydrogels were frozen at −80 °C for 2 h, followed by lyophilization over 24 h. The dried samples were weighted 3 times to obtain the dry weight for the respective samples. Water content of the hydrogels was calculated using the formula: water content (%) = 100 × (weightWET – weightDRY)/weightWET.

3.10.2 Tensile Tests

Tensile tests were carried out using Instron 5544 and a custom setup to provide a temperature-controlled liquid environment for the test. Liquid is cycled between a heater and the test chamber to maintain our desired temperature of 37 °C during the tests. Before loading each gel, hydrogel profile pictures were taken to measure their width and thickness. After the gels were loaded, an additional picture was taken to measure the gauge length. Once loaded, the gels were allowed to equilibrate for 30 in warm PBS. During the test, the extension rate was kept constant at 10 mm/min for the tensile tests.

The elastic modulus for each gel was calculated using the stress data between strains of 15% and 30%. Failure strain and ultimate tensile stress were determined as the strain and stress values, respectively, at the failure point for each gel. Sample size was 5 for each gel type tested to perform statistical analysis.

3.10.3 Resilience Tests

Resilience tests were carried out using the same instrument and setup. After the gels were equilibrated for 30 min, the cyclic test was performed at a strain rate of 1/min. Each gel underwent 6 cycles of stretching and relaxation. Elastic recovery was calculated as the ratio between energy of relaxation and the energy of extension. Sample size was 5 for each gel type tested to perform statistical analysis. Sample size was 3 for V75CK1 hydrogels in the presence of GuHCl.

Chapter 4 Adhesive hydrogels

4.1 Introduction

Adhesives, unlike sutures and staples, provide a convenient and non-invasive method to bond surfaces together. For biomedical applications, adhesives are useful for bonding tissues post incisions and for closing wounds without introducing further trauma. In general, a good adhesive needs to not only bond well to the target surface, but also crosslink to form a strong and stable bridge upon curing. Some of the most common adhesives are derivatives of cyanoacrylate glues, which undergo free-radical polymerization upon exposure to a nucleophile such as water and bond to tissues in the process of curing.[184] Since their first use to seal wounds in the late 1950s, cyanoacrylates have seen significant developments to achieve the FDA approved 2-octyl cyanoacrylate or Dermabond in 1998.[183,184] Cyanoacrylate based glues show high adhesion strengths, eliminate the dangers involved with suturing, allow wounds to heal faster and show good cosmetic results.[182,183] However, the volatile organic solvents that are a part of these glues can cause inflammation and necrosis and show cytotoxicity at typical concentrations prior to curing.[182] Additionally, the degradation of these glues and any long-term effects *in vivo* have not been adequately evaluated.[182]

Alternatives to cyanoacrylate glues comprise of hydrogel adhesives that contain synthetic and natural polymers, and animal-derived proteins. However, since the adhesives target the same subset of reactive groups such as amines, thiols and imidazoles, they commonly use formaldehyde, glutaraldehyde or UV-based strategies for bonding.[214] A major risk with the use of formaldehyde and glutaraldehyde is their toxicity, while UV exposure can cause unwanted mutations. Another significant drawback for common hydrogels is swelling that can lead to mechanical failure in aqueous environments.[5] In addition, synthetic polymers require careful design to manage degradation and biocompatibility,[1] which makes proteins such as fibrin, gelatin and collagen the simpler alternative. However, since the protein-based adhesives are from xenogenic sources, there is batch-to-batch variability, and risk of allergic reaction and disease transfer.[215,216] Hydrogels also lack flexibility that would be advantageous for long-term endurance of adhesives.

To this end, we pursue the development of a biocompatible adhesive that is not only adhesive to wet biological tissues, but also flexible. Our elastin-like polypeptides are an ideal candidate for this work. ELP are recombinant proteins, which makes them monodispersed and genetically tunable. ELP are also known for their elasticity and stimuli-responsiveness.[181] Thus, in addition to flexibility, hydrogels containing ELP can naturally deswell at the relatively high temperatures and ionic strengths encountered in our body.[181,185] We can achieve adhesion by incorporating mussel-inspired catechol groups on our polymers.[217] It is well-known that mussels can adhere to many different types of organic and inorganic surfaces. This is accomplished through their byssal thread proteins with a high content of L-3,4-dihydroxyphenylalanine (L-DOPA) and lysine

residues.[217] In fact, L-DOPA residues populate up to 30% of amino acids in mussel foot protein-2 and are a result of post-translational modification of tyrosine via tyrosinase enzymes.[217] The catechol residue on L-DOPA is similar to polyphenolic compounds found in wine, coffee and tea with the ability to react with inorganics such as metal oxides as well as organics such as amino acids containing amine, thiol, imidazole and many synthetic polymers.[218] Since amine, thiol and imidazole groups are already present in biological tissues, catechols are a good candidate for adhesion purposes. By incorporating the flexible ELP and adhesive catechols, we can accomplish our goal of synthesizing a flexible adhesive.

4.2 Strategy for adhesive synthesis

In order to create a flexible adhesive, we use genetic engineering to engineer elastin-like polypeptides (ELP) and design a polypeptide that can be chemically functionalized to yield adhesive properties. We have already shown the extent of flexibility that can be achieved with the material.[181] By imparting the ability to adhere and crosslink *in situ*, we can create a flexible and biocompatible adhesive. First, we designed the core sequence of our ELP, which has a variable guest residue, 'X,' in the pentapeptide repeat unit, 'VPGXG'. In this work, we chose glutamate as the guest residue, since the carboxylate functional group can be chemically modified with dopamine for catechol incorporation (Figure 4.1a & Figure 4.2). Lysine is another candidate for this purpose, however since catechol can bond with amine in addition to other catechols, the protein would undergo unwanted reactions with unmodified amines and reduce the number of catechols available for adhesion to tissues.[218] Tyrosine can also be a good guest residue as it can be converted to L-DOPA by enzymatic modification in a scheme similar to mussel foot proteins.[217] However, protein purification to remove the enzymes after the modification would result in significant loss of the material. In addition, the presence of tyrosine would greatly increase the hydrophobicity of the protein, and lead to difficulty in protein handling and processing. Comparatively, the carboxylate functional glutamate is the ideal choice to develop our material since upon chemical modification of the ELP, all small molecule reactants and products can be removed by dialysis.

Once functionalized, the proteins can be applied to a target substrate for adhesion. Generally, catechol containing adhesives crosslink or cure as the catechol groups are oxidized. During oxidation, quinones can react with tissue specific residues such as amine, thiol and imidazole via Michael addition or Schiff base formation (Figure 4.1b).[218] Additionally, the catechol and the oxidized quinone groups can dimerize to crosslink the polymer chains together.[218] Through these reactions, the adhesive can both, adhere to the tissue and form a stable bridging material to bond the target surfaces (Figure 4.1c). Previous research has also shown the effectiveness of adhesion even with small quantities of catechol, however, it requires an oxidant to work efficiently.[219-221] Since our ELPs will contain significantly low amounts of catechols compared to mussel foot proteins, we will incorporate sodium periodate, which is a mild oxidant and has shown success with other previous works.[219-221]

In the remainder of this chapter, I will describe the design and synthesis of the ELP. This will be followed by the functionalization of the ELP with dopamine and its characterization. We characterize the curing of functionalized ELPs through rheometry and highlight the deswelling behavior of these materials in addition to flexibility. Finally, we study the adhesion strengths of the proteins on porcine skin and conclude with a remark about a pathway to create adhesives using rubber-like hydrogels in Chapter 3.

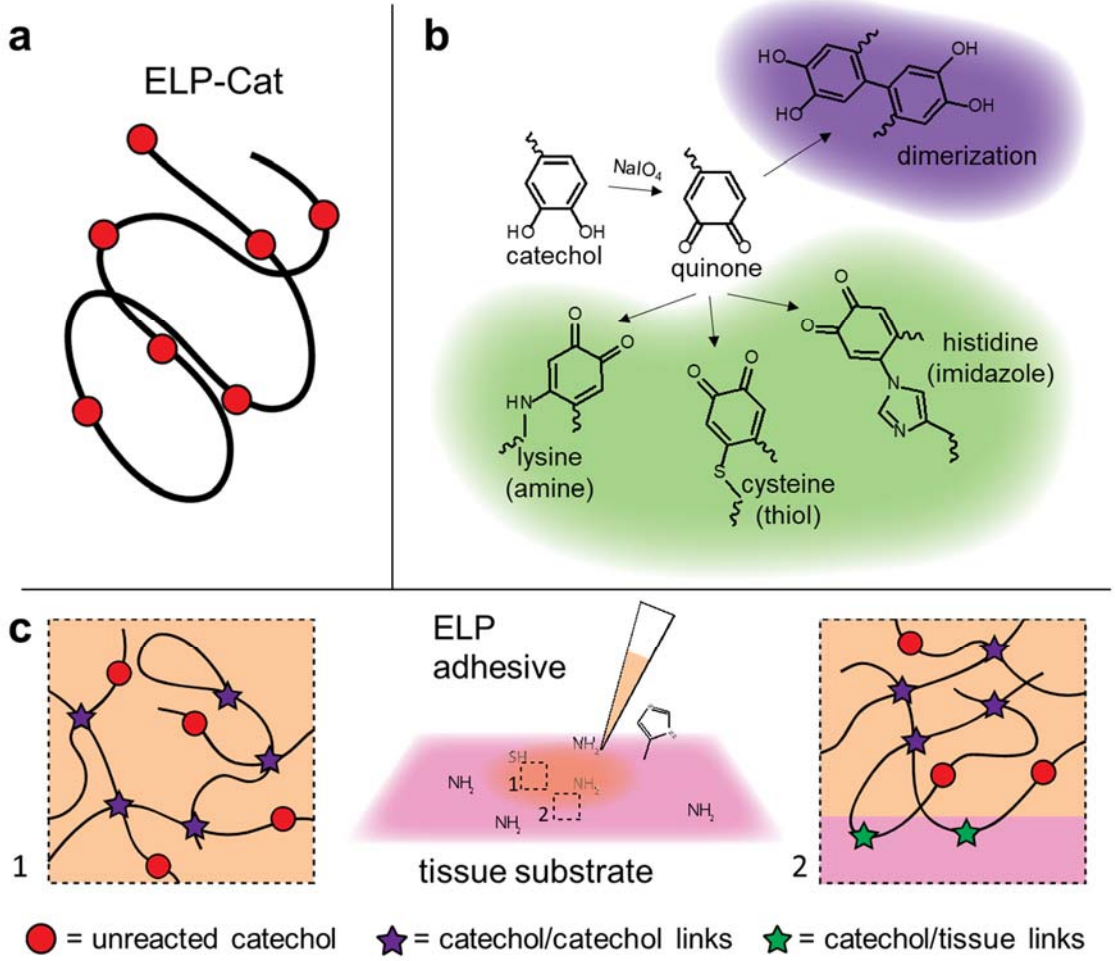

Figure 4.1 Adhesive hydrogel schematic *a) ELP will be modified with dopamine to produce ELP/Cat. b) In oxidative conditions, ELP/Cat can bind to tissues by reacting with amine, thiol and imidazole, and form a network by dimerizing. c) ELP/Cat can be easily applied on tissues, on which it will solidify and bind*

4.3 ELP synthesis and material design

In this work, our goal was to create an adhesive polymer that cures and bonds soft tissues. We approach this issue by designing an ELP glutamate, which contains carboxylate that can be chemically modified with dopamine. The ELP, called V4E125, is composed of two types of pentapeptides – 'VPGVG' and 'VPGEG' – with a full sequence of $([VPGVG]_2VPGEG[VPGVG]_2)_{25}$. The protein name is derived from its

repeat units, each of which contains 4 repeats of pentapeptides with guest residue 'V' and 1 repeat of pentapeptide with guest residue 'E'. Each protein contains a total of 125 pentapeptides. V4E125 was synthesized previously by Dr. Eddie Wang using genetic engineering methods described in chapter 2.[18] Once the V4E125 gene was synthesized, the protein was synthesized by over-expression in terrific broth with glycerol and the antibiotic, kanamycin.[191] The expressed protein was purified by lysing the cells and removing the cell debris, followed by inverse temperature cycling to remove all other contaminants. The protein solution was dialyzed against ultra-pure water over two days and lyophilized over two more days to yield a pure protein sample. Our previous mass spectrometry results show the protein to be 52.5 kDa as expected. In addition, since the negative charge at physiological pH leads to repulsion, the protein does not show any transition in physiological conditions compared to V50CK1, V75CK1 and V100CK1 in chapter 3.

4.4 Chemical functionalization of V4E125

Adhesives bond multiple surfaces together by not only adhering to each surface, but also forming a network that bridges across these surfaces. Furthermore, since our goal is to develop an adhesive to treat biological tissues, we are limited to natural tissue surfaces that contain reactive groups such as amines, thiols and imidazoles in aqueous conditions. We can target all these groups by using catechols that undergo Michael addition in oxidative conditions to form strong bonds.[218] Additionally, since catechols can also react with each other, they can form a strong network that will lead to a successful adhesion (Figure 4.1b). We introduce catechols into our carboxylate containing V4E125 proteins using amine containing dopamine. The 26 carboxylates (25 glutamate residues and one carboxylate at the C-terminal), can be easily modified with dopamine using the EDC/NHS chemistry. Since NHS is a good leaving group, activating a carboxylate with NHS ester can provide a high yield strategy to functionalize our protein with dopamine (Figure 4.2). Unlike enzymatic modification strategies, our method allows us to control the amount of modification by controlling the ratio of reactants. Furthermore, purification of protein is extremely simple as all reactants, unwanted products, and organic solvents are small molecules that can diffuse through the 10 kDa molecular weight cut-off dialysis membrane. We can recover 99% of the protein modified with this method.

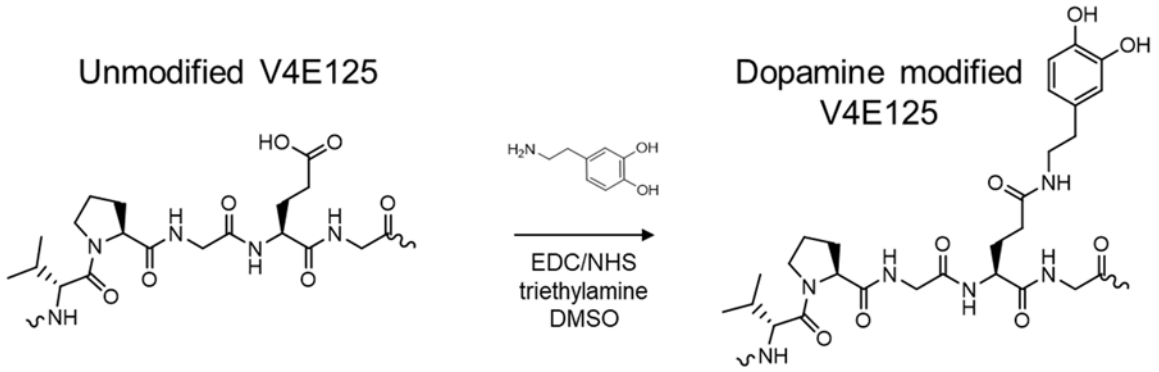

Figure 4.2 Chemical functionalization scheme for modifying V4E125 with dopamine. *Glutamate can be activated using EDC/NHS. The NHS ester functional V4E125 can react efficiently with primary amines on dopamine to create the modified ELP/Cat*

A significant effect of the functionalization of V4E125 was observed in the transition temperature of the proteins. Unmodified V4E125 has an extremely high to no transition due to charge-charge repulsion. However, once the proteins are modified, their hydrophobicity increases along with the loss of charged carboxylates. This leads to a decrease in the transition temperature of the proteins even below the room temperature.[39] Once the protein was purified, the transition temperature of each protein was quantified using turbidity measurements. We expected the transition temperature to decrease as the amount of modification increases. This is both due to the addition of a relatively hydrophobic moiety and the loss of a charged residue. As shown in Figure 4.3, the transition temperature of ELP/Cat solutions in phosphate buffered saline changes from 28°C for 50% modification ratio to 16°C for 100% modification ratio (Figure 4.3). This provides us with qualitative proof that the proteins are being modified and increasing the modification ratio makes them more hydrophobic as expected. The relatively low transition temperature also indicates an increased potential for any resulting hydrogel network to deswell as the temperature increases from cold temperatures to 37°C.

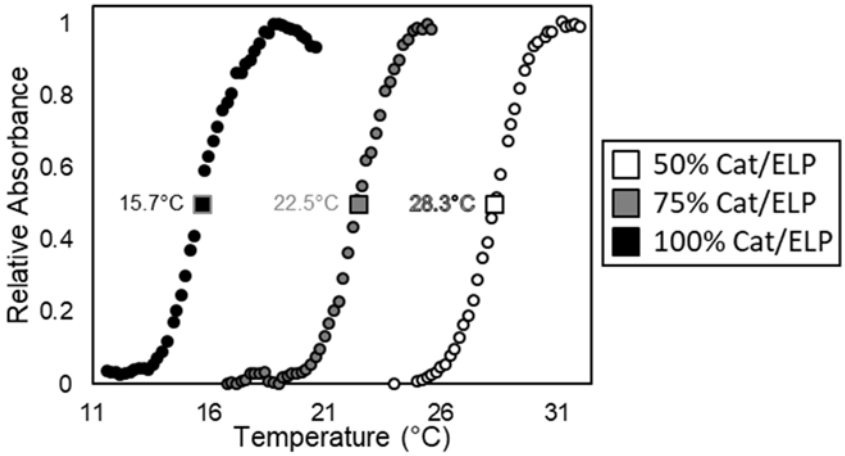

Figure 4.3 Transition temperature measurements of ELP/Cat. *As the amount of modification increases, the protein loses negatively charged residues that result in a decrease in its transition temperature.*

In order to confirm and quantify the presence of catechol on ELP/Cat, we investigate our samples using NMR spectroscopy. 50%, 75% and 100% ELP/Cat samples showed reaction yields of 90%, 86% and 79%, respectively. (Figure 4.4) Polymeric materials are generally difficult to examine using NMR due to their broad dispersity and branching. However, our recombinantly synthesized ELP show excellent signal due to their highly repetitive nature and monodispersed size. In addition, since the unmodified V4E125 does not have any phenyl groups, we can confirm dopamine functional groups by observing NMR signals around 6.8 ppm. (Figure 4.4) Compared to unmodified V4E125, all three ELP/Cat samples show peaks between 6.5 and 7 ppm. (Figure 4.6) To further quantify the number of dopamine present, we compare the integration of signal from three protons on the catechol/quinone groups to that of the six protons on methyl groups of valine at 0.9 ppm. (Figure 4.4) Through this we calculated the actual modification ratio of 45% for the 50% ELP/Cat sample, 64.5% for the 75% ELP/Cat sample, and 80% for 100% ELP/Cat. (Figure 4.5 & Figure 4.6)

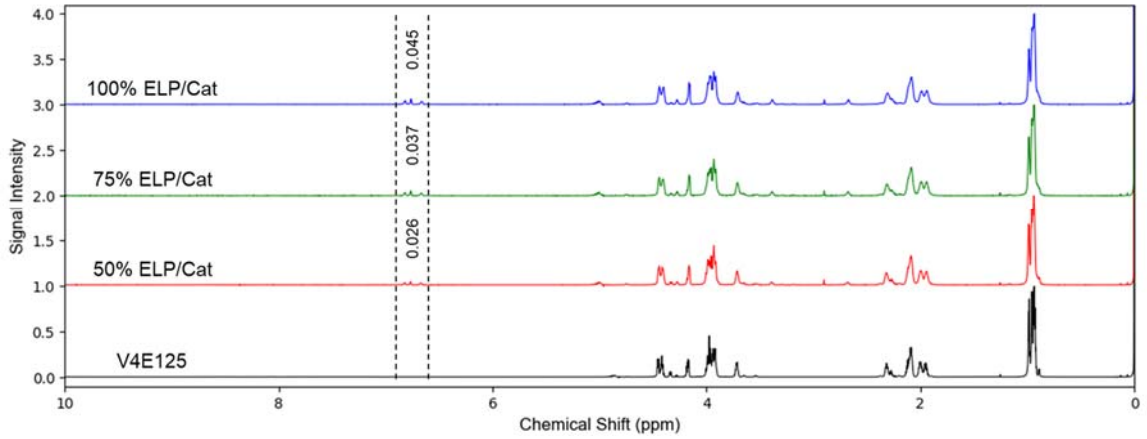

Figure 4.4 ^{1}H NMR spectra (900 MHz) of ELP/Cat. *Protons on the valine methyl groups (0.9 ppm) can be used to quantify catechol/quinone protons (6.5 – 7 ppm)*

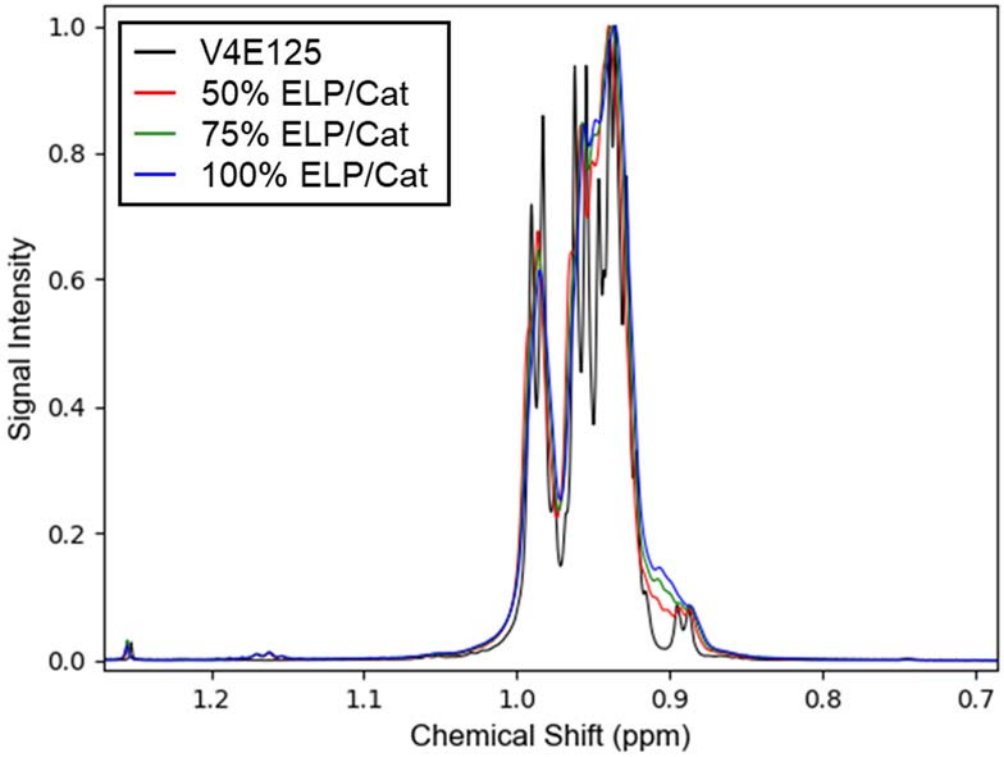

Figure 4.5 ^{1}H NMR signal of valine methyl protons. *Methyl protons were used to normalize the signals and quantify catechol protons.*

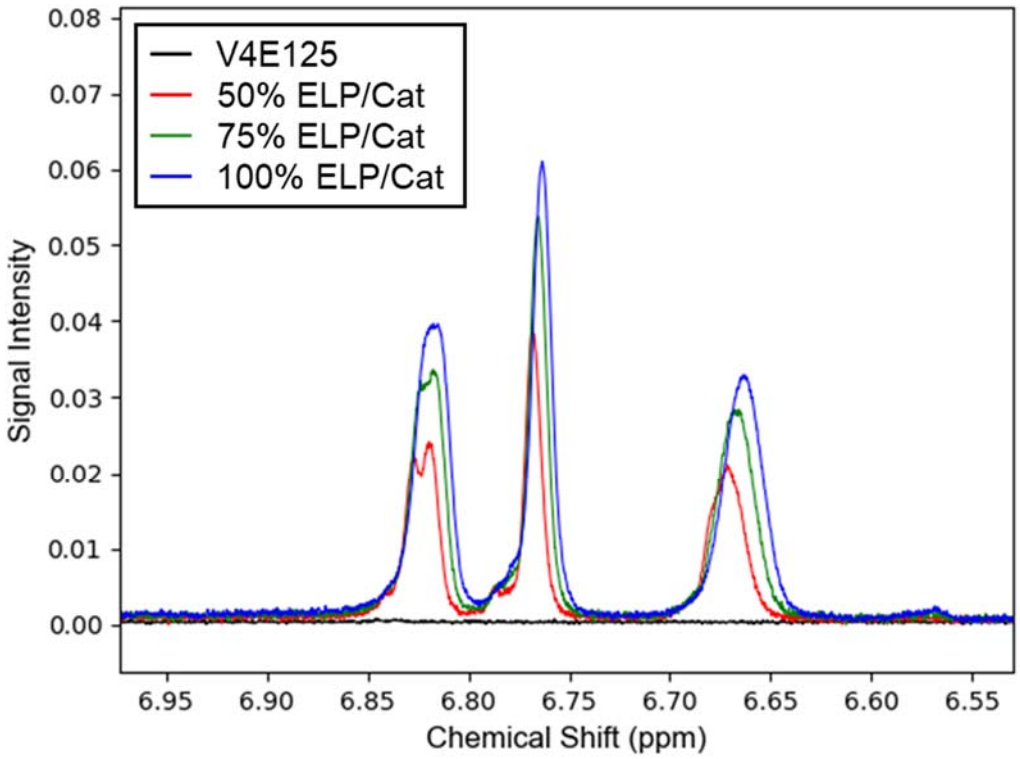

Figure 4.6 ^{1}H NMR signal of catechol/quinone signal. *50% ELP/Cat showed 90% reaction yield, while 75% ELP/Cat showed 86% and 100% ELP/Cat showed 79% reaction yield*

4.5 Rheological properties of ELP/Cat

The ELP/Cat polymers must crosslink to from a stable hydrogel network for our adhesive to function as intended. Since the starting state of the adhesive is a liquid that should solidify over time, we chose rheometry as the appropriate technique. Rheometry can be used to measure material characteristics over time by applying shear in an oscillatory manner. Our first priority was to measure how fast our materials cure at the physiological temperature of 37°C. We prepare the adhesive hydrogel mixture on ice and immediately transfer it to the rheometer stage cooled to 4°C. We observe that until the temperature is raised, there are no changes in the storage and loss moduli. Once the temperature is ramped to 37°C, all the samples show an increase in storage modulus within 1 to 3 minutes and it increases slowly over an hour (Figure 4.7). Although 75% and 100% ELP/Cat samples consistently show changes in the storage modulus from 100 to 1000 Pa, many of the 50% ELP/Cat samples showed no changes. Such low moduli would indicate extremely soft hydrogels; however, we were able to easily handle the cured hydrogels and even stretch it. We hypothesized that the hydrogels were shrinking as they crosslink, and this led to loss of contact between the material and the probe.

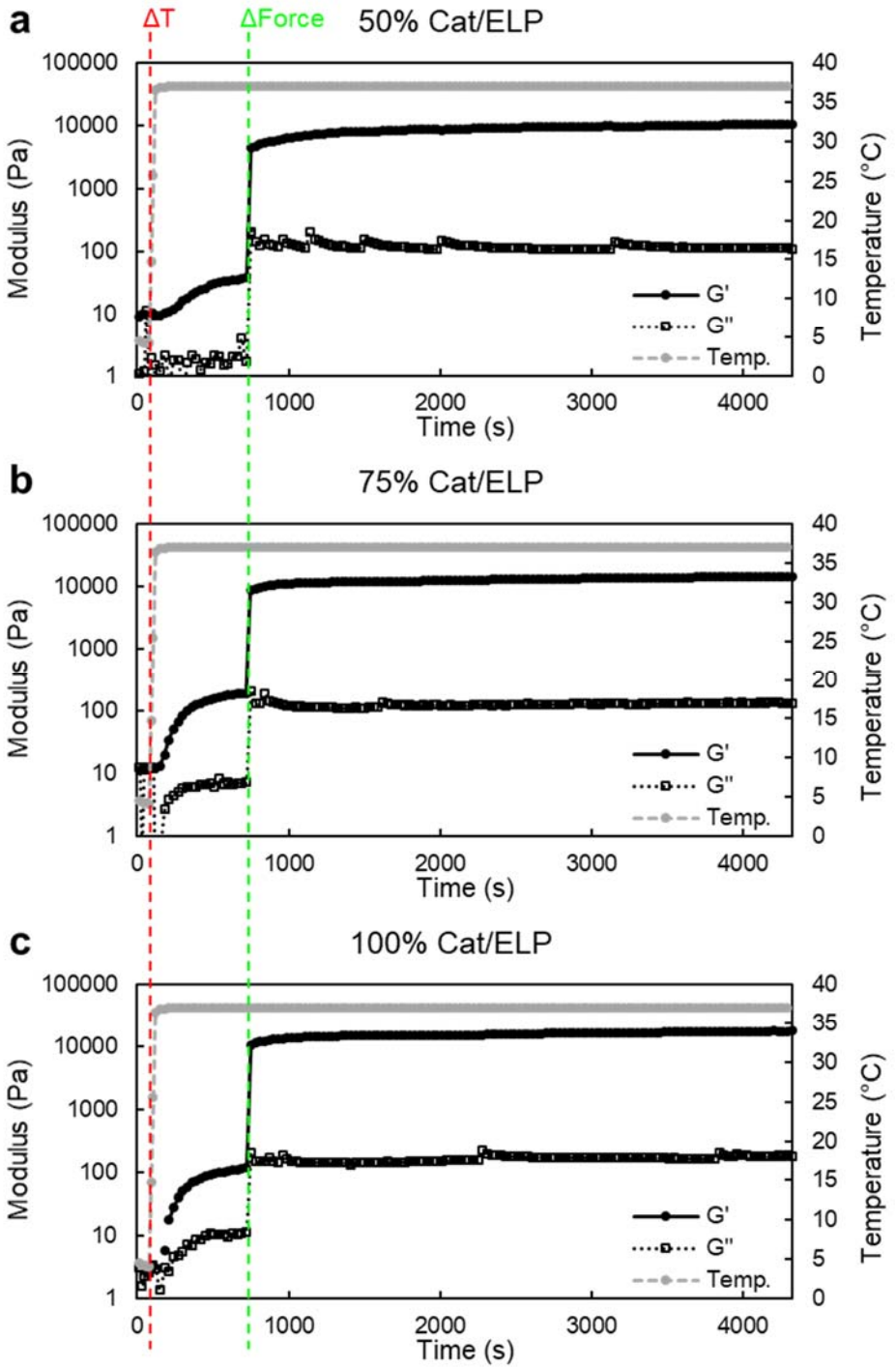

Figure 4.7 Representative rheology test data. *Rheology tests for ELP/Cat hydrogels show small moduli until normal force is applied (ΔForce); This is due to hydrogel deswelling, which is common for ELP-based hydrogels. a) 50% ELP/Cat. b) 75% ELP/Cat. c) 100% ELP/Cat*

We addressed this issue by applying a constant normal force on the material so that the gap is adjusted to account for hydrogel deswelling. But, before we begin applying

the force, we allow the hydrogels to crosslink for 10 minutes at 37°C to prevent premature expulsion of uncrosslinked mixture. Figure 4.7 shows the representative measurements for each type of ELP/Cat and Figure 4.8 shows the average values of storage and loss moduli after 1 hour of measurements. The loss moduli remain small and indistinguishable among the three sample types; However, the storage moduli show a positive relationship with an increase in dopamine content as expected. 100% ELP/Cat samples show moduli as high as 19 kPa.

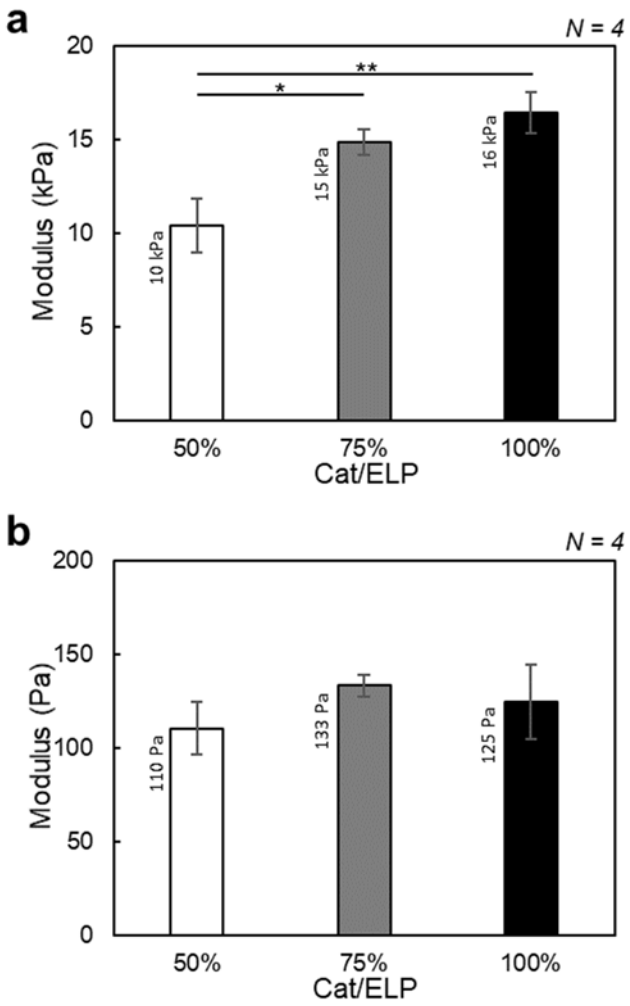

Figure 4.8 Rheological properties of ELP/Cat hydrogels. *a) Storage modulus, elastic component, increases with an increase in the amount of catechol. b) Loss modulus, viscous component, remains constant. (N, number of samples; statistically significant differences noted with '*' for $p < 0.05$ & '**' for $p < 0.01$)*

After the 1 hour of measurements, we further test the gels with a strain sweep by linearly ramping the strain from 0.1% to 300% (Figure 4.9). We observe the damping factor, which is a ratio of storage to loss modulus, and use a value of 1 as the failure point of the hydrogel. The ELP/Cat protein with lowest modification ratio of 50% shows the highest failure strain with an average of 161%. This can be attributed to the fact that decreasing the crosslink density leaves larger inter-crosslink distances so that the polymer

chains can stretch before rupturing. (Figure 4.10) And although the 100% ELP/Cat adhesives show the least flexibility, they can still withstand a shear strain beyond 100%.

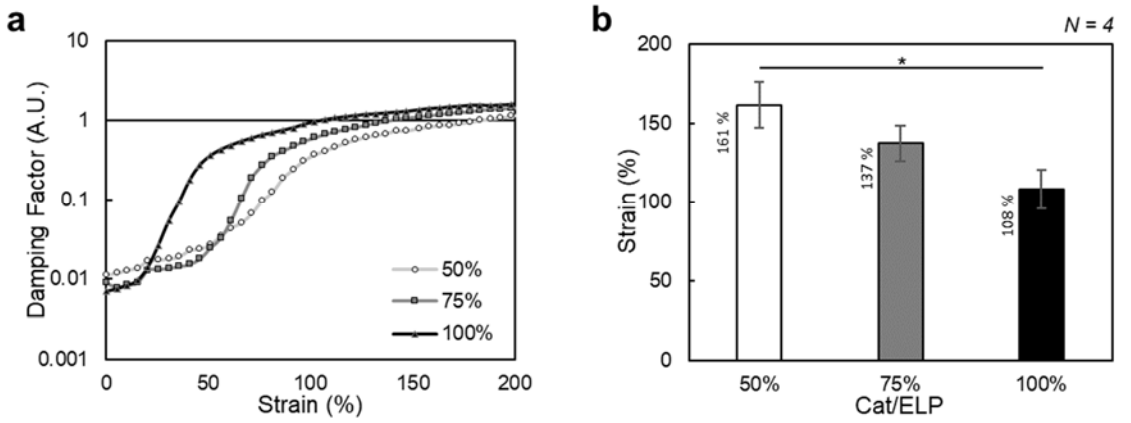

Figure 4.9 ELP/Cat hydrogel flexibility. *a) Representative plots showing the changes in damping factor during strain sweeps. b) Average strain at which the damping factor reaches 1; 50% ELP/Cat hydrogels maintain their integrity to shear strain as high as 190%. (N, number of samples; statistically significant differences noted with '*' for $p < 0.05$)*

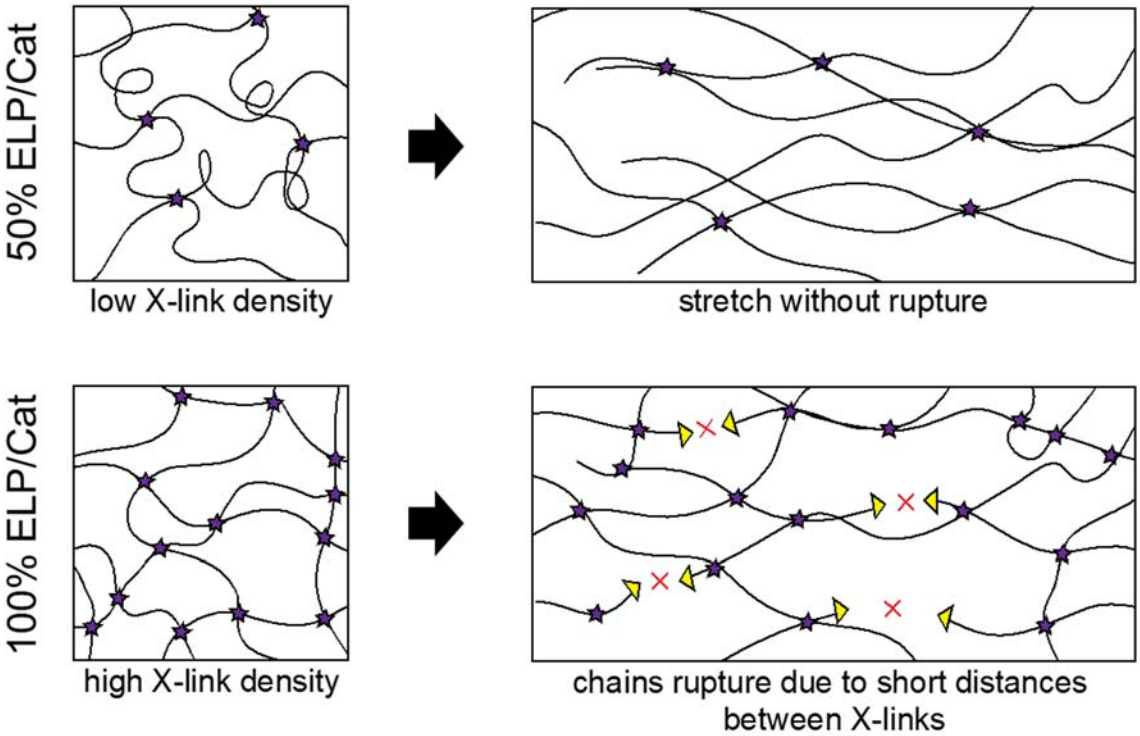

Figure 4.10 Schematic showing the effects of crosslink density and strain. *50% ELP/Cat hydrogels show higher flexibility because a larger portion of the polymer chain is available for stretching compared to highly crosslinked 100% ELP/Cat*

4.6 Adhesive properties of ELP/Cat

Once we measured the curing characteristics of our materials, we investigated their adhesiveness to biological tissues, specifically to porcine skin. We first test the tensile strength of the adhesives and find that the ELP/Cat with 100% modification show the highest strength of 35 kPa and the strength decreases with a decrease in the amount of modification (Figure 4.11). We chose porcine skin as a model system for testing as it is readily available and is typically used to test adhesives. Since skin is rather flexible, we secure them on aluminum supports and in particular, we use T-bar shaped aluminum stubs for tensile tests. Figure 4.11a shows a representative test for each type of adhesive. Typically, the samples remain stable until a peak load is reached, at which point the adhesive fails and the load decreases immediately. Although the material ruptures, the photograph shown in Figure 4.12 shows that some of the material still bridges across the two skin surfaces due to its flexibility.

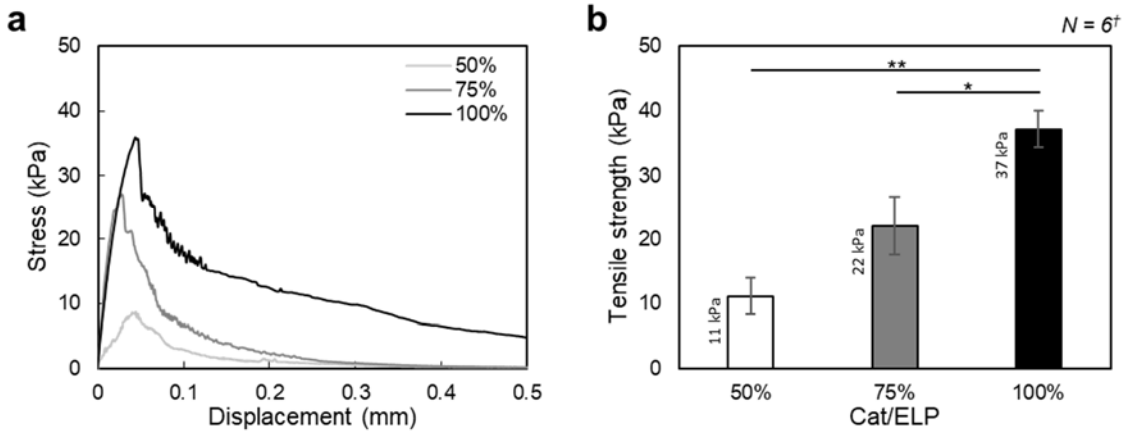

Figure 4.11 Adhesive tensile strength tests. *a) Representative data for each type of ELP/Cat adhesive. b) Average tensile strength for adhesives; 100% modified samples show the highest strength, which correlates with the amount of catechol (N, number of samples; †: N = 5 for 100% ELP/Cat; statistically significant differences noted with '*' for p < 0.05 & '**' for p < 0.01)*

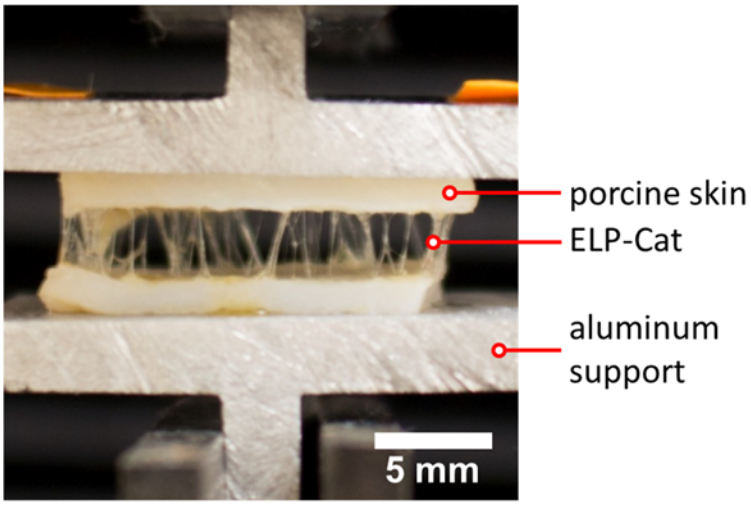

Figure 4.12 Photograph of tensile pull-off test showing 50% ELP/Cat spanning between two pieces of skin

In addition to the tensile tests, we also tested the ELP/Cat adhesives for their shear strength using lap-shear testing. We find similar strengths for the three different sample types with the 100% ELP/Cat samples showing an average of 39 kPa (Figure 4.13). As expected, decreasing the quantity of catechols decreases the shear strength to 20 kPa for 50% ELP/Cat samples. For the lap-shear tests, we use a flat rectangular piece of aluminum as the support for skin. While the parallel plates of aluminum are displaced, the skin and adhesive assembly in the middle are sheared. Figure 4.13a shows a representative test for each sample type. In practical terms, both the tensile and shear tests show that 1.5 cm x 1.5 cm pieces of skin adhered with ELP/Cat can withstand loads as high as 1 kg before rupturing. Considering that the catechol groups make up for a maximum of only 4% of the number of amino acids per chain, our material works quite well. This may be related to the deswelling phenomenon that we observe during rheology. Although we use 12% wt/vol protein content for the adhesives, the final amount increases as the polymer chains transition to a hydrophobic state and expel water.

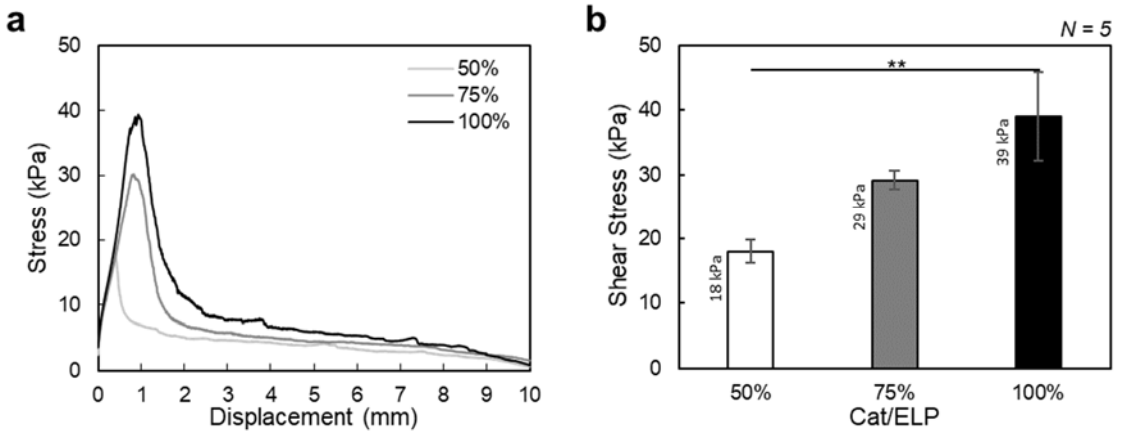

Figure 4.13 Adhesive shear strength tests. *a) Representative data for each type of ELP/Cat adhesive. b) Average shear strength for adhesives; 100% modified samples*

*show the highest strength, which correlates with the amount of catechol (N, number of samples; statistically significant differences noted with '**' for $p < 0.01$)*

4.7 Conclusion

In this work, we designed and synthesized V4E125 that could be chemically functionalized with dopamine. We modified the ELP with dopamine and characterized it using NMR and showed how the loss of negative charge leads to a decrease in the transition temperature of the proteins. Through rheometry, we show that our materials can form stable hydrogel networks and they deswell as the ELP transitions to a hydrophobic state. We also showed that the materials can adhere well to porcine skin. Further work involves testing the materials *in vitro* to investigate their biocompatibility and finally test them *in vivo* in murine models as a surgical adhesive.

In the future, we can create a highly flexible adhesive by combining the ELP/Cat adhesives developed in this chapter with the rubbery hydrogels in chapter 3. This can be done by synthesizing a new set of telechelic ELPs (containing glutamates) with cysteine at both terminals. Hydrogels can be synthesized by crosslinking them with a maleimide functional 4-arm PEG and modifying them with dopamine. ELP/Cat can then be used as a bridging material to bind biological tissues to the elastic hydrogels. Highly extensible adhesives will be advantageous to bond to tissues that undergo repetitive deformations such as skeletal and cardiac muscles as well as blood vessels.

4.8 Method

4.8.1 Functionalizing V4E125 with Dopamine

The modification of V4E125 with dopamine is performed using 2% w/v protein concentration in a 3:1 mixture of DMSO:DMF in the presence of 0.5, 0.75 or 1 equimolar dopamine to carboxylates. The ratio of dopamine:EDC:NHS is kept constant at 1:1.5:1.2. 1 equimolar triethylamine to dopamine is added to the reaction mixture as a catalyst. The reaction mixture is prepared on ice and then moved to 37°C incubator and rotated end-over-end for 6 hours. This is followed by 10x dilution of the mixture with chilled 100 mM acetate buffer at pH 4.0. In addition to hydrolysis of the remaining water sensitive reactants, the low pH prevents oxidation of catechols to quinones. The chilled solutions are then transferred to 10 kDa MWCO dialysis cassettes and dialyzed against dilute HCl solution (3.5 L ultrapure water with 1 mL concentrated HCl) with pH < 3.0 at 4°C. Dilute HCl solution is changed 8 times over 3 days. At the end, the cassettes are dialyzed against ultra-pure water for at least 4 hours. The functionalized protein solutions are then removed from the cassettes and transferred to glass scintillation vials. The vials are frozen at -80°C for 2 hours and lyophilized for 3 days. Once lyophilized, the vials are stored with loosened caps in a vacuum chamber with desiccant until use.

4.8.2 ^{1}H NMR

5.25 mg/mL solution of proteins were made using 50 mM phosphate buffer, pH 5.0. The phosphate buffer contained D_2O as the solvent to prevent signal from water. Samples were tested at the Central California 900 MHz NMR facility.

4.8.3 Adhesive preparation

ELP/Cat adhesives are prepared with the addition to sodium periodate to promote oxidation of catechol. The adhesive solution is prepared to have a final protein concentration of 12% w/v. All buffers and solutions are chilled on ice throughout synthesis. ELP is weighed out and dissolved in phosphate buffered saline at a concentration of 20% w/v. Separately, a stock solution of 30 mg/mL $NaIO_4$ in water is prepared. 0.5 equimolar $NaIO_4$ to dopamine solution is prepared for each protein sample by diluting the stock solution with an appropriate amount of water. Immediately prior to use, the appropriate volume of $NaIO_4$ solution is added to the protein solution. The mixture is stirred using a clean pipette tip and pipetted on the test surface.

4.8.4 Rheology

Adhesive curing and flexibility in shear regime were characterized using rheometry (MCR 302 Modular Compact Rheometer, Anton Paar) with temperature control. 8 mm probe was used for all tests. The rheometer stage is chilled to 4°C. Adhesive was prepared as described and pipetted on the stage. Probe was lowered until the liquid mixture completely filled the gap between probe and stage. During our tests, we realized that as the adhesives cure, they shrink and lose contact with the rheometer probe. In order to maintain contact, we applied 1 N of normal force after allowing the materials to crosslink at 37°C for 10 minutes. The table below describes the details of the rheometer program used for testing. After allowing the hydrogel to cure for 1 hour at 1% strain, 1 Hz frequency, 37°C and 1 N of normal force, a strain sweep was applied to test its flexibility. Strain was ramped linearly from 0.1% to 300%, while other settings were kept constant. Storage modulus and loss modulus were collected for each test. Damping factor was also collected for strain sweep tests.

4.8.5 Skin preparation for adhesion tests

Split thickness porcine skin (I-188) was purchased from Stellen Medical and kept frozen at -20°C. Prior to sectioning the necessary size of testing targets, the skin was moved to -80°C for 30 minutes to ensure that it remains frozen. Dissection pan and a scalpel were chilled in 4°C cold room during this time. After 30 minutes, skin was sectioned in 4°C cold room and immediately transferred to -20°C for storage. The target skin samples were sectioned into 1.5 cm x 1.5 cm for pull-off tests and 1 cm x 2.5 cm for lap-shear tests. Each section of skin was thawed and hydrated by soaking in room temperature PBS for 30 minutes. To attach skin to aluminum supports, the epidermis side was wiped dry using a paper wipe. Cyanoacrylate glue was applied to the prepared aluminum surface and the epidermis side of skin was carefully centered on the support. Skin was gently pressed down for 30 seconds and excess glue was wiped away. Each skin assembly was kept hydrated until test by covering it with a PBS soaked gauze pad.

4.8.6 Tensile pull-off test

For pull-off tests, a 1” x 1” aluminum T-bar was used as support. Each support was roughened using 50 grit sandpaper and cleaned prior to attaching the skin samples. Test samples were prepared by securing a (wet gauze pad covered) skin assembly using a table vise. Gauze pad was removed, and excess water was removed using a damp paper wipe. Adhesive mixture was prepared and immediately spread on the skin surface. Second skin assembly was placed on top and the material was allowed to cure for 5 minutes at room temperature without being disturbed. The test sample was clamped using two clips (OXO Good Grips Magnetic All-Purpose Clips, Cat. 13141700V1), evenly balanced on either side. Test sample assembly was covered with wet gauze pad and moved to a sealed container with water to maintain 100% relative humidity. The container was incubated at 37°C for 12 to 13 hours prior to testing.

Tests were carried out using an Instron 5544 tester. Sample to be tested was taken out of the incubator and the clips were gently removed. Sample was then secured into the lower grips of the Instron, followed by the upper grips. Samples were loaded until failure at an extension rate of 1 mm/minute to a final extension of 5 mm. Each pair of target skin substrates were photographed to measure the cross-sectional area. Smaller area was used in each case to calculate stress from load.

4.8.7 Lap-shear test

For lap-shear tests, a flat 1” x 2” aluminum bar was used as support. Samples were prepared in a nearly identical manner to pull-of test samples. The test sample was finally clamped using a single clip. Similar to pull-off test samples, the sample assembly was incubated at 37°C in a humid environment for 12 to 13 hours prior to testing.

Tests were carried out using an Instron 5544 tester. Sample to be tested was taken out of the incubator and the clip was gently removed. Sample was then secured into the lower grips of the Instron, followed by the upper grips. Samples were loaded until failure at an extension rate of 1 mm/minute to a final extension of 10 mm. Each pair of target skin substrates were photographed to measure the cross-sectional area. Smaller area was used in each case to calculate stress from load.

Chapter 5 Self-healing hydrogels

5.1 Introduction

Functional hydrogels designed to be biocompatible, injectable, stimuli-responsive and self-healing are valuable for many biomedical applications including wound healing,[222,223] tissue engineering,[224,225] as well as carriers for drug or cell delivery.[226,227] In particular, *in situ* forming hydrogels are interesting as they can be applied to a target site without the need for pre-defined shapes.[228] An aqueous precursor mixture of an *in situ* forming hydrogel can be injected into the target site, where it forms a stable structure over-time by itself or in response to stimuli such as light, temperature, and pH.[229,230] *In situ* forming hydrogels have been synthesized with a variety of natural and synthetic polymers with physical and chemical crosslinking[226,228,231] such as Michael addition between thiol-modified hyaluronic acid and poly(ethylene glycol) vinylsulfone,[232] electrostatic interaction between alginate and slow released calcium ions from $CaSO_4$.[233] Although previous strategies have shown control over individual characteristics, they have limited scope of combining desired functionalities such as tunable mechanical properties, biocompatible and stimuli-responsive crosslinking, and direct integration of cell stimulating motifs without labor intensive chemical synthesis.

5.2 Strategy for self-healing

In order to develop functional *in situ* forming hydrogels with self-healing properties, our strategy was to use a customizable and stimulus-responsive polymer, and a crosslinking scheme with dynamic chemical bonds. We focused on recombinant polypeptides as they can be easily customized using standard genetic engineering techniques to mimic natural extracellular matrix.[11,15] Specifically, we chose the mammalian elastin derived elastin-like polypeptides (ELP).[234] ELP have a simple repetitive sequence composed of the pentapeptide 'Val-Pro-Gly-X-Gly', where the guest residue 'X' can be any amino acid other than proline. These polypeptides are highly flexible due to weak hydrophobic interactions and hydrogen bonds that enable the chains to extend and retract like a spring.[98,181,234] ELP can also reversibly phase separate in response to environmental factors such as temperature, pH and ionic strength as well as intrinsic properties such as size of the ELP molecule and the hydrophobicity of the guest residue.[39] These advantageous properties of ELP and its biocompatibility have already motivated its use in developing biomaterials for tissue engineering,[18,103,235-237] biocatalysis,[238] drug delivery,[239] and hydrogel actuators.[99] Although available, current *in situ* forming ELP hydrogels[102-104] use crosslinking molecules that can diffuse out and affect the surrounding tissues. Moreover, while irreversible chemical crosslinks are mechanically stable, the materials cannot heal when damaged. Thus, we chose to use Schiff base chemistry based crosslinking scheme to form reversible imine bonds between aldehyde and primary amines.[225,240] Reactants and products remain at equilibrium in this

scheme with high pH favoring imines (specifically, aldimines) and low pH favoring aldehyde and amines.[241] The dynamic nature of imine bonds[242] can also impart self-healing properties making our materials robust. Furthermore, direct functionalization of ELP with reactive groups through genetic and chemical modifications eliminates the need for extraneous reactive molecules that can leach into surrounding tissues.

Our strategy to form high pH triggered aldimine crosslinks requires a way to increase the pH without using toxic buffer systems. We can realize this using the biocompatible inorganic, bioglass (BG).[243] BG is a well-known bioactive inorganic material that can induce bone mineralization, enhance angiogenesis, promote wound healing and even prevent bacterial growth through the release of ions into its surroundings.[244-248] Based on these appealing properties, BG has been used to develop materials for surface coatings,[249] cell encapsulation,[250] tissue engineering,[247,251,252] and drug delivery.[253] Thus, by combining aldimine forming ELP with BG, we can create a composite material in which the two components work synergistically to form crosslinked hydrogels in a safe and tunable manner. Previously, BG has been incorporated with ELP and collagen,[254] however the role of BG and ELP are unclear as the materials likely solidify primarily through physical crosslinking among collagen. In this work, we first synthesize ELP containing either primary amine or carboxylic acid functional groups using genetic engineering and recombinant expression. We chemically modify carboxylic acids to create ELP with aldehyde functional groups. We then combine the organic and inorganic components to create ELP/BG composite hydrogels and show their tunable gelling characteristics and mechanical properties (Figure 5.1). We also demonstrate the self-healing property of the hydrogels by successfully reattaching severed hydrogels along with the rheological tests. Additionally, we show the strength of genetically engineering to easily customize the ELPs with 'RGD' sequences to promote cell adhesion without the need for serum proteins. In the future, the robust *in situ* forming ELP/BG hydrogels with dynamic crosslinks will be useful for delivering cells and drug molecules to promote soft tissue regeneration.

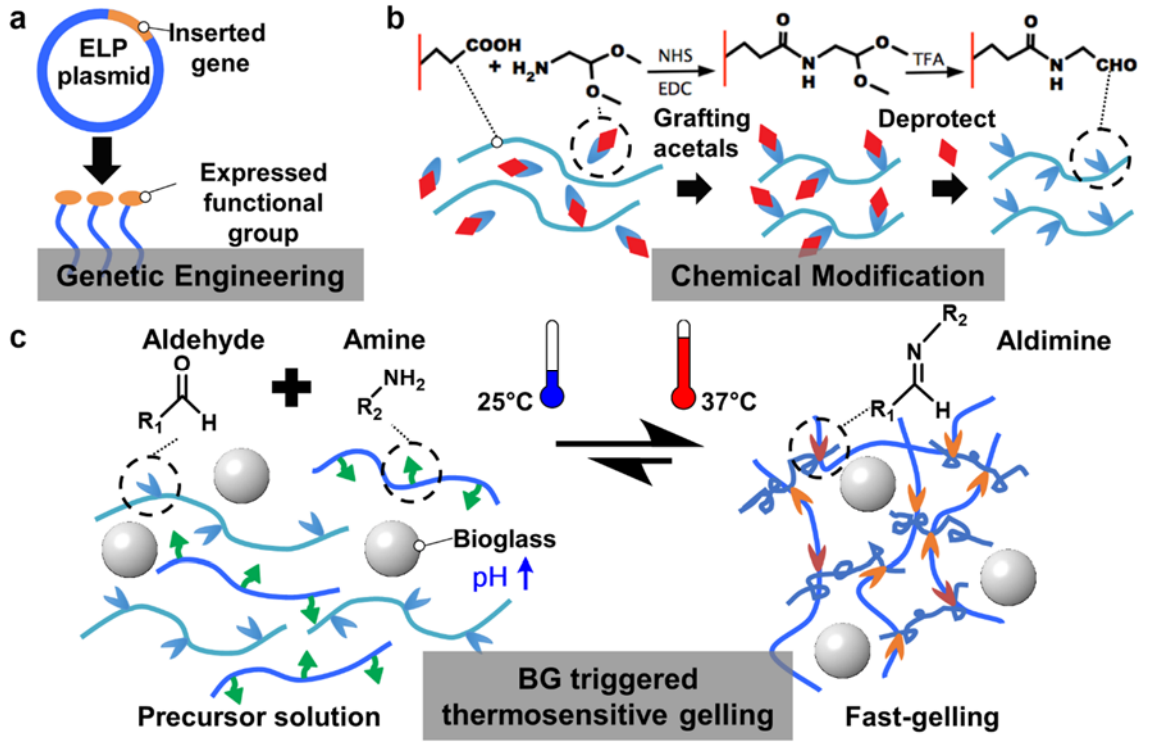

Figure 5.1 ELP can be designed through *a) genetic engineering and b) chemical modification. c) ELP/BG biocomposite undergoes bioglass driven thermosensitive gelling.*

5.3 ELP design and synthesis

We designed the ELPs to create *in situ* forming hydrogel with BG. In order to enable our polymers to cross-link, we employ Schiff base formation between primary amines and aldehydes. The Schiff base formation is favored in a high pH environment, which can be achieved by BG that releases ions and increases the local pH.[255] We used recombinant DNA techniques to design and synthesize two ELP backbone sequences, $[(VPGVG)_2(VPG\mathbf{K}G)(VPGVG)_2]_{25}$ for K125 and $[(VPGVG)_2(VPG\mathbf{E}G)(VPGVG)_2]_{25}$ for E125, where the charged pentapeptides were spaced with hydrophobic "VPGVG" to lower product toxicity to the host *E. coli.*[18,99,256] The K125 backbone was further engineered to add functional motifs (Table 5.1, Figure 5.1a). We functionalized both N-/C-termini of K125 with cell adhesive "RGD" sequence[256] to produce K125-RGD; whereas, only C-terminus of K125 was modified with hydroxyapatite adhesive "EEEEEEEE"[18] to produce K125-E8 used during material characterization (Table 5.1). On the other hand, glutamic acids in E125 were chosen to accomplish a simple modification of the carboxylic acid side chains to display aldehydes (Figure 5.1b). Together, ELP functionalized with primary amines and aldehydes can form aldimine cross-links to achieve gelation (Figure 5.1c).

ELP mass and purity were measured using MALDI-TOF mass spectrometer to confirm that they match the theoretical values. Figure 5.2 shows that all the synthesized

ELP are monodisperse and highly pure. The molecular weights of E125 (52.55 kDa), K125-E8 (53.66 kDa), and K125-RGD (53.50 kDa) closely matched their theoretical mass (52.43 kDa, 53.60 kDa, and 53.67 kDa, respectively).

Table 5.1 ELP nomenclature and sequences

Name	N-terminal	Backbone	C-terminal
E125	SGVG	$[(VPGVG)_2VPGEG(VPGVG)_2]_{25}$	VPG
K125-E8	SGVG	$[(VPGVG)_2VPGKG(VPGVG)_2]_{25}$	VPGSEEEEEEEE
K125-RGD	SGRGDSG	$[(VPGVG)_2VPGKG(VPGVG)_2]_{25}$	VPGSGRGDSGK

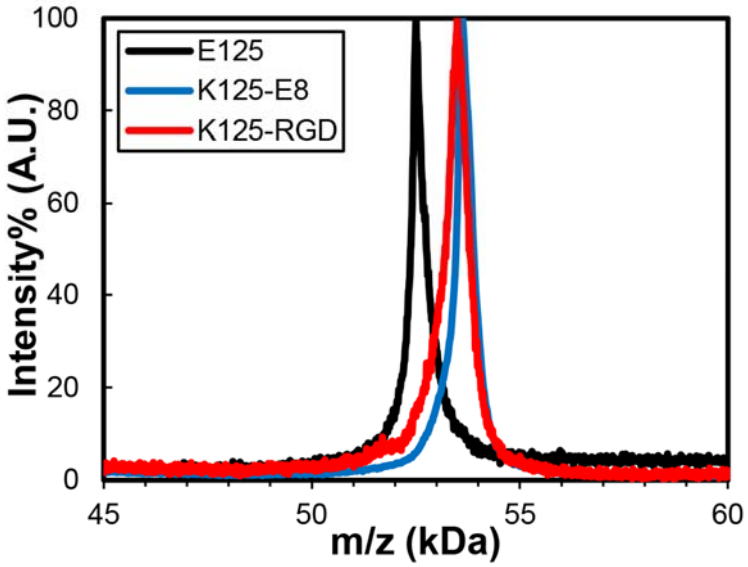

Figure 5.2 MALDI-TOF spectra of E125 (52.55 kDa), K125-E8 (53.66 kDa) and K125-RGD (53.50 kDa).

5.4 Functionalizing ELP with aldehyde

After synthesis of E125, we chemically functionalized the carboxylic acid groups on E125 with aldehydes using NHS/EDC chemistry (Figure 5.1b). We coupled aminoacetaldehyde dimethyl acetal on E125 and converted acetal end groups to aldehyde in the presence of trifluoroacetic acid (Figure 5.1b) to produce the modified E125 (M-E125). We verified the ELP modification and acetal deprotection by NMR (Figure 5.3). The ^{1}H NMR spectrum of M-E125 shows a peak at 9.42 ppm (blue line) from the aldehyde proton while E125 and midproducts (before deprotection) show no signal in the same range (purple and red lines, respectively). The midproducts show a peak at 3.13 ppm (red line), which confirmed the presence of dimethylacetal groups.[117] Furthermore, we quantify the amount of the aldehyde groups in M-E125 by titrating it with hydroxylamine hydrochloride. The reaction between aldehyde and hydroxylamine hydrochloride results in HCl generation that lowers the pH of the M-E125 solution (Figure 5.4).[257] Consequently, E125 solution does not exhibit any pH change. Based on the amount of the titrant that induced pH changes,[257] we estimated that 40–45% of the

glutamates were modified with aldehydes in M-E125. Molecular weight of M-E125 was not measured due to dispersity following chemical modification.

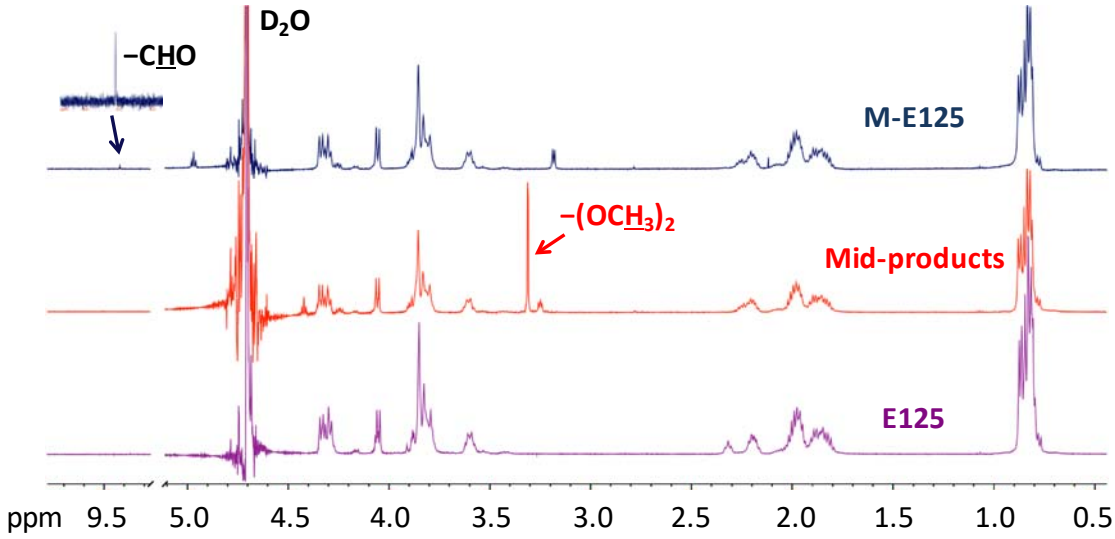

Figure 5.3 ^{1}H NMR spectra (500 MHz) of E125, the mid-products during modification and modified M-E125. Peaks for aldehyde [-CHO, 9.42 ppm] and acetal [-(OCH$_3$)$_2$, 3.13 ppm] are labeled on the spectra for M-E125 and Mid-products, respectively.

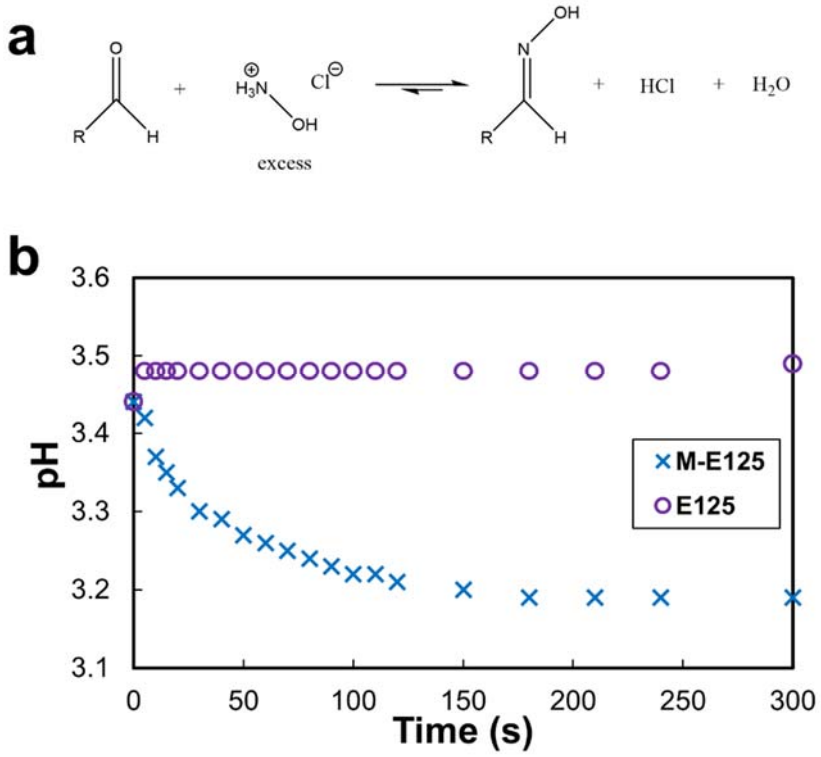

Figure 5.4 Hydroxylamine hydrochloride assay. *a) Aldehydes react with hydroxylamine to produce oxime and release hydrochloric acid. b) In the presence of M-E125 (blue crosses), the pH decreases due to release of hydrochloric acid, however there is no*

change for unmodified E125 (purple circles). Change in pH was used to calculate the quantity of aldehyde on modified ELP.

5.5 Transition temperature of ELPs

ELP transition properties were characterized by measuring solution turbidity with a rise in temperature. ELP remain hydrated and soluble at low temperature; however, the chains collapse and phase separate when the temperature goes above their transition temperature (T_t).[40] As described by Urry et al., T_t depends on many factors including the hydrophobicity of the guest residue.[40] In the case of K125 and E125, the highly charged guest residues "Lys" and "Glu" drastically increase the T_t due to charge–charge repulsion. K125-E8 and K125-RGD possess similar T_t of 57 °C as they share the same positively charged backbone sequences (Figure 5.5). On the other hand, E125 did not exhibit T_t in PBS even up to 60 °C likely from the strong repulsion from the glutamate residues (Figure 5.6, blue line). Interestingly, after aldehyde modification of E125 to M-E125, we see a dramatic decrease in T_t to 36 °C (Figure 5.6, orange line). We hypothesized that the near physiological T_t of M-E125 could make it easier to initiate polypeptide aggregation and cross-linking during hydrogel synthesis.

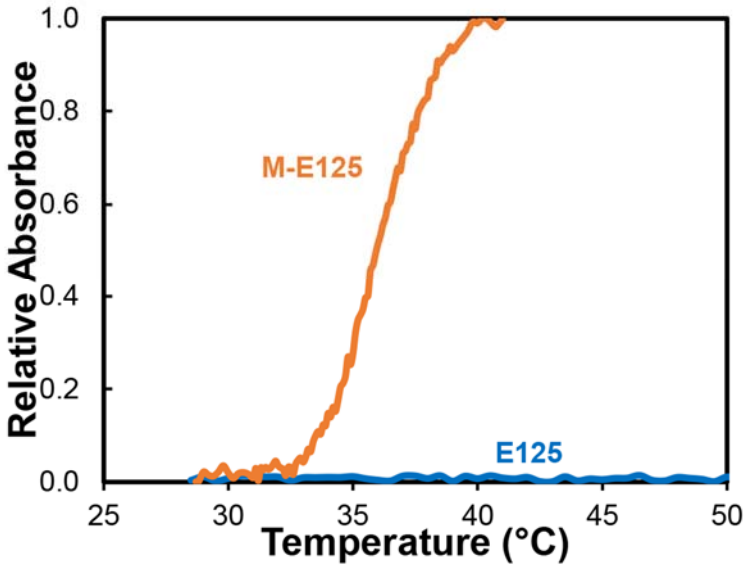

Figure 5.5 Inverse transition patterns of E125 (blue) and chemical modified M-E125 (orange).

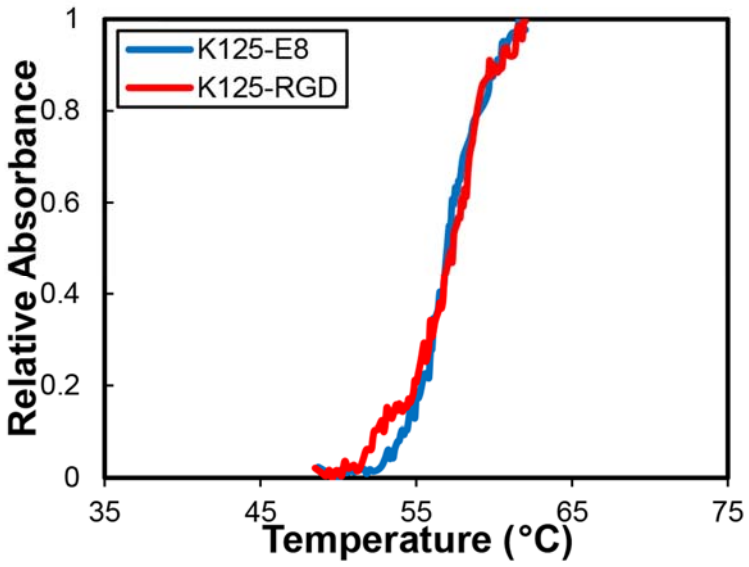

Figure 5.6 ITT measurement for K125-E8 and K125-RGD. *Positively charged backbone results in a high transition temperature of 57 °C for both proteins.*

5.6 Hydrogel Synthesis

We synthesized the *in situ* forming composite hydrogels using ELP and BG. Considering that K125-E8 contains 25 primary amine containing lysines (Table 5.1), while nearly half of the amino acids in M-E125 have aldehyde groups, we mixed the two components at a ratio of 1:2 to have similar amounts of amine and aldehyde. Cross-linking between K125-E8 and M-E125 occurs as soon as the solution pH increases with the addition of BG powders to the mixture. In order to determine the influence of BG on the gelation kinetics, we first characterized solution pH changes with increasing concentration of BG. We observed that the solution pH changes more rapidly and equilibrates at a higher level with greater BG concentration (Figure 5.7a). As aldimine formation is favored at high pH, an increase in the amount of BG concentration should allow for faster gelation. Using rheology tests, we were able to observe rapid gelation within 100s with 1% w/v BG (Figure 5.7b). In addition, higher amounts of BG results in statistically significant increases in the storage modulus of the hydrogels (Figure 5.7c). Since the solution pH increases with more BG, we hypothesize that the reaction between amines and aldehydes proceeds closer to completion and raises the storage modulus. This imparts tunability to our hydrogel gelling time and elastic properties with a simple change in BG concentration.

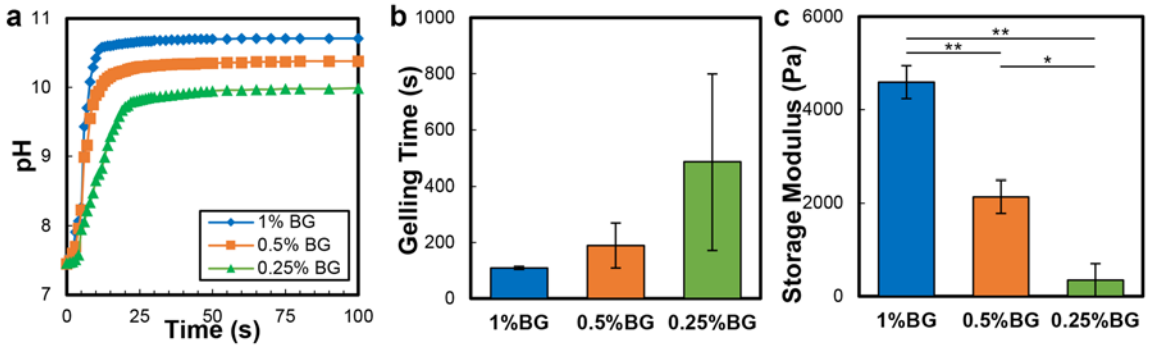

Figure 5.7 Rheometry *a) BG increased the pH of PBS solution. b) Gelling time of the ELP/BG hydrogels with different BG content. c) Storage moduli of hydrogels after one hour gelling with different BG content. (n = 3; statistically significant differences denoted by '*' for p < 0.05; '**' for p < 0.01)*

5.7 Thermosensitive gelling

We further study the cross-linking in our ELP/BG composite system by characterizing their gelation kinetics in response to temperature. We observed that the ELP/BG solutions remain fluid at 25 °C, but quickly set at the physiological temperature of 37 °C and turn more turbid (Figure 5.8a). In order to show this more clearly, we conducted rheology tests by first maintaining 25 °C and then quickly raising the temperature to 37 °C. The plot in Figure 5.8b shows how the storage modulus remains unchanged at low temperature and quickly increases once the temperature is increased to 37 °C. This test also mimics the temperature change that would occur if the liquid precursor is injected into an *in vivo* target site where the high temperature will cause it to solidify rapidly. Based on our observations, we hypothesize that the cross-linking of ELP/BG hydrogels at 37 °C is partly because of ELP thermoresponsiveness. The reversible transition properties of ELP play a critical role in the thermosensitive cross-linking. We showed that unlike highly charged E125, M-E125 have a T_t of 36 °C that will cause them to aggregate at physiological temperature. Similarly, although K125 containing ELPs have a T_t of 57 °C, the high pH environment around BG will result in a neutralization of positive charge and a drastic decrease in T_t from 57 °C to lower than 37 °C for the large ELP.[39,181] At the physiological temperature, both proteins will aggregate, bringing their reactive groups closer together and promoting faster cross-linking of the hydrogels (Figure 5.1c). Therefore, in addition to the typical temperature and pH driven increase in reaction rates, the thermosensitive aggregation of ELP also enables our ELP/BG hydrogels to solidify quickly, a useful feature for an *in situ* forming material. Moreover, as observed with other ELP hydrogels,[98,181] the ELP/BG hydrogels also have temperature dependent swelling (Figure 5.9). The water content of hydrogels at 25 °C is significantly higher than at 37 °C, which was caused by the deswelling of the ELP networks. Unlike typical hydrogels that swell in physiological conditions, the ELP/BG hydrogels will maintain their robust mechanical stability.

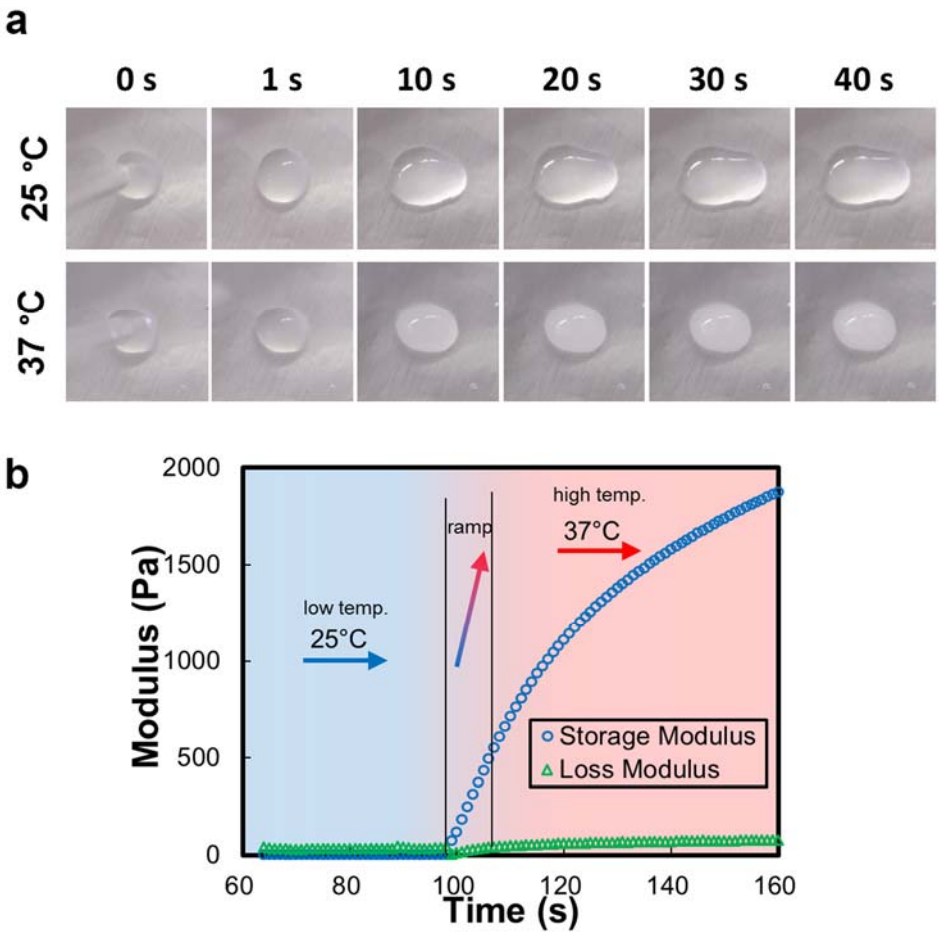

Figure 5.8 The thermosensitive gelling process of ELP/BG hydrogels. *a) Gelling process at 25°C compared to 37°C. At low temperature, the reaction mixture remains in the form of a clear liquid, while at physiological temperature, it turns opaque as it solidifies; b) Rheology test shows a rapid increase in storage modulus once the temperature is increased.*

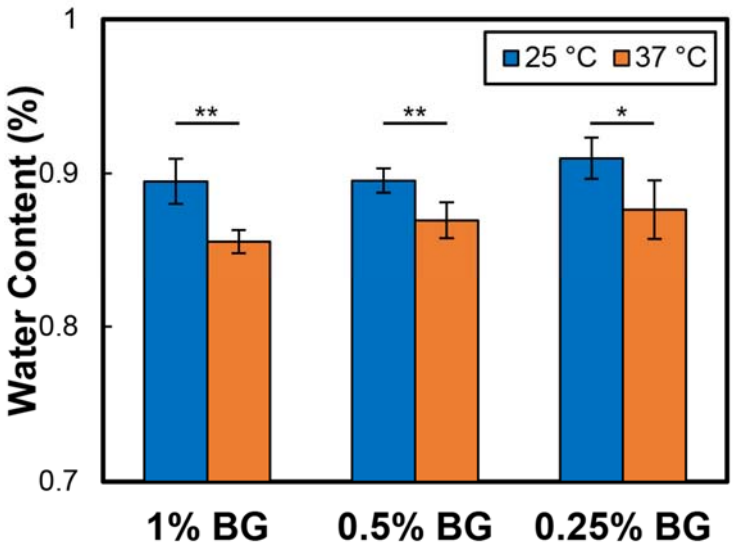

Figure 5.9 Water content of different ELP/BG hydrogels at 25 °C and 37 °C. (n = 4; statistically significant differences denoted by '*' for p < 0.05; '**' for p < 0.01)

5.8 Self-healing

We exploited the dynamic nature of Schiff base reaction to realize the self-healing properties of our ELP/BG hydrogels. Imine bonds, or more specifically, aldimine bond are reversible chemical bonds and this property makes them useful to design self-healing hydrogel system due to constant bond association and dissociation.[258-260] We tested self-healing properties of our materials by first preparing rectangular hydrogels (width = 2 mm, height = 1 mm, and length = 4 mm) and cutting them using a blade (Figure 5.10a). We attached the severed pieces together and after a 24 h incubation period at room temperature, the hydrogels showed uniform appearance and remained intact when stretched (Figure 5.10b). The self-healing property of the hydrogel was also confirmed using cyclic strain sweep rheological tests. At low strain (γ = 1%) that is below the deformation limit, the storage modulus of the ELP/BG is higher than its loss modulus (Figure 5.10c). At higher strain (γ = 100%), the storage modulus decreases below the loss modulus, which indicates hydrogel rupture and loss of mechanical integrity.[258] The rheology results showed that the storage modulus of the gel quickly recovers when the high strain is removed. This suggests that the resulting ELP/BG hydrogels can quickly recover from network collapse by rapid formation of aldimine bonds. The self-healing properties of this system need to be tested *in vivo* in the future, and we can improve the self-healing capability of our system by employing additional dynamic bonds (such as Diels–Alder reaction,[261] acylhydrazone bonds[262] and disulfide bonds[263]) and other self-healing strategies, such as release of healing agents and miscellaneous technologies.[264]

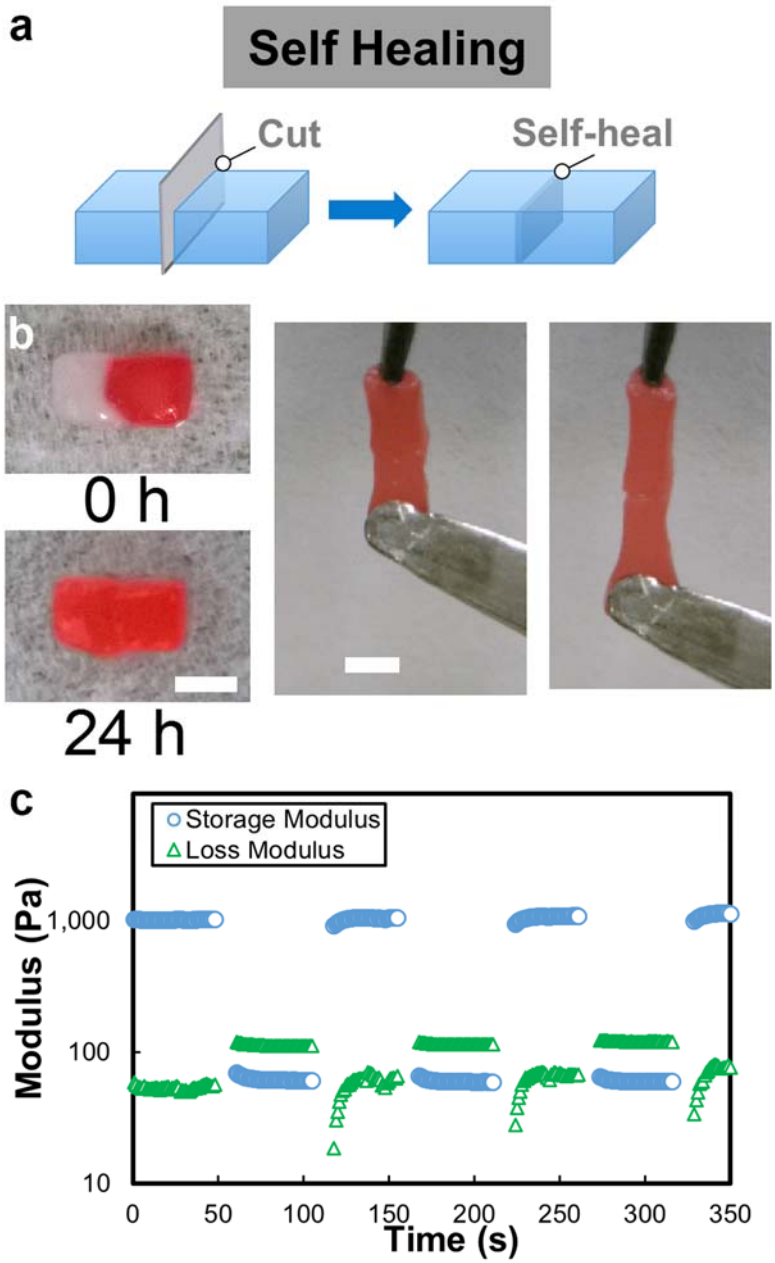

Figure 5.10 Self-healing of ELP/BG hydrogel. *a) Schematic diagram showing demonstration. b) Separated hydrogel pieces healed into one after 24 hours, bar = 2mm. c) The cyclic strain sweep of hydrogel in the rheological test. (During 0~50s, 100~150s, 200~250s, and 300~350s, γ = 1%; During50~100s, 150~200s, and 250~300s, γ = 100%).*

5.9 Cytocompatibility and cell adhesion

The ELP/BG biocomposite hydrogels exhibit good cytocompatibility. We characterized the cytocompatibility of ELP/BG composites using MC3T3-E1 cells. We performed WST-1 proliferation assay to determine the relative cell number during the

course of 7 days in the presence of ELP/BG hydrogels, while cells cultured without the hydrogels were used as control. Using the WST-1 assay, cell growth ratio was calculated as C_t/C_0 (Figure 5.11a) and it showed similar growth curves between experimental and control groups. The results demonstrate that the ELP/BG composites have good cytocompatibility. In addition to the simple cytocompatibility tests, we also demonstrated the strength of genetic engineering to functionalize ELP and enhance its ability to stimulate cells. We used RGD fused K125 backbone (K125-RGD) to synthesize cell adhesive hydrogels and characterized how well the cells bind to RGD containing hydrogels compared to those composed of K125-E8. We observed significantly greater cell spreading area and higher density of attached cells on hydrogels with RGD compared to hydrogels without RGD (Figure 5.11b). The binding assay showed that the introduction of RGD peptide in the ELP/BG hydrogels enhances cell adhesion and spreading without the need for serum proteins (Figure 5.11c). The same strategy can be used to further customize the hydrogels by directly fusing functionalities such as wound healing stimulating peptide (PHSRN)[265,266] and additional cell stimulating peptides (REDV, IKVAV, and YIGSR)[267] to the engineered ELP. Furthermore, directed evolution technologies can also be used to discover and optimize previously unknown peptide motifs.[268]

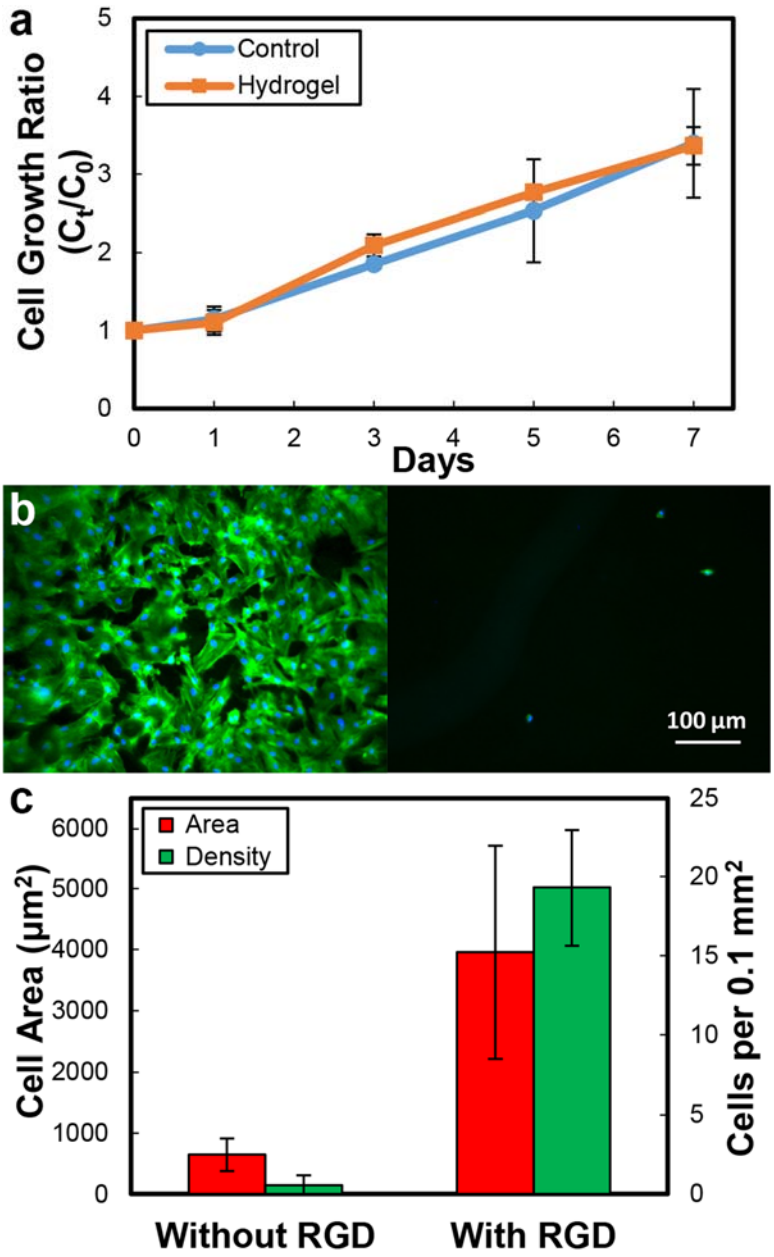

Figure 5.11 Cytocompatibility and cell binding characterization. *a) Growth ratio of MC3T3-E1 cells cultured with ELP/BG hydrogel or without hydrogel (control). b) The fluorescence images of MC3T3-E1 cells on different hydrogel that contain K125-RGD (RGD) or K125-E8 (E8), actin filaments (green) and nuclei (blue) are labeled. c) Average cells area and cells density on the surface of different hydrogels after 6 hours binding test.*

5.10 Conclusion

In summary, we designed novel *in situ* forming biocomposite hydrogels using ELP and BG. We synthesized sequence specific ELP with functional motifs and

chemically modified them. The hydrogels form through dynamic aldimine cross-links favored at a high local pH achieved through BG. The resulting ELP/BG biocomposite showed thermosensitive gelling and mechanical properties that can be easily tuned by changing BG content. We also demonstrated self-healing by successfully reattaching severed hydrogels as well as through rheology. Moreover, we showed the effectiveness of fusing ELP with RGD peptide to enhance cell spreading and binding. Our novel self-healable biocomposite materials can be easily customized using genetic engineering and their rapid and dynamic cross-links makes them useful as injectable biomedical materials. In future designs, we can further develop the *in situ* forming ELP/BG hydrogels as injectable scaffolds to deliver cells to target sites *in vivo* in a minimally invasive manner. Additionally, BG can also be doped with trace elements to achieve therapeutic functions[269,270] and be modulated into mesoporous structures to allow for controlled release of loaded molecules.[271,272]

5.11 Methods

5.11.1 pH measurement of BG solution

PBS (pH = 7.4) with continuous stirring was monitored using a pH meter. BG (diameter =10 μm) was added to PBS to reach 1.0%, 0.5% or 0.25% w/v concentration. pH changes with time were recorded for each group.

5.11.2 Hydrogel Synthesis

K125-E8 or K125-RGD was first dissolved in PBS and then thoroughly mixed with BG. In the meantime, M-E125 was also dissolved in PBS. The two solutions were mixed to achieve ELP/BG solution and injected into a PDMS mold to form ELP/BG hydrogels with desired shapes and sizes. The M-E125 concentration was 5% w/v. K125-E8 or K125-RGD concentration was 2.5% w/v, and BG concentrations were 1.0%, 0.5% or 0.25% w/v. ELP/BG hydrogels with K125-RGD were only used in cell binding experiment.

5.11.3 Rheology – Gelling point

Rheometer (MCR 302 Modular Compact Rheometer, Anton Paar) with an 8 mm diameter plate and a 0.2 mm gap was used for all rheology studies. All hydrogel components were mixed, and 35 μL of the ELP/BG solution was transferred onto the rheometer. In order to mimic in vivo environment, the test temperature was kept at 25 °C for 90 s followed by a ramp to 37 °C. Measurements were performed at a frequency of 1 Hz and strain of 1%. Storage moduli (G′) and loss moduli (G″) were collected, and the gelling point was determined at the time point when G′ and G″ were equal. After measuring the gelling point, the storage moduli of samples were also collected after incubating them for 1 h at 37 °C.

5.11.4 Rheology - Step Strain Sweep

ELP/BG hydrogels were loaded into the rheometer at a fixed plate gap (0.2 mm) and frequency (1 Hz). Strains were switched from small strain (γ = 1%) to large strain (γ = 100%), and each strain interval spanned for 50 s. G′ and G″ were collected.

5.11.5 Water Content

ELP/BG solution (20 μL) was injected into PDMS molds (width = 2 mm, height = 1 mm) and allowed to gel for 4 h after which it was transferred to PBS and kept at 25 °C for 24 h. After removing the residual water on the gel surface, the hydrogels were weighed at 25 °C (W25C). Then, the hydrogels were transferred to PBS and kept at 37 °C for 24 h. They were similarly weighed at 37 °C (W37C). Dry weight (Wdry) of each hydrogel was measured after freeze-drying. Water content of hydrogels at 25 and 37 °C was calculated as (W25C – Wdry)/W25C × 100% and (W37C – Wdry)/W37C × 100%.

5.11.6 Self-Healing

Bar-shaped ELP/BG hydrogels (width = 2 mm, height = 1 mm, and length = 4 mm) were prepared and gelled for 4 h, and then they were cut in the middle. After cutting, we dyed one severed piece with Allura Red AC (McCormick & Company Inc., Sparks, MD) while keeping the other half unchanged and reconnected the pieces. After allowing them to heal for 24 h, the gel integrity was determined by stretching and documenting with photographs.

5.11.7 Cytocompatibility and Cell Binding Assays

In order to test for cytocompatibility, mouse preosteoblastic cells (MC3T3-E1, subclone = 4–7) were obtained from ATCC and cultured in α-MEM supplemented with 10% (v/v) FBS and 1% (v/v) P/S at 37 °C with 5% CO2 and >90% relative humidity. Cells were seeded into 96-well plates (4000 cells/well) and 10 μL ELP/BG solution (1% w/v BG) was added into each well to form hydrogel on top of the cells after cells adhered to the well bottom. Cells cultured without any hydrogel were used as the control group. WST-1 cell proliferation assay was used to determine the relative cell number Ct at day t (t = 0, 1, 3, 5, 7) according to the manufacturer's instructions. Cell growth ratio was calculated as Ct/C0. Cell binding assays were conducted using K125-RGD that contains the cell binding motif Arg-Gly-Asp (RGD) at the C-terminal. ELP/BG hydrogels (BG = 1% w/v) were prepared on the cover glass in 6-well plates. MC3T3-E1 cells were seeded into each well (5 × 105 cells/well) with only α-MEM media. FBS was excluded in order to avoid nonspecific cell adhesion, and P/S was not necessary due to the short duration of the experiment. After incubating the cells at 37 °C for 6 h, cover glasses with hydrogel were taken out and washed three times with PBS. Then, they were fixed with 4% formaldehyde in PBS for 10 min at room temperature. The samples were washed three times with PBS again before permeabilization with 0.1% Triton X-100 for 3 min, followed by three more washes with PBS. The fixed cells were then incubated in 100 nM rhodamine phalloidin for 30 min, and the samples were washed three times with PBS and incubated in 300 nM 4′,6-diamidino-2-phenylindole (DAPI) for 5 min. The samples were washed three final times with deionized H2O before imaging to reduce background fluorescence. Four samples of each group were imaged at a minimum of four random nonoverlapping fields at 100× magnification. The cell density (cells per 0.1 mm2) and cell area (μm2) of the attached cells on each sample were analyzed by ImageJ (NIH).

5.11.8 Statistical Analysis

One-way analysis of variance was used to determine differences between groups of three hydrogel types, specifically, to compare storage modulus and gelling time for hydrogel with different bioglass contents. Differences were further analyzed by posthoc Tukey HSD test. Student's t-test was used to compare two sample types, specifically to compare water content at two different temperatures for each hydrogel composition.

Chapter 6 Hydrogel beads for bio-lasing

6.1 Introduction

Fluorescent dyes and proteins are used heavily in biological sciences.[273-276] Fluorophores can be used to study biological phenomena by tagging biomolecules, and detecting their presence, localization and interactions.[273,274] However, the relatively low output signal of fluorescent systems limits their ability to detect rare incidents.[188] This can be addressed by creating a device that amplifies light through lasing. Traditionally, lasers are semiconductor devices that are used as sources of coherent light in devices ranging from CD readers/writers to cutting-edge quantum computers. The concept of lasing has also been used to develop bio-lasers that integrate biological components for light amplification.[188] Instead of thinking about them as sources of coherent light, biolasers should be thought of as sensors; since biolasers amplify light signals, any small change in their characteristics is also amplified and can be observed in their output spectra.[188]

The acronym, LASER, is derived from the phenomenon of light amplification by stimulated emission of radiation. Just like a semiconductor-based laser, a biolaser requires several key components to function: gain medium, pumping source, and optical resonance.[188,189] The gain medium consists of sources of spontaneous and stimulated emission. As their names suggest, spontaneous emission sources release photons spontaneously after being excited, while their counterparts release photons upon being stimulated with another photon.[189] In order for a gain medium to be effective, more than 50% of its population (stimulated emission sources) must be in the exited state in a phenomenon known as population inversion.[189] Simulated emission and population inversion is possible in chemical fluorophores and fluorescent proteins due to their fluorescence lifetimes in the range of nanoseconds. An optical pumping source such as a pulsed laser can be used to excite the gain medium. In addition to pumping, amplification of coherent light requires stimulating the excited fluorophores that can be achieved by confined light through repeated reflection.[188,189] Typically, mirrors are used to create an optical cavity for such applications, however an optical cavity can be integrated into a self-contained micro-scale system through total internal reflection (TIR) and whispering gallery mode (WGM) generation, both of which will be described in section 6.2.[190,277]

Development of biolasers for biomolecule sensing has shown promising results with many examples of fluidic gain media containing optofluidic biolasers.[188,278,279] Biolasing has also been shown in live cells and tissues using fluorescent proteins and dyes.[280-282] Though the developed systems have potential, optofluidic devices can only be used in confined environments, while live-cell biolasers can only be used in cells that are spherical, which is rare if not absent in biological tissues.[280,281] In order to create a more broadly applicable device, our goal is to develop a fully protein-based biolaser[283] that has the characteristics of a gain material and an optical resonator. Specifically, we will use stimuli-responsive elastin-like polypeptides (ELPs) as our core material. Advantages of

such a system include stimuli-responsive changes of material density that will be reflected in its signal, in addition to the capabilities of genetic engineering and the full range of available cell and biomolecule interacting peptide motifs.[11] Additionally, the flexibility of ELP-based materials will ensure that our devices are mechanically durable and can also be used to study biomechanics of cell interactions with their environments.[181]

6.2 Strategy for fluorescent hydrogel bead synthesis

Our goal in this project is to create a stimuli-responsive hydrogel bead capable of lasing. (Figure 6.1) In order to create it, our device needs to have the dual properties of a gain medium and an optical resonator. We chose ELP as our core polymer since we have already proven our ability to synthesize optically clear hydrogels with stimuli-responsive size and protein density.

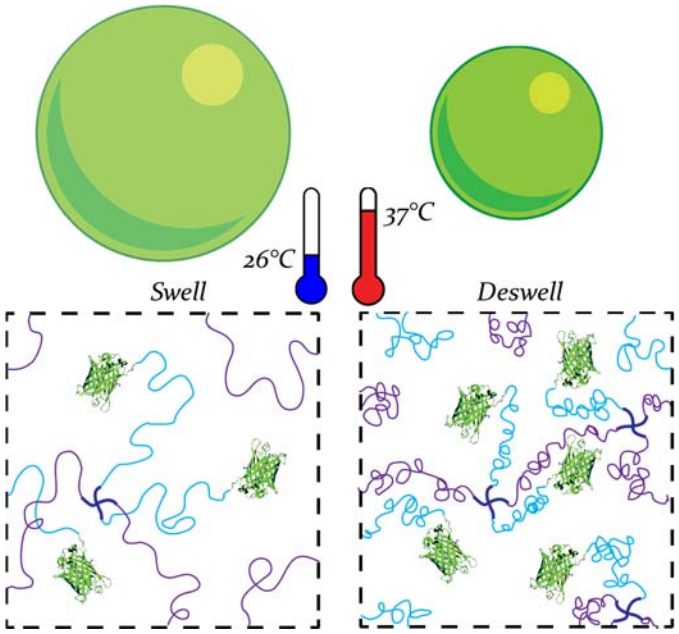

Figure 6.1 Schematic of stimuli-responsive beads and protein density changes

To accomplish our first task of creating a gain medium, we can incorporate fluorophores on the proteins using two distinct pathways. For our first path, we will chemically modify ELP ('V4K125' with lysine) with a commercially available fluorescent dye, such as Alexa Fluor 488, with an amine reactive N-hydroxysuccinimidyl ester functionality. The fluorescent ELP can then be mixed with unmodified ELP to create hydrogels with a tunable ratio of fluorophores. V4K125 can be also be crosslinked into a hydrogel using disuccinimidyl suberate. We can yield an optically clear hydrogel by crosslinking the hydrogel in organic solvents to avoid unwanted ELP transition that can lead to uneven crosslinking.[98] An advantage of this strategy is our ability to easily functionalize ELP with other dyes and fluorophores such as quantum dots.[284] However, a

potential drawback is the likely limited range of swelling/deswelling that can be realized due to a high degree of crosslinking. This property is critical as it dictates the range of protein densities, and therefore the range of refractive indices, that the hydrogels can achieve.[190]

We will simultaneously explore an alternate strategy to create the gain medium by genetically incorporating fluorescent proteins with ELP. Through this pathway, we also exploit the unique advantage of recombinant protein engineering that allows us to fuse ELPs with other proteins. We will use the telechelic V50 ELP similar to those used to create elastomeric hydrogels in chapter 3. However, to avoid side-reactions with the fluorescent protein functional groups, we must employ thiol/maleimide crosslinking scheme rather than amine/NHS ester. Compared to the chemical pathway, these hydrogels may be able to undergo larger overall volume changes, which will be advantageous. However, due to their low crosslink density, the hydrogels will need time to equilibrate upon deswelling before they regain their optical clarity. In addition, potential complications with fluorescent protein folding and side-reactions during crosslinking may cause problems during hydrogel synthesis.

Finally, we need to fabricate optical resonators that can trap light in order to amplify coherent light and induce lasing.[189] To trap light, we have to use the phenomena of total internal reflection (TIR) and whispering gallery mode (WGM).[189,190] TIR can occur when light passes from a medium with high refractive index to low. The phenomenon can be understood using Snell's law, which describes refraction by relating the refractive indices of materials to the incident (θ_1) and refraction angles (θ_2) of light. (Equation 1 & Figure 6.2)

Equation 1 Snell's law

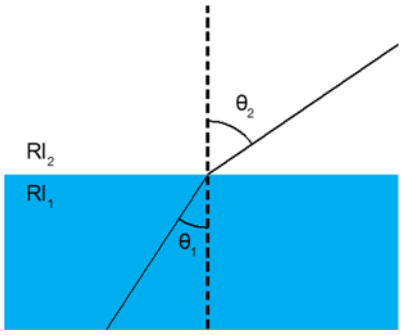

Figure 6.2 Schematic of light refraction

When refractive index of the first medium is larger than the second medium, we can find θ_1 (called critical angle, θ_c) at which $\theta_2 = 90°$. When $\theta_1 \geq \theta_c$, the incident light will undergo TIR. In order to trap light through TIR, we need a geometry that can sustain WGM. WGM arises from the acoustic phenomenon discovered at the whispering gallery of St. Paul's Cathedral.[190] The sound waves at specific resonance frequencies create

corresponding oscillatory patterns or modes, termed WGM. WGM can also be produced in optical systems in the shape of cylinders and spheres.[188,190,277,279,281] Incident light that is internally reflected can remain trapped in a defect-free spherical object (Figure 6.3) and create WGM that can be measured spectroscopically. Furthermore, the larger the contrast between refractive indices of the object and its environment, the more light can be trapped and the better the response.

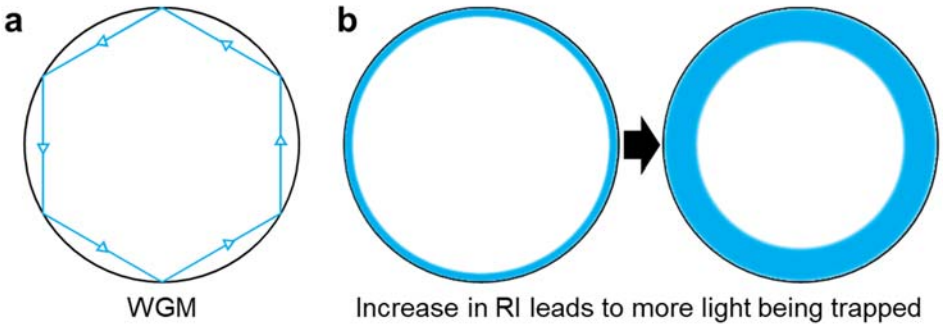

Figure 6.3 Total internal reflection and whispering gallery modes. *a) Spherical beads can achieve optical WGM by trapping light. b) Amount of light that can be trapped in a system depends on the contrast between refractive index of the device and its environment*

Using this concept, we can fabricate our optical resonators by molding the ELP hydrogels into spheres. We can create spherical hydrogels by creating an emulsion of the crosslinking mixture in an immiscible medium.[285] Unlike standard emulsions, the end result of our synthesis is solid hydrogel beads, which also eliminates the need for a surfactant and simplifies the synthesis process.[285] Due to the stimuli-responsiveness of ELPs, the hydrogel spheres or beads will be able to reversibly deswell and create a condition that will be ideal for lasing. In the rest of this chapter, I will describe the synthesis, modification and characterization of our ELPs and hydrogel beads. I will conclude the chapter with the critical experiments and material characteristics required for the future success of this project.

6.3 Fluorescent ELP synthesis

We develop fluorescent ELPs using two pathways – chemical modification of V4K125 with Alexa Fluor 488 and genetic modification of V50.

6.3.1 V4K125 modification with Alexa Fluor 488 (V4K125/Alexa488)

V4K125 was synthesized previously using methods described in chapter 2. With the peptide sequence of "SGVG($[VPGVG]_2$VPGKG$[VPGVG]_2)_{25}$VPG," V4K125 contains 25 lysine residues and an amine at the N-terminal.[18,185] Fluorescent V4K125 were produced by functionalizing the amine groups with NHS-ester terminated Alexa Fluor 488. (Figure 6.4) We intended to modify 25% of amines with the dye molecules.

Figure 6.5 shows photographs of protein solutions and the excitation/emission spectra of the proteins.

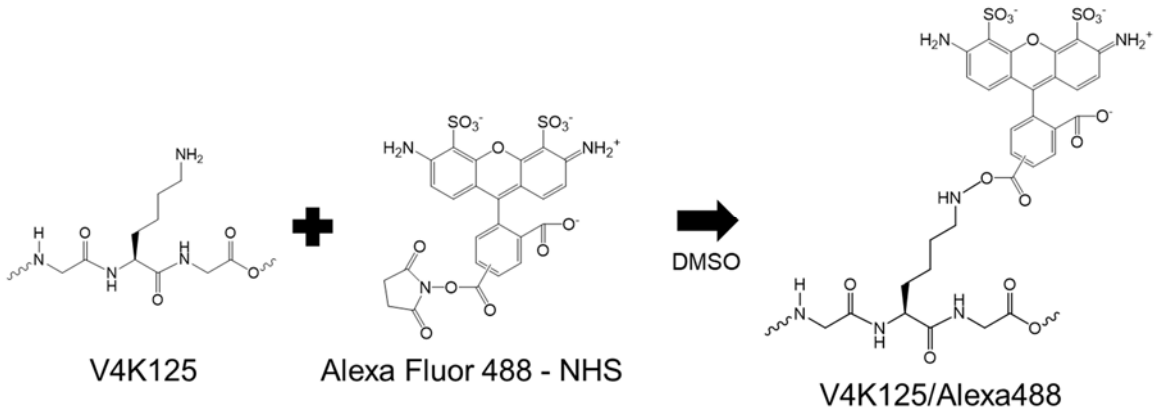

Figure 6.4 V4K125 functionalization scheme

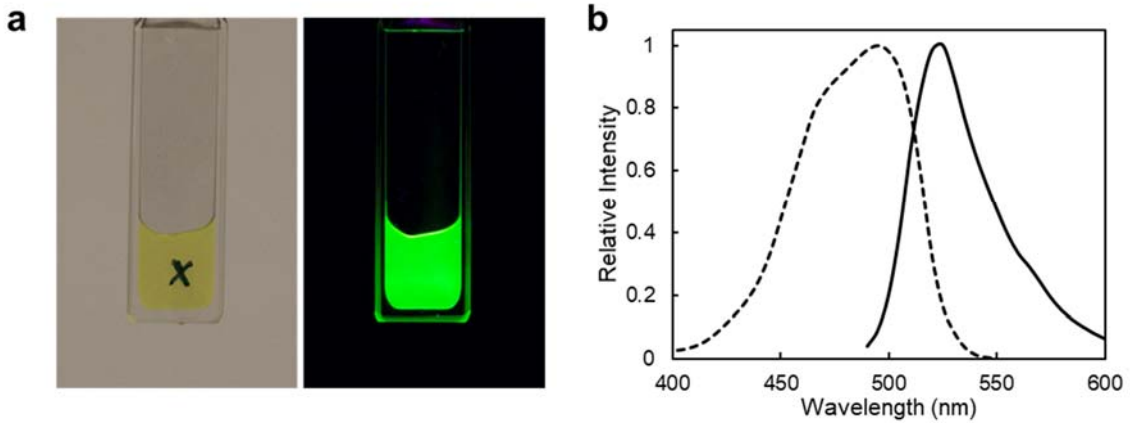

Figure 6.5 V4K125/Alexa488 protein fluorescence. *a) Photograph of 1 mg/mL solution of protein in visible light (left) and long-wave UV light (right); b) Fluorescence spectra showing ex/em peaks at 495nm/525nm, respectively.*

6.3.2 Genetic engineering of V50/fluorescent protein (V50/FP) fusions

V50 ELP gene was synthesized previously with the core sequence of $[VPGVG]_{50}$.[99,181,256] For this project, we first modify the expression vector pet28b by inserting the fluorescent protein genes on the C-terminal side, followed by the ELP gene at the N-terminal. The N-terminal of the fusion protein contains a cysteine for crosslinking. The proteins have the general sequence – $[SGCG(VPGVG)_{50}VPGGG$-FluorProtein]. Detailed procedures for gene synthesis are described in section 6.8.1. Standard procedures were used to express. Since the fusion proteins include ELP, which acts as a thermal tag, the proteins can be purified using Inverse Temperature Cycling process as usual. (Figure 6.6) Together, we synthesized four different fusion proteins with ELP, and turquoise, green, yellow and red fluorescent proteins. (Figure 6.7 & Figure 6.8)

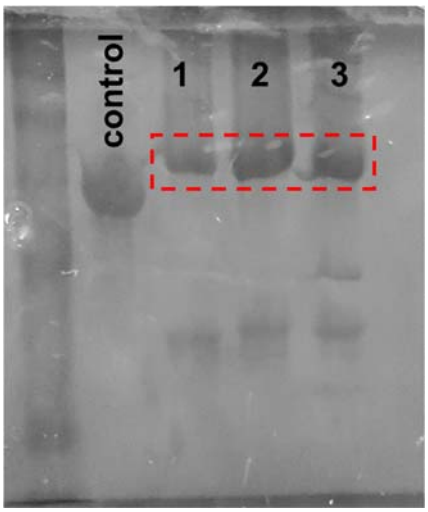

Figure 6.6 SDS page gel. *Control sample is V100CK1, 42 kDa compared to 48 kDa fusion proteins [1] V50/mTurquoise2, [2] V50/sfGFP and [3] V50/mRFP. Faint bands seen on at the bottom half of the gel are likely from cleaved V50 segments.*

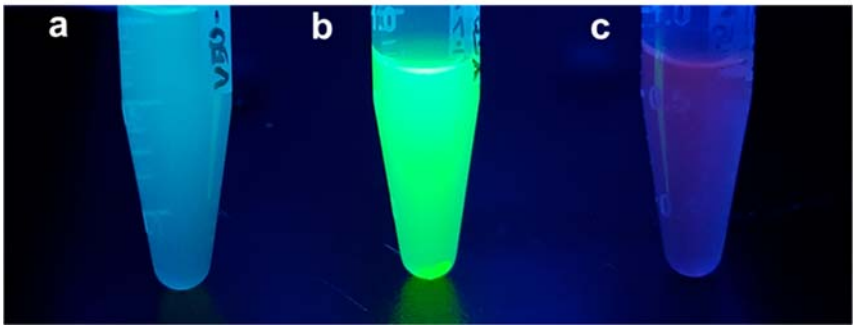

Figure 6.7 Photograph of ELP/FP fusion proteins. *a) V50/mTurquoise2; b) V50/sfGFP; c) V50/mRFP*

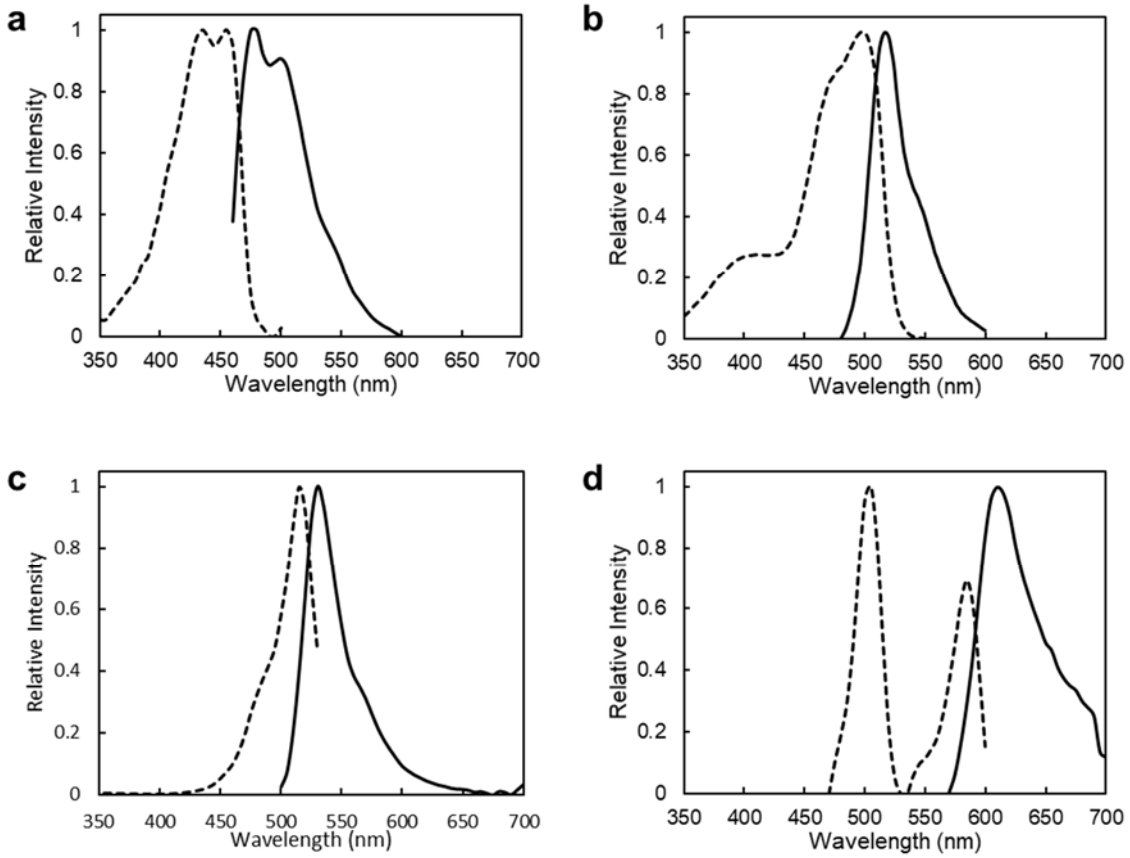

Figure 6.8 Fluorescence spectra of ELP/FP. *a) V50/mTurquoise2 (ex/em – 498/516 nm); b) V50/sfGFP (ex/em – 498nm/516nm); c) V50/SYFP2 (ex/em – 515nm/530nm); d) V50/mRFP (ex/em – 585nm/610nm; second excitation peak at 505 nm)*

6.3.3 Genetic engineering of V50NCC1

FPs contain many lysines throughout their sequence. In order to avoid side reactions that can potentially disrupt the proteins, we synthesize thiol containing V50NCC1 proteins. Similar to V50CK1, these telechelic proteins contain a thiol group at each terminal through cysteine residues. V50NCC1 have the sequence – [SGCG(VPGVG)$_{50}$VPGCG].

6.4 ELP/FP transition and FRET

It is known that upon transition of ELP from a hydrophilic to a hydrophobic state, the protein aggregates and phase separates. However, since ELP aggregates scatter light, most studies cannot reveal more about ELP behavior post-transition. We took advantage of the ELP/FP fusion proteins to study the post-transition properties of ELP using förster resonance energy transfer (FRET). FRET is the phenomenon of nonradiative dipole-dipole coupling that allows a donor fluorophore that is in close proximity to an acceptor fluorophore to transfer energy. Since FRET is highly dependent on the distance between fluorophores, we can use it to study ELP behavior. Figure 6.8a shows the fluorescence

spectra of a 1mg/mL solution of 1:1 V50/sfGFP:V50/mRFP in 0.5 M NaCl. The solution was excited at 440 nm and the spectra were recorded with a rise in temperature. Similarly, Figure 6.8c shows the fluorescence spectra of a 1mg/mL solution of 1:1 V50/mTurquoise2:V50/SYFP2 in 0.5 M NaCl. The solution was excited at 400 nm and the spectra were recorded with a rise in temperature. Both the plots (Figure 6.8 a & c) show a decrease in signal for the donor fluorophore (sfGFP or mTurquoise2) and an increase in signal for the acceptor (mRFP or SYFP2). Figure 6.8 b & d show the decrease in donor signal with a rise in temperature, which is clear in both cases. We observe that as the temperature increases, the distance between the aggregated proteins decreases gradually, which means that the protein dehydrates in correlation with the temperature. Since the observation of FRET requires the proteins to be within nanometer of each other, this process likely happens after the transition of ELP into an aggregated state. Our observations correlate with the deswelling of ELP hydrogels in Chapter 3. Since hydrogels already begin with a high concentration of ELP (15% to 20% w/v), an increase in temperature results in gradual deswelling that continues with temperature increase rather than an abrupt event at a cut-off temperature. This also correlates to the gradual refractive index changes observed in section 6.7.

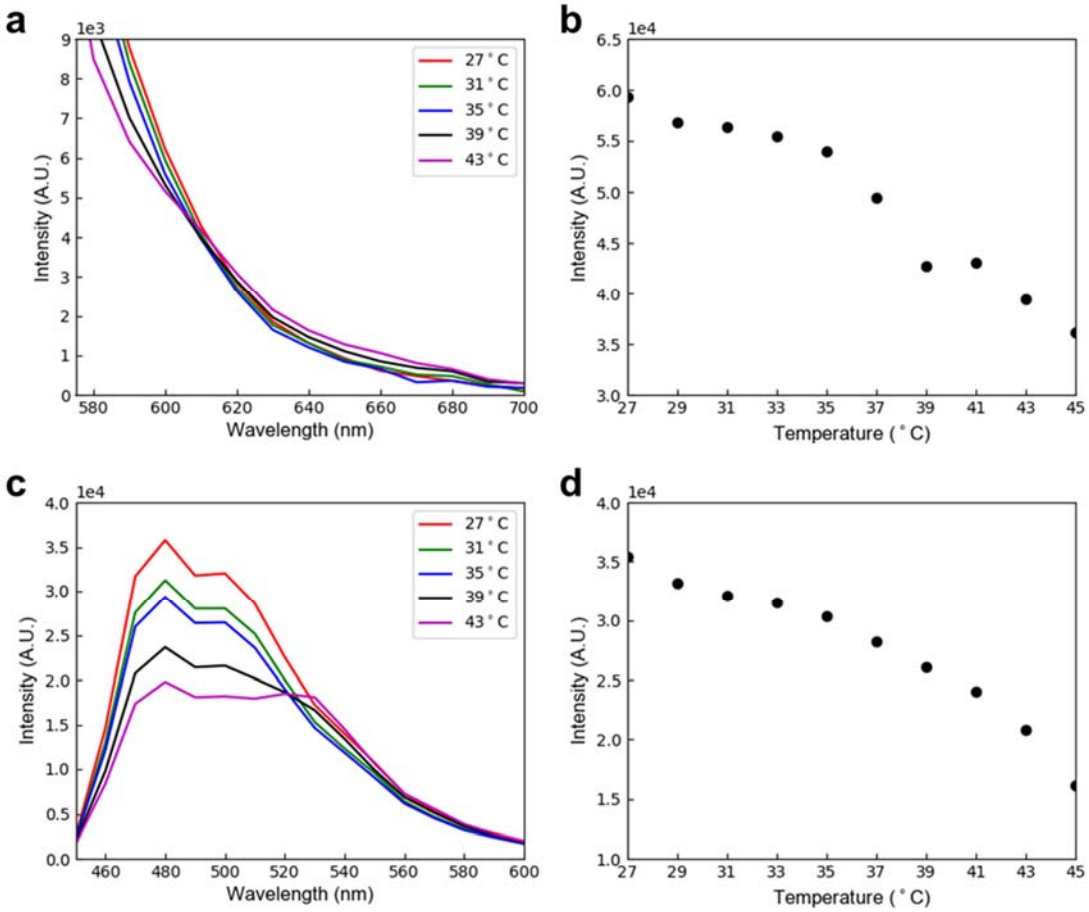

Figure 6.9 FRET measurements of ELP/FP fusions. *a) V50/sfGFP & V50/mRFP solution was excited at 440 nm and spectra were recorded with a rise in temperature; b) data shows a decrease in sfGFP signal and an increase in mRFP signal; c)*

V50/mTurquoise & V50/SYFP2 solution was excited at 400 nm and spectra were recorded with a rise in temperature; d) data shows a clear decrease in mTurquoise2 signal. mTurquoise2/SYFP2 pair generally shows a stronger FRET signal compared to sfGFP/mRFP

6.5 Hydrogel bead synthesis

The V4K125/Alexa488 hydrogels (10% w/v) are synthesize in an organic solvent mixture containing a 3:1 ratio of DMSO:DMF. The use of organic solvents prevents ELP transition during crosslinking. Disuccinimidyl suberate is used for crosslinking V4K125 into hydrogels and the V4K125:NHS-ester ratio is kept constant at 1:9 during hydrogel synthesis. Hydrogels are solidified by incubating the prepared mixtures at 37°C. On the other hand, V50/FP hydrogels (12% w/v) are synthesized using water as the solvent. Although DMSO:DMF mixture is ideal for creating optically clear hydrogels, we discovered that the V50/FP fusion proteins are insoluble in organic solvents. However, the greater stability of maleimide functional groups compared to NHS-esters in aqueous conditions still allows us to use water in our system. To yield clear hydrogels, we maintain the beads at a low temperature overnight followed by further incubation at room temperature for 24 hours.

The main challenge in this case was the synthesis of spherical hydrogel beads using both the hydrogel combinations we developed. We overcome this by generating emulsions between our organic solvents or water based crosslinking mixtures with an immiscible solvent. Typically, the crosslinking mixture is injected into a glass vial filled with 10 to 15 mL of an immiscible solvent. For our first trial, we used hexane and observed that the hydrophilic mixtures quickly drop to the bottom of the vessel and spread on the glass surface. (Figure 6.10) We attempted to tackle this issue by coating the glass vessels with a hydrophobic trichloro(1*H*,1*H*,2*H*,2*H*-perfluorooctyl)silane. After coating, although the mixtures did not spread, they deform as they rest on the vessel surface. Next, we use the coated vessels with more viscous mineral oil, but due to a marginal increase in viscosity, the beads still deformed. Finally, we employed a viscous mixture of silicone oil with a 3:2 ratio of 30,000 cSt:10 cSt oils. Due to the viscosity of the silicone oil mixture, the crosslinking mixture droplets slowly migrate to the bottom of the vessel. By the time they reach the bottom, they are already crosslinked into stable beads. After incubation is complete, the silicone oil is removed, and the beads are washed with hexane to remove the remaining oil. The beads are then hydrated in phosphate buffered saline solutions. (Figure 6.11 & Figure 6.12)

Figure 6.10 Hydrogel bead synthesis attempt in hexane with untreated glass

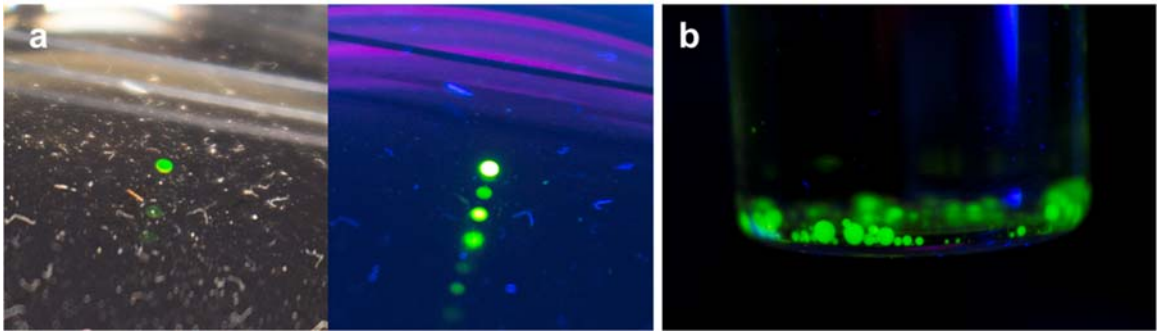

Figure 6.11 V4K125/Alexa488 hydrogel beads. *a) Photographs of a bead in visible light (left) and long range UV light (right); b) Photograph of beads illuminated by long range UV showing an array of sizes (for reference, glass vial has an outer diameter of 28 mm)*

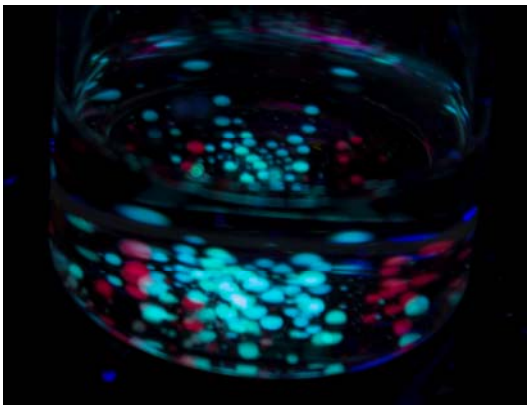

Figure 6.12 V50/FP hydrogel beads. *The photograph shows turquoise, green and red beads illuminated by long range UV light.*

6.6 Stimuli-response of hydrogel beads

Clear hydrogel beads with unmodified ELP are used for this characterization. In order to show stimuli-responsiveness of the hydrogel beads, we change the solution ionic strength or temperature and record the changes in bead size. A hydrogel bead is first equilibrated at an initial condition followed by quick transfer to the target condition. Changes in bead size are evaluated from videos recorded using a microscope. V4K125 bead with a diameter of 900 μm shows a volumetric change of 45-55% over a period of 60 minutes between 1x concentrated PBS and 5x PBS. (Figure 6.13 & Figure 6.14) On the other hand, the beads undergo a volumetric change of 30-40% as they are warmed from 4°C to 25°C and 60% change as they are cooled from 37°C to 25°C. (Figure 6.15) More conditions will be tested in the future to thoroughly characterize the stimuli-responses of the hydrogel beads. Stimuli-response of V4K125/Alexa488 and V50/FP hydrogel beads will also be characterized.

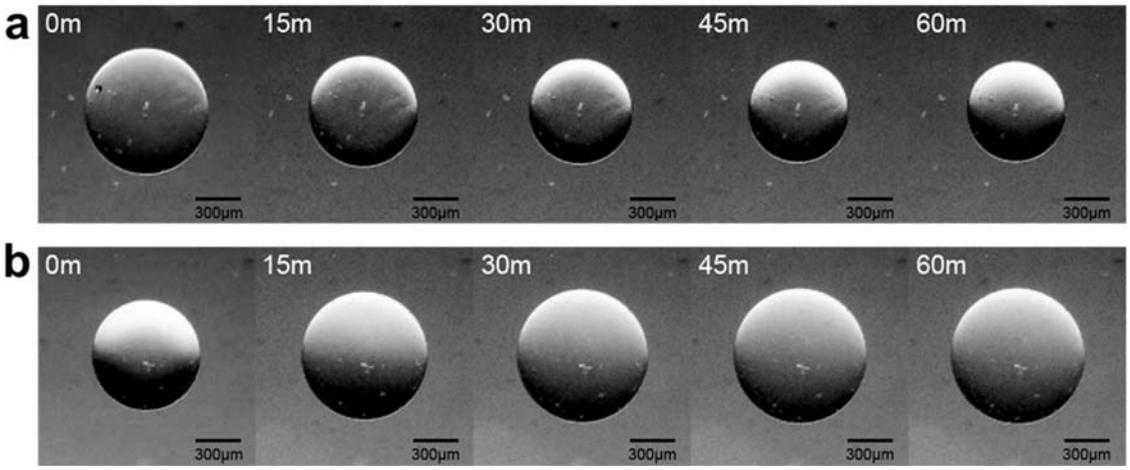

Figure 6.13 V4K125 bead swelling/deswelling in response to ionic strength. *a) Bead equilibrated in 1x PBS deswells in 5x PBS over time; b) Once bead is returned from 5x PBS to 1x PBS, it returns to its original state*

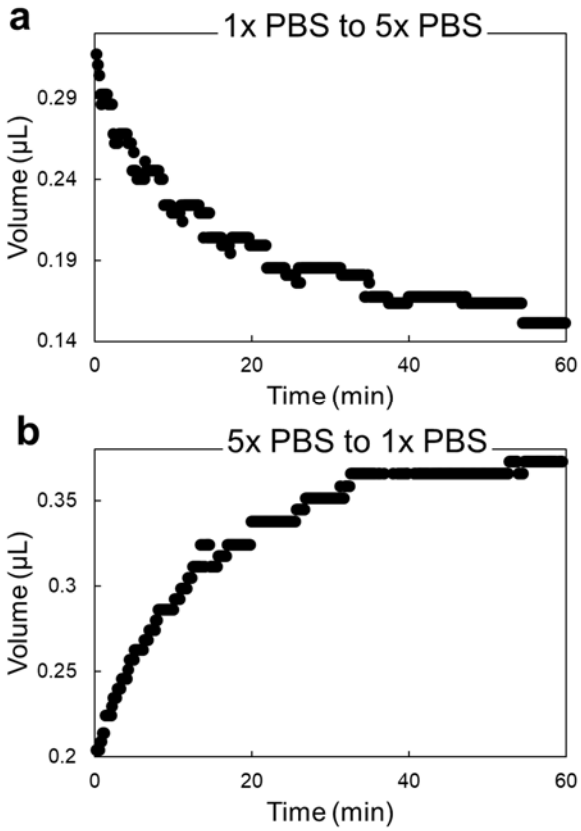

Figure 6.14 V4K125 bead swelling/deswelling in response to ionic strength. *a) Bead deswells as it equilibrates in 5x PBS and shows a 53% decrease in volume; b) Bead swells as it equilibrates in 1x PBS and shows a 46% increase in volume*

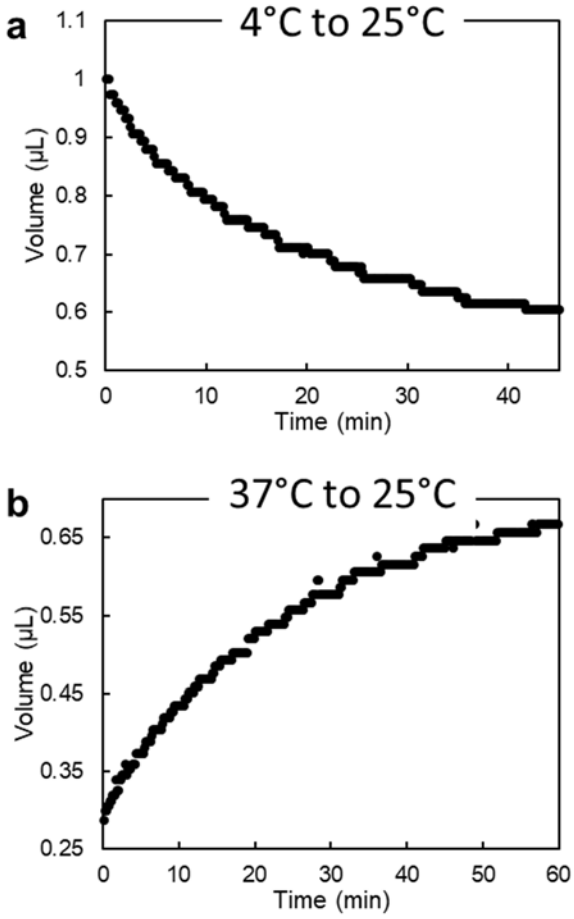

Figure 6.15 V4K125 bead thermo-responsive swelling/deswelling. *a) Bead deswells as it warms from 4°C to room temperature and shows a 40% decrease in volume; b) Bead swells as it cools to room temperature from 37°C and shows a 57% increase in volume*

6.7 Refractive index of bulk hydrogels

We measure the refractive index of bulk hydrogels using a portable refractometer (Atago™ Digital Hand-Held Pocket Refractometer: PAL-RI). We expect that as the hydrogels deswell and their protein content increases, their refractive index will increase. Since the refractive index of water is 1.33, we need to maximize the protein content in order to achieve desirable conditions for lasing. Figure 6.16a shows the measurements of refractive index (RI) of bovine serum albumin (BSA) solutions. Using the equation of the fitted line, we can extrapolate that in order to reach RI>1.45, the protein concentration would need to be greater than 80% w/v. Figure 6.16b shows the changes in the RI of V4K125 hydrogels. As can be seen, the RI increases to 1.41 as the hydrogels are heated to 50°C. Similar tests need to be carried out with V50NCC1 hydrogels to compare along with water content measurements that can be used as secondary method to confirm the relationship between RI and protein concentration.

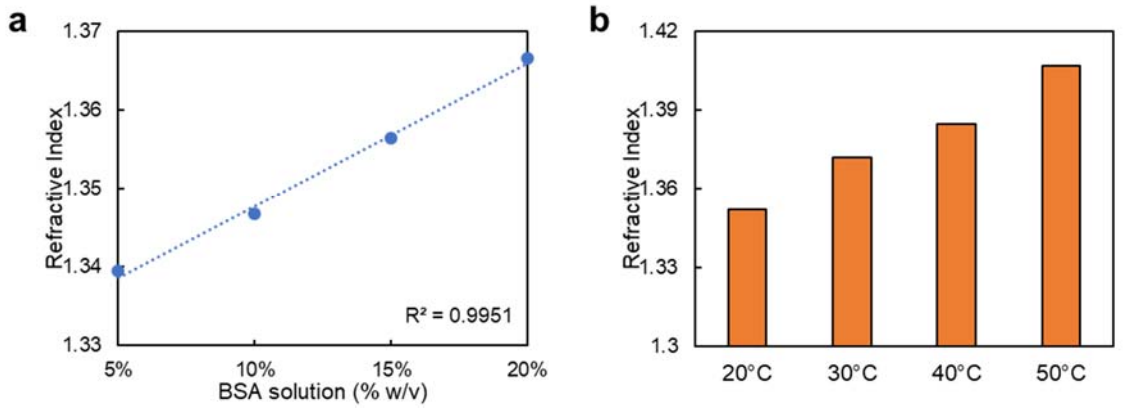

Figure 6.16 Protein concentration dependent refractive index changes. *a) BSA solutions show an increase in RI with concentration; b) V4K125 hydrogels show an increase in RI from 1.35 to 1.41 as temperature rises from 20°C to 50°C*

6.8 Further work

In this chapter, I described our ongoing work for the development of stimuli-responsive hydrogel beads for bio-lasing. Successful synthesis of a biolaser requires that our optically clear hydrogel beads have a high refractive index and spherical shape for its function as an optical resonator. The most significant experiment that is currently in progress is that of lasing. Since this experiment requires a specialized setup including a high energy pulsed laser for pumping and a precise spectrometer for signal detection, we are working with collaborators to complete the work. In the process, we will need to optimize our hydrogel bead properties by tuning protein and fluorophore concentration as well as the environmental conditions that maximize the refractive index contrast. Throughout our measurements, we will also continue collecting more data to thoroughly characterize the properties of our material.

The success of this project will introduce not only a new class of optical sensors, but also add valuable scientific insight into the design and development of biolaser devices. Our recombinant protein-based approach will be advantageous due to the ease of enhancing function and the ability to quickly tackle a broad range of applications in biosensing.

6.9 Methods

6.9.1 Genetic engineering of V50/FP

Plasmids containing the fluorescent protein (FP) genes for turquoise (mTurquoise2), green (superfolder-GFP), yellow (SYFP2) and red (mRFP) fluorescent proteins were a generous gift from Prof. John Dueber. The FP genes were PCR cloned from the plasmids using primers in Table 6.1. The primers add Eco31I recognition sites such that the full sequence of the FP was preserved when the amplicon is digested to yield sticky ends. The cloning site of pet28b plasmid was prepared by digesting it with

the enzymes NcoI and BamHI and ligating inserts 1 and 2 in Table 6.2. The modified plasmid was digested with Eco31I to create matching sticky ends to the respective FP insert. Once inserted, the plasmid containing FP gene was digested with NcoI and Eco31I, and inserts 3 and 4, with the N-terminal protein sequence and ELP insert site were ligated. (Table 6.2) The new plasmid was digested once more with Eco31I enzyme and V50 insert (see section 2.2.2) was inserted to yield the full V50/FP fusion protein gene. All other proteins were engineered in a similar manner and the insert sequences are listed in section 8.1. Full DNA sequence of each fusion protein can also be found in section 8.2.

Table 6.1 Primers used to PCR clone fluorescent protein genes

Protein		Sequence (5' → 3')
mTurquoise2	for	CAGGTCTCAATGGTTTCTAAAGGTGAAGAATTATTCAC
	rev	GAGGTCTCATTTGTACAATTCATCCATACCCAAGG
sfGFP	for	CAGGTCTCAATGCGTAAAGGCGAAGAGC
	rev	GAGGTCTCATTTGTACAGTTCATCCATACCATGCG
SYFP2	for	CAGGTCTCAATGGTATCAAAAGGTGAAGAATTATTCAC
	rev	GAGGTCTCATTTGTACAATTCATCCATACCCAAGG
mRFP	for	CAGGTCTCAATGGCGAGTAGCGAAGAC
	rev	GAGGTCTCAAGCACCGGTGGAGTG

Table 6.2 Inserts for sfGFP engineering

	Direction	Sequence (5' → 3')
Insert 1	for	CATGGGAACAACCACGGTCTC
	rev	GTGACGCATGGAGACCGTGGTTGTTCC
Insert 2	for	CATGCGTCACGGTCTCCCAAATAATAA
	rev	GATCTTATTATTTGGGAGACC
Insert 3	for	CATGAGCGGCTGCGGCGTCCTGAGACC
	rev	GTGACCAGTGGGTCTCAGGACGCCGCAGCCGCT
Insert 4	for	CACTGGTCACGGTCTCGGTCCCGGGTGGCGGC
	rev	GCATGCCGCCACCCGGGACCGAGACC

Chapter 7 Conclusion & Future Perspective

7.1 Elastin-like polypeptides

Recombinant proteins have great potential for use in developing unique materials due to their high purity and monodispersity. Elastin-like polypeptides are particularly interesting due to their stimuli-responsive properties and elasticity. Throughout my work, I have focused on using ELP to synthesize different types of hydrogels that utilize the properties that make the protein distinct.

In Chapter 3, we used ELP to create rubber-like extensible hydrogels. Unlike majority of previous chemically crosslinked hydrogels, our hydrogels reach strains as high as 1500% and maintained resilience as high as 94% up to a strain of 600%. We accomplish this by minimizing the crosslink density. As our hydrogels deswell due to the transition of ELP, the ELP chains contract into dense coils that can then use their entire length to stretch. Our strategy led to observations of clear correlations between the molecular architectures of polymer networks and hydrogel extensibility as well as reversibility. We also delve into the hysteresis characteristics we observe among the different types of hydrogels. Using guanidinium, we show how the hydrophobic interaction driven cohesion leads to hysteresis.

Practical implications of our research lie in the selection of polymer based on what is needed for a particular application. For example, V100CK1 show the greatest extensibility, however long-term use with repetitive loading would lead to material failure. In addition to the exceptional properties described, the ELP hydrogels also have a biologically relevant elastic modulus matching soft tissues and numerous studies have already shown its excellent biocompatibility.[14] Unlike many other hydrogels that lack the ability to deform reversibly, these ELP hydrogels can be used as tissue engineering materials to develop extraordinarily robust scaffolds. These hydrogels can be further developed into tissue engineering scaffolds for extensible tissues such as cardiac and skeletal muscles, blood vessels and even skin.

In Chapter 4, I continued with the idea of flexibility to develop flexible tissue adhesives using ELPs. We synthesized our adhesives using catechol containing dopamine groups as the broadly reactive molecules to bond with amino acid residues such as amines, thiols and imidazoles in oxidative conditions. Our adhesives achieved tensile and shear strengths as high as 35 to 40 kPa. A major advantage of this material compared to other hydrogel adhesives is their deswell at high temperatures, which likely boosts their adhesion strength and improves their integrity in general. Through rheometry, we also determined that the resulting hydrogels are flexible as they maintain their integrity to shear strains as high as 160%. We hope to prove the biocompatibility and efficacy of our adhesive both *in vitro* and *in vivo*. In the future, the ELP adhesives will be useful for sealing soft tissues including skin, muscles and neuronal tissues. Furthermore, with the development of rubber-like flexible hydrogels in chapter 3, we also have a potential path

to the formulation of a rubber-like adhesive. The development of a truly flexible adhesive will help us establish a new class of adhesives with great potential in surgical sealing applications in the future.

Next, we designed an *in situ* forming biocomposite hydrogel using ELP and bioglass. We designed the ELPs to form dynamic aldimine cross-links that are favored at a high local pH achieved through BG. The resulting ELP/BG biocomposite showed thermosensitive gelling and mechanical properties that can be easily tuned by changing BG content. We also demonstrated self-healing by successfully reattaching severed hydrogels as well as through rheology. Similar to the adhesive hydrogels, these materials can form in situ, which makes them injectable. The ELP/BG hydrogels will be useful for wound healing and as carriers for cell and drug delivery. The advantageous qualities of bioglass including its ability to promote biomineralization and even antibacterial properties in addition to the self-healing properties of the hydrogels will make them valuable for tissue engineering applications.

Finally, I discussed our ongoing efforts to develop a biolaser using protein-based hydrogel beads. In addition to chemical modification of ELPs to create fluorescent proteins, we also synthesize fusion proteins with ELP and fluorescent proteins using genetic engineering. Such a pathway is only conceivable by employing genetic engineering and recombinant protein technologies. We synthesized hydrogel beads using our proteins and show their stimuli-responsive behavior. As we test their capability to undergo lasing, we will optimize their composition and anticipate the realization of a stimuli-responsive biolaser. Such a device will be broadly applicable for sensing biomolecules, environmental changes and even mechanical perturbations that result from cellular movements.

7.2 Protein-based polymers

I want to conclude my thesis with thoughts on the broader field of recombinant protein-based polymers. Proteins are fundamental parts of all biological systems and structural proteins such as elastin, collagen and even insect-derived proteins such as silk and resilin have shown their worth in the development of new materials useful for tissue engineering and bioengineering in general. Understanding the properties of these proteins and being able to design new mimics can help us tackle the challenge of replicating ECM-like environments as well as creating completely novel smart materials through protein self-assembly and stimuli response. The functional biosignal domains in addition to the smart structural domains add to the value of protein-based polymers allowing one to also stimulate cells physically and biochemically.

As we make progress, it is important to note the upcoming revolution with the infusion of data mining and computational modelling into recombinant protein development. Modular design of PBP with different structural and functional motifs is already paving the way for the future of precisely and purposefully designed bionanomaterials. Computational modelling will significantly enhance our abilities to

design and evaluate new PBPs for future biomedical applications.[286,287] I hope to keep learning and innovating, and to remain at the forefront research throughout my career. I also hope to use my skills and knowledge to train a future generation of scientists, because in the end, our ingenuity is our greatest asset as individuals and for humanity as a whole.

Chapter 8 Supplemental Information

8.1 Insert sequences for ELP/fluorescent protein fusions

Table 8.1 Inserts for V50/mTurquoise2 engineering

	Direction	Sequence (5' → 3')
Insert 1	for	CATGGGAACAACCACGGTCTC
	rev	GTGACCCATGGAGACCGTGGTTGTTCC
Insert 2	for	CATGGGTCACGGTCTCCCAAATAATAA
	rev	GATCTTATTATTTGGGAGACC
Insert 3	for	CATGAGCGGCTGCGGCGTCCTGAGACC
	rev	GTGACCAGTGGGTCTCAGGACGCCGCAGCCGCT
Insert 4	for	CACTGGTCACGGTCTCGGTCCCGGGTGGCGGC
	rev	CCATGCCGCCACCCGGGACCGAGACC

Table 8.2 Inserts for V50/SYFP2 engineering

	Direction	Sequence (5' → 3')
Insert 1	for	CATGGGAACAACCACGGTCTC
	rev	GTGACCCATGGAGACCGTGGTTGTTCC
Insert 2	for	CATGGGTCACGGTCTCCCAAATAATAA
	rev	GATCTTATTATTTGGGAGACC
Insert 3	for	CATGAGCGGCTGCGGCGTCCTGAGACC
	rev	GTGACCAGTGGGTCTCAGGACGCCGCAGCCGCT
Insert 4	for	CACTGGTCACGGTCTCGGTCCCGGGTGGCGGC
	rev	CCATGCCGCCACCCGGGACCGAGACC

Table 8.3 Inserts for V50/mRFP engineering

	Direction	Sequence (5' → 3')
Insert 1	for	CATGGGAACAACCACGGTCTC
	rev	GTGACCCATGGAGACCGTGGTTGTTCC
Insert 2	for	CATGGGTCACGGTCTCCCAAATAATAA
	rev	GATCTTATTATTTGGGAGACC
Insert 3	for	CATGAGCGGCTGCGGCGTCCTGAGACC
	rev	GTGACCAGTGGGTCTCAGGACGCCGCAGCCGCT
Insert 4	for	CACTGGTCACGGTCTCGGTCCCGGGTGGCGGC
	rev	CCATGCCGCCACCCGGGACCGAGACC

8.2 ELP/fluorescent protein sequences

```
   1 GAAGGAGATA TACCATGAGC GGCTGCGGCG TCCCAGGTGT GGGCGTACCG GGCGTTGGTG TTCCTGGTGT CGGCGTGCCG
  81 GGCGTGGGTG TTCCGGGCGT AGGTGTCCCA GGTGTGGGCG TACCGGGCGT TGGTGTTCCT GGTGTCGGCG TGCCGGGCGT
 161 GGGTGTTCCG GGCGTAGGTG TCCCAGGTGT GGGCGTACCG GGCGTTGGTG TTCCTGGTGT CGGCGTGCCG GGCGTGGGTG
 241 TTCCGGGCGT AGGTGTCCCA GGTGTGGGCG TACCGGGCGT TGGTGTTCCT GGTGTCGGCG TGCCGGGCGT GGGTGTTCCG
 321 GGCGTAGGTG TCCCAGGTGT GGGCGTACCG GGCGTTGGTG TTCCTGGTGT CGGCGTGCCG GGCGTGGGTG TTCCGGGCGT
 401 AGGTGTCCCA GGTGTGGGCG TACCGGGCGT TGGTGTTCCT GGTGTCGGCG TGCCGGGCGT GGGTGTTCCG GGCGTAGGTG
 481 TCCCAGGTGT GGGCGTACCG GGCGTTGGTG TTCCTGGTGT CGGCGTGCCG GGCGTGGGTG TTCCGGGCGT AGGTGTCCCA
 561 GGTGTGGGCG TACCGGGCGT TGGTGTTCCT GGTGTCGGCG TGCCGGGCGT GGGTGTTCCG GGCGTAGGTG TCCCAGGTGT
 641 GGGCGTACCG GGCGTTGGTG TTCCTGGTGT CGGCGTGCCG GGCGTGGGTG TTCCGGGCGT AGGTGTCCCA GGTGTGGGCG
 721 TACCGGGCGT TGGTGTTCCT GGTGTCGGCG TGCCGGGCGT GGGTGTTCCG GGCGTAGGTG TCCCGGGTGG CGGCATGCGT
 801 AAAGGCGAAG AGCTGTTCAC TGGTGTCGTC CCTATTCTGG TGGAACTGGA TGGTGATGTC AACGGTCATA AGTTTTCCGT
 881 GCGTGGCGAG GGTGAAGGTG ACGCAACTAA TGGTAAACTG ACGCTGAAGT TCATCTGTAC TACTGGTAAA CTGCCGGTTC
 961 CTTGGCCGAC TCTGGTAACG ACGCTGACTT ATGGTGTTCA GTGCTTTGCT CGTTATCCGG ACCATATGAA GCAGCATGAC
1041 TTCTTCAAGT CCGCCATGCC GGAAGGCTAT GTGCAGGAAC GCACGATTTC CTTTAAGGAT GACGGCACGT ACAAAACGCG
1121 TGCGGAAGTG AAATTTGAAG GCGATACCCT GGTAAACCGC ATTGAGCTGA AAGGCATTGA CTTTAAAGAA GACGGCAATA
1201 TCCTGGGCCA TAAGCTGGAA TACAATTTTA ACAGCCACAA TGTTTACATC ACCGCCGATA AACAAAAAAA TGGCATTAAA
1281 GCGAATTTTA AAATTCGCCA CAACGTGGAG GATGGCAGCG TGCAGCTGGC TGATCACTAC CAGCAAAACA CTCCAATCGG
1361 TGATGGTCCT GTTCTGCTGC CAGACAATCA CTATCTGAGC ACGCAAAGCG TTCTGTCTAA AGATCCGAAC GAGAAACGCG
1441 ATCATATGGT TCTGCTGGAG TTCGTAACCG CAGCGGGCAT CACGCATGGT ATGGATGAAC TGTACAAATA ATAAGATCCG
1521 AATTCGAGCT CCGTC

    Features:
    V50     15-779
    sfGFP   795-1508
```

Figure 8.1 V50/sfGFP sequence

```
   1 GAAGGAGATA TACCATGAGC GGCTGCGGCG TCCCAGGTGT GGGCGTACCG GGCGTTGGTG TTCCTGGTGT CGGCGTGCCG
  81 GGCGTGGGTG TTCCGGGCGT AGGTGTCCCA GGTGTGGGCG TACCGGGCGT TGGTGTTCCT GGTGTCGGCG TGCCGGGCGT
 161 GGGTGTTCCG GGCGTAGGTG TCCCAGGTGT GGGCGTACCG GGCGTTGGTG TTCCTGGTGT CGGCGTGCCG GGCGTGGGTG
 241 TTCCGGGCGT AGGTGTCCCA GGTGTGGGCG TACCGGGCGT TGGTGTTCCT GGTGTCGGCG TGCCGGGCGT GGGTGTTCCG
 321 GGCGTAGGTG TCCCAGGTGT GGGCGTACCG GGCGTTGGTG TTCCTGGTGT CGGCGTGCCG GGCGTGGGTG TTCCGGGCGT
 401 AGGTGTCCCA GGTGTGGGCG TACCGGGCGT TGGTGTTCCT GGTGTCGGCG TGCCGGGCGT GGGTGTTCCG GGCGTAGGTG
 481 TCCCAGGTGT GGGCGTACCG GGCGTTGGTG TTCCTGGTGT CGGCGTGCCG GGCGTGGGTG TTCCGGGCGT AGGTGTCCCA
 561 GGTGTGGGCG TACCGGGCGT TGGTGTTCCT GGTGTCGGCG TGCCGGGCGT GGGTGTTCCG GGCGTAGGTG TCCCAGGTGT
 641 GGGCGTACCG GGCGTTGGTG TTCCTGGTGT CGGCGTGCCG GGCGTGGGTG TTCCGGGCGT AGGTGTCCCA GGTGTGGGCG
 721 TACCGGGCGT TGGTGTTCCT GGTGTCGGCG TGCCGGGCGT GGGTGTTCCG GGCGTAGGTG TCCCGGGTGG CGGCATGGTT
 801 TCTAAAGGTG AAGAATTATT CACTGGTGTT GTCCCAATTT TGGTTGAATT AGATGGTGAT GTTAATGGTC ACAAATTTTC
 881 TGTCTCCGGT GAAGGTGAAG GTGATGCTAC TTACGGTAAA TTGACCTTAA AATTTATTTG TACTACTGGT AAATTGCCAG
 961 TTCCATGGCC AACCTTAGTC ACTACTTTAT CTTGGGGTGT TCAATGTTTT GCAAGATACC CAGATCATAT GAAACAACAT
1041 GACTTTTTCA AGTCTGCCAT GCCAGAAGGT TATGTTCAAG AAAGAACTAT TTTTTTCAAA GATGACGGTA ACTACAAGAC
1121 CAGAGCTGAA GTCAAGTTTG AAGGTGATAC CTTAGTTAAT AGAATCGAAT TAAAAGGTAT TGATTTTAAA GAAGATGGTA
1201 ACATTTTAGG TCACAAATTG GAATACAATT ATTTCTCTGA CAATGTTTAC ATCACTGCTG ACAAACAAAA GAATGGTATC
1281 AAAGCTAACT TCAAAATTAG ACACAACATT GAAGATGGTG GTGTTCAATT AGCTGACCAT TATCAACAAA ATACTCCAAT
1361 TGGTGATGGT CCAGTCTTGT TACCAGACAA CCATTACTTA TCCACTCAAT CTAAGTTATC CAAAGATCCA AACGAAAAGA
1441 GGGACCACAT GGTCTTGTTA GAATTTGTTA CTGCTGCTGG TATTACCTTG GGTATGGATG AATTGTACAA ATAATAAGAT
1521 CCGAATTCGA GCTCCGTC

    Features:
    V50             15-779
    mTurquoise2     795-1511
```

Figure 8.2 V50/mTurquoise2 sequence

```
   1 GAAGGAGATA TACCATGAGC GGCTGCGGCG TCCCAGGTGT GGGCGTACCG GGCGTTGGTG TTCCTGGTGT CGGCGTGCCG
  81 GGCGTGGGTG TTCCGGGCGT AGGTGTCCCA GGTGTGGGCG TACCGGGCGT TGGTGTTCCT GGTGTCGGCG TGCCGGGCGT
 161 GGGTGTTCCG GGCGTAGGTG TCCCAGGTGT GGGCGTACCG GGCGTTGGTG TTCCTGGTGT CGGCGTGCCG GGCGTGGGTG
 241 TTCCGGGCGT AGGTGTCCCA GGTGTGGGCG TACCGGGCGT TGGTGTTCCT GGTGTCGGCG TGCCGGGCGT GGGTGTTCCG
 321 GGCGTAGGTG TCCCAGGTGT GGGCGTACCG GGCGTTGGTG TTCCTGGTGT CGGCGTGCCG GGCGTGGGTG TTCCGGGCGT
 401 AGGTGTCCCA GGTGTGGGCG TACCGGGCGT TGGTGTTCCT GGTGTCGGCG TGCCGGGCGT GGGTGTTCCG GGCGTAGGTG
 481 TCCCAGGTGT GGGCGTACCG GGCGTTGGTG TTCCTGGTGT CGGCGTGCCG GGCGTGGGTG TTCCGGGCGT AGGTGTCCCA
 561 GGTGTGGGCG TACCGGGCGT TGGTGTTCCT GGTGTCGGCG TGCCGGGCGT GGGTGTTCCG GGCGTAGGTG TCCCAGGTGT
 641 GGGCGTACCG GGCGTTGGTG TTCCTGGTGT CGGCGTGCCG GGCGTGGGTG TTCCGGGCGT AGGTGTCCCA GGTGTGGGCG
 721 TACCGGGCGT TGGTGTTCCT GGTGTCGGCG TGCCGGGCGT GGGTGTTCCG GGCGTAGGTG TCCCGGGTGG CGGCATGGTA
 801 TCAAAAGGTG AAGAATTATT CACTGGTGTT GTCCCAATTT TGGTTGAATT AGATGGTGAT GTTAATGGTC ACAAATTTTC
 881 TGTCTCCGGT GAAGGTGAAG GTGATGCTAC TTACGGTAAA TTGACCTTAA AATTGATTTG TACTACTGGT AAATTGCCAG
 961 TTCCATGGCC AACCTTAGTC ACTACTTTAG GTTATGGTGT GCAATGTTTT GCTAGATACC CAGATCATAT GAAACAACAT
1041 GACTTTTTCA AGTCTGCCAT GCCAGAAGGT TATGTTCAAG AAAGAACTAT TTTTTCAAA GATGACGGTA ACTACAAGAC
1121 CAGAGCTGAA GTCAAGTTTG AAGGTGATAC CTTAGTTAAT AGAATCGAAT TAAAAGGTAT TGATTTTAAA GAAGATGGTA
1201 ACATTTTAGG TCACAAATTG GAATACAACT ATAACTCTCA CAATGTTTAC ATCACTGCTG ACAAACAAAA GAATGGTATC
1281 AAAGCTAACT TCAAAATTAG ACACAACATT GAAGATGGTG GTGTTCAATT AGCTGACCAT TATCAACAAA ATACTCCAAT
1361 TGGTGATGGT CCAGTCTTGT TACCAGACAA CCATTACTTA TCCTATCAAT CTAAATTATC CAAAGATCCA AACGAAAAGA
1441 GAGATCACAT GGTCTTGTTA GAATTTGTTA CTGCTGCTGG TATTACCTTG GGTATGGATG AATTGTACAA ATAATAAGAT
1521 CCGAATTCGA GCTCCGTC

     Features:
     V50      15-779
     SYFP2    795-1511
```

Figure 8.3 V50/SYFP2 sequence

```
   1 GAAGGAGATA TACCATGAGC GGCTGCGGCG TCCCAGGTGT GGGCGTACCG GGCGTTGGTG TTCCTGGTGT CGGCGTGCCG
  81 GGCGTGGGTG TTCCGGGCGT AGGTGTCCCA GGTGTGGGCG TACCGGGCGT TGGTGTTCCT GGTGTCGGCG TGCCGGGCGT
 161 GGGTGTTCCG GGCGTAGGTG TCCCAGGTGT GGGCGTACCG GGCGTTGGTG TTCCTGGTGT CGGCGTGCCG GGCGTGGGTG
 241 TTCCGGGCGT AGGTGTCCCA GGTGTGGGCG TACCGGGCGT TGGTGTTCCT GGTGTCGGCG TGCCGGGCGT GGGTGTTCCG
 321 GGCGTAGGTG TCCCAGGTGT GGGCGTACCG GGCGTTGGTG TTCCTGGTGT CGGCGTGCCG GGCGTGGGTG TTCCGGGCGT
 401 AGGTGTCCCA GGTGTGGGCG TACCGGGCGT TGGTGTTCCT GGTGTCGGCG TGCCGGGCGT GGGTGTTCCG GGCGTAGGTG
 481 TCCCAGGTGT GGGCGTACCG GGCGTTGGTG TTCCTGGTGT CGGCGTGCCG GGCGTGGGTG TTCCGGGCGT AGGTGTCCCA
 561 GGTGTGGGCG TACCGGGCGT TGGTGTTCCT GGTGTCGGCG TGCCGGGCGT GGGTGTTCCG GGCGTAGGTG TCCCAGGTGT
 641 GGGCGTACCG GGCGTTGGTG TTCCTGGTGT CGGCGTGCCG GGCGTGGGTG TTCCGGGCGT AGGTGTCCCA GGTGTGGGCG
 721 TACCGGGCGT TGGTGTTCCT GGTGTCGGCG TGCCGGGCGT GGGTGTTCCG GGCGTAGGTG TCCCGGGTGG CGGCATGGCG
 801 AGTAGCGAAG ACGTTATCAA AGAGTTCATG CGTTTCAAAG TTCGTATGGA AGGTTCCGTT AACGGTCACG AGTTCGAAAT
 881 CGAAGGTGAA GGTGAAGGTC GTCCGTACGA AGGTACCCAG ACCGCTAAAC TGAAAGTTAC CAAAGGTGGT CCGCTGCCGT
 961 TCGCTTGGGA CATCCTGTCC CCGCAGTTCC AGTACGGTTC CAAAGCTTAC GTTAAACACC CGGCTGACAT CCCGGACTAC
1041 CTGAAACTGT CCTTCCCGGA AGGTTTCAAA TGGGAACGTG TTATGAACTT CGAAGACGGT GGTGTTGTTA CCGTTACCCA
1121 GGACTCCTCC CTGCAAGACG GTGAGTTCAT CTACAAAGTT AAACTGCGTG GTACCAACTT CCCGTCCGAC GGTCCGGTTA
1201 TGCAGAAAAA AACCATGGGT TGGGAAGCTT CCACCGAACG TATGTACCCG GAAGACGGTG CTCTGAAAGG TGAAATCAAA
1281 ATGCGTCTGA AACTGAAAGA CGGTGGTCAC TACGACGCTG AAGTTAAAAC CACCTACATG GCTAAAAAAC CGGTTCAGCT
1361 GCCGGGTGCT TACAAAACCG ACATCAAACT GGACATCACC TCCCACAACG AAGACTACAC CATCGTTGAA CAGTACGAAC
1441 GTGCTGAAGG TCGTCACTCC ACCGGTGCTT AATAAGATCC GAATTCGAGC TCCGTC

     Features:
     V50      15-779
     mRFP     795-1469
```

Figure 8.4 V50/mRFP sequence

References

1 Drury, J. L. & Mooney, D. J. Hydrogels for tissue engineering: scaffold design variables and applications. *Biomaterials* **24**, 4337-4351, doi:10.1016/s0142-9612(03)00340-5 (2003).

2 Discher, D. E., Janmey, P. & Wang, Y. L. Tissue cells feel and respond to the stiffness of their substrate. *Science* **310**, 1139-1143, doi:10.1126/science.1116995 (2005).

3 Nerem, R. M. & Sambanis, A. Tissue engineering: from biology to biological substitutes. *Tissue engineering* **1**, 3-13, doi:10.1089/ten.1995.1.3 (1995).

4 Khademhosseini, A. & Langer, R. Microengineered hydrogels for tissue engineering. *Biomaterials* **28**, 5087-5092, doi:10.1016/j.biomaterials.2007.07.021 (2007).

5 Ahmed, E. M. Hydrogel: Preparation, characterization, and applications: A review. *J. Adv. Res.* **6**, 105-121, doi:10.1016/j.jare.2013.07.006 (2015).

6 Calo, E. & Khutoryanskiy, V. V. Biomedical applications of hydrogels: A review of patents and commercial products. *Eur. Polym. J.* **65**, 252-267, doi:10.1016/j.eurpolymj.2014.11.024 (2015).

7 Van Vlierberghe, S., Dubruel, P. & Schacht, E. Biopolymer-Based Hydrogels As Scaffolds for Tissue Engineering Applications: A Review. *Biomacromolecules* **12**, 1387-1408, doi:10.1021/bm200083n (2011).

8 Nguyen, Q. V., Huynh, D. P., Park, J. H. & Lee, D. S. Injectable polymeric hydrogels for the delivery of therapeutic agents: A review. *Eur. Polym. J.* **72**, 602-619, doi:10.1016/j.eurpolymj.2015.03.016 (2015).

9 Kaur, S. & Dhillon, G. S. The versatile biopolymer chitosan: potential sources, evaluation of extraction methods and applications. *Crit. Rev. Microbiol.* **40**, 155-175, doi:10.3109/1040841x.2013.770385 (2014).

10 Lee, K. Y. & Mooney, D. J. Alginate: Properties and biomedical applications. *Progress in Polymer Science* **37**, 106-126, doi:10.1016/j.progpolymsci.2011.06.003 (2012).

11 Desai, M. S. & Lee, S.-W. Protein-based functional nanomaterial design for bioengineering applications. *Wiley Interdisciplinary Reviews: Nanomedicine and Nanobiotechnology* **7**, 69-97, doi:10.1002/wnan.1303 (2015).

12 Rosano, G. L. & Ceccarelli, E. A. Recombinant protein expression in Escherichia coli: advances and challenges. *Frontiers in microbiology* **5**, 172, doi:10.3389/fmicb.2014.00172 (2014).

13 Werkmeister, J. A. & Ramshaw, J. A. M. Recombinant protein scaffolds for tissue engineering. *Biomedical Materials* **7**, 012002, doi:10.1088/1748-6041/7/1/012002 (2012).

14 Nettles, D. L., Chilkoti, A. & Setton, L. A. Applications of elastin-like polypeptides in tissue engineering. *Advanced Drug Delivery Reviews* **62**, 1479-1485, doi:10.1016/j.addr.2010.04.002 (2010).

15 DiMarco, R. L. & Heilshorn, S. C. Multifunctional Materials through Modular Protein Engineering. *Advanced Materials* **24**, 3923-3940, doi:10.1002/adma.201200051 (2012).

16 Vashi, A. V. *et al.* Controlled surface modification of tissue culture polystyrene for selective cell binding using resilin-inspired polypeptides. *Biofabrication* **5**, 035005, doi:10.1088/1758-5082/5/3/035005 (2013).
17 Wohlrab, S. *et al.* Cell adhesion and proliferation on RGD-modified recombinant spider silk proteins. *Biomaterials* **33**, 6650-6659, doi:10.1016/j.biomaterials.2012.05.069 (2012).
18 Wang, E., Lee, S.-H. & Lee, S.-W. Elastin-Like Polypeptide Based Hydroxyapatite Bionanocomposites. *Biomacromolecules* **12**, 672-680, doi:10.1021/bm101322m (2011).
19 Li, L., Tong, Z., Jia, X. & Kiick, K. L. Resilin-like polypeptide hydrogels engineered for versatile biological function. *Soft Matter* **9**, 665, doi:10.1039/c2sm26812d (2013).
20 Xia, X.-X., Xu, Q., Hu, X., Qin, G. & Kaplan, D. L. Tunable Self-Assembly of Genetically Engineered Silk–Elastin-like Protein Polymers. *Biomacromolecules* **12**, 3844-3850, doi:10.1021/bm201165h (2011).
21 An, B. *et al.* The influence of specific binding of collagen–silk chimeras to silk biomaterials on hMSC behavior. *Biomaterials* **34**, 402-412, doi:10.1016/j.biomaterials.2012.09.085 (2013).
22 Bracalello, A. *et al.* Design and Production of a Chimeric Resilin-, Elastin-, and Collagen-Like Engineered Polypeptide. *Biomacromolecules* **12**, 2957-2965, doi:10.1021/bm2005388 (2011).
23 Annabi, N. *et al.* Elastomeric recombinant protein-based biomaterials. *Biochemical Engineering Journal* **77**, 110-118, doi:10.1016/j.bej.2013.05.006 (2013).
24 Arias, F. J., Santos, M., Fernández-Colino, A., Pinedo, G. & Girotti, A. Recent contributions of elastin-like recombinamers to biomedicine and nanotechnology. *Current topics in medicinal chemistry* **14**, 819-836, doi:10.2174/1568026614666140118223412 (2014).
25 MacEwan, S. R. & Chilkoti, A. Elastin-like polypeptides: biomedical applications of tunable biopolymers. *Biopolymers* **94**, 60-77, doi:10.1002/bip.21327 (2010).
26 McDaniel, J. R., Dewhirst, M. W. & Chilkoti, A. Actively targeting solid tumours with thermoresponsive drug delivery systems that respond to mild hyperthermia. *International Journal of Hyperthermia* **29**, 501-510, doi:10.3109/02656736.2013.819999 (2013).
27 Silva, N. H. C. S. *et al.* Protein-based materials: from sources to innovative sustainable materials for biomedical applications. *Journal of Materials Chemistry B* **2**, 3715-3740, doi:10.1039/c4tb00168k (2014).
28 Yu, S. M., Li, Y. & Kim, D. Collagen mimetic peptides: progress towards functional applications. *Soft Matter* **7**, 7927, doi:10.1039/c1sm05329a (2011).
29 Omenetto, F. G. & Kaplan, D. L. New Opportunities for an Ancient Material. *Science* **329**, 528-531, doi:10.1126/science.1188936 (2010).
30 Rising, A., Widhe, M., Johansson, J. & Hedhammar, M. Spider silk proteins: recent advances in recombinant production, structure–function relationships and biomedical applications. *Cellular and Molecular Life Sciences* **68**, 169-184, doi:10.1007/s00018-010-0462-z (2011).

31 Schacht, K. & Scheibel, T. Processing of recombinant spider silk proteins into tailor-made materials for biomaterials applications. *Current Opinion in Biotechnology* **29**, 62-69, doi:10.1016/j.copbio.2014.02.015 (2014).
32 Spiess, K., Lammel, A. & Scheibel, T. Recombinant Spider Silk Proteins for Applications in Biomaterials. *Macromolecular Bioscience* **10**, 998-1007, doi:10.1002/mabi.201000071 (2010).
33 Li, L. & Kiick, K. L. Resilin-Based Materials for Biomedical Applications. *ACS Macro Letters* **2**, 635-640, doi:10.1021/mz4002194 (2013).
34 Su, R. S.-C., Kim, Y. & Liu, J. C. Resilin: Protein-based elastomeric biomaterials. *Acta Biomaterialia* **10**, 1601-1611, doi:10.1016/j.actbio.2013.06.038 (2014).
35 Wise, S. G., Mithieux, S. M. & Weiss, A. S. in *Advances in Protein Chemistry and Structural Biology* Vol. 78 1-24 (Elsevier, 2009).
36 Vrhovski, B. & Weiss, A. S. Biochemistry of tropoelastin. *European Journal of Biochemistry* **258**, 1-18, doi:10.1046/j.1432-1327.1998.2580001.x (1998).
37 Sandberg, L. B., Weissman, N. & Gray, W. R. Structural features of tropoelastin related to the sites of cross-links in aortic elastin. *Biochemistry* **10**, 52-56, doi:10.1021/bi00777a008 (1971).
38 Sandberg, L. B., Weissman, N. & Smith, D. W. Purification and partial characterization of a soluble elastin-like protein from copper-deficient procine aorta. *Biochemistry* **8**, 2940-2945, doi:10.1021/bi00835a037 (1969).
39 McDaniel, J. R., Radford, D. C. & Chilkoti, A. A Unified Model for De Novo Design of Elastin-like Polypeptides with Tunable Inverse Transition Temperatures. *Biomacromolecules* **14**, 2866-2872, doi:10.1021/bm4007166 (2013).
40 Urry, D. W. *et al.* Temperature of polypeptide inverse temperature transition depends on mean residue hydrophobicity. *Journal of the American Chemical Society* **113**, 4346-4348, doi:10.1021/ja00011a057 (1991).
41 Urry, D. W. Entropic elastic processes in protein mechanisms. I. Elastic structure due to an inverse temperature transition and elasticity due to internal chain dynamics. *Journal of Protein Chemistry* **7**, 1-34, doi:10.1007/bf01025411 (1988).
42 Baldock, C. *et al.* Shape of tropoelastin, the highly extensible protein that controls human tissue elasticity. *Proceedings of the National Academy of Sciences* **108**, 4322-4327, doi:10.1073/pnas.1014280108 (2011).
43 Ohgo, K. *et al.* Resolving Nitrogen-15 and Proton Chemical Shifts for Mobile Segments of Elastin with Two-dimensional NMR Spectroscopy. *Journal of Biological Chemistry* **287**, 18201-18209, doi:10.1074/jbc.M111.285163 (2012).
44 Yao, X. L. & Hong, M. Structure distribution in an elastin-mimetic peptide (VPGVG)3 investigated by solid-state NMR. *Journal of the American Chemical Society* **126**, 4199-4210, doi:10.1021/ja036686n (2004).
45 Maeda, I. *et al.* Structural requirements essential for elastin coacervation: favorable spatial arrangements of valine ridges on the three-dimensional structure of elastin-derived polypeptide (VPGVG)n. *Journal of Peptide Science* **17**, 735-743, doi:10.1002/psc.1394 (2011).
46 Serrano, V., Liu, W. & Franzen, S. An Infrared Spectroscopic Study of the Conformational Transition of Elastin-Like Polypeptides. *Biophysical Journal* **93**, 2429-2435, doi:10.1529/biophysj.106.100594 (2007).

47 Leach, J. B., Wolinsky, J. B., Stone, P. J. & Wong, J. Y. Crosslinked alpha-elastin biomaterials: towards a processable elastin mimetic scaffold. *Acta Biomaterialia* **1**, 155-164, doi:10.1016/j.actbio.2004.12.001 (2005).
48 Duvenage, L., Hitzeroth, I. I., Meyers, A. E. & Rybicki, E. P. Expression in tobacco and purification of beak and feather disease virus capsid protein fused to elastin-like polypeptides. *Journal of Virological Methods* **191**, 55-62, doi:10.1016/j.jviromet.2013.03.028 (2013).
49 Meyer, D. E. & Chilkoti, A. Purification of recombinant proteins by fusion with thermally-responsive polypeptides. *Nature biotechnology* **17**, 1112-1115, doi:10.1038/15100 (1999).
50 Ricard-Blum, S. The Collagen Family. *Cold Spring Harbor Perspectives in Biology* **3**, a004978-a004978, doi:10.1101/cshperspect.a004978 (2011).
51 Söderhäll, C. *et al.* Variants in a Novel Epidermal Collagen Gene (COL29A1) Are Associated with Atopic Dermatitis. *PLoS Biology* **5**, e242, doi:10.1371/journal.pbio.0050242 (2007).
52 *Structure and function of collagen types*. (Academic Press, 1987).
53 Fratzl, P. *Collagen structure and mechanics*. (Springer, 2008).
54 Shoulders, M. D. & Raines, R. T. Collagen Structure and Stability. *Annual Review of Biochemistry* **78**, 929-958, doi:10.1146/annurev.biochem.77.032207.120833 (2009).
55 Fallas, J. A., O'Leary, L. E. R. & Hartgerink, J. D. Synthetic collagen mimics: self-assembly of homotrimers, heterotrimers and higher order structures. *Chemical Society Reviews* **39**, 3510, doi:10.1039/b919455j (2010).
56 Jalan, A. A., Demeler, B. & Hartgerink, J. D. Hydroxyproline-Free Single Composition ABC Collagen Heterotrimer. *Journal of the American Chemical Society* **135**, 6014-6017, doi:10.1021/ja402187t (2013).
57 Xu, Y. Streptococcal Scl1 and Scl2 Proteins Form Collagen-like Triple Helices. *Journal of Biological Chemistry* **277**, 27312-27318, doi:10.1074/jbc.M201163200 (2002).
58 Yoshizumi, A. *et al.* Self-association of *streptococcus pyogenes* collagen-like constructs into higher order structures. *Protein Science* **18**, 1241-1251, doi:10.1002/pro.134 (2009).
59 Yu, Z., An, B., Ramshaw, J. A. M. & Brodsky, B. Bacterial collagen-like proteins that form triple-helical structures. *Journal of Structural Biology* **186**, 451-461, doi:10.1016/j.jsb.2014.01.003 (2014).
60 Chung, W.-J. *et al.* Biomimetic self-templating supramolecular structures. *Nature* **478**, 364-368, doi:10.1038/nature10513 (2011).
61 Rele, S. *et al.* D-Periodic Collagen-Mimetic Microfibers. *Journal of the American Chemical Society* **129**, 14780-14787, doi:10.1021/ja0758990 (2007).
62 Askarieh, G. *et al.* Self-assembly of spider silk proteins is controlled by a pH-sensitive relay. *Nature* **465**, 236-238, doi:10.1038/nature08962 (2010).
63 Gosline, J. M., DeMont, M. E. & Denny, M. W. The structure and properties of spider silk. *Endeavour* **10**, 37-43, doi:10.1016/0160-9327(86)90049-9 (1986).
64 Tokareva, O., Michalczechen-Lacerda, V. A., Rech, E. L. & Kaplan, D. L. Recombinant DNA production of spider silk proteins. *Microbial biotechnology* **6**, 651-663, doi:10.1111/1751-7915.12081 (2013).

65 Adrianos, S. L. *et al.* Nephila clavipes Flagelliform Silk-Like GGX Motifs Contribute to Extensibility and Spacer Motifs Contribute to Strength in Synthetic Spider Silk Fibers. *Biomacromolecules* **14**, 1751-1760, doi:10.1021/bm400125w (2013).
66 Teulé, F. *et al.* Combining flagelliform and dragline spider silk motifs to produce tunable synthetic biopolymer fibers. *Biopolymers* **97**, 418-431, doi:10.1002/bip.21724 (2012).
67 Chung, H., Kim, T. Y. & Lee, S. Y. Recent advances in production of recombinant spider silk proteins. *Current Opinion in Biotechnology* **23**, 957-964, doi:10.1016/j.copbio.2012.03.013 (2012).
68 Xia, X.-X. *et al.* Native-sized recombinant spider silk protein produced in metabolically engineered Escherichia coli results in a strong fiber. *Proceedings of the National Academy of Sciences* **107**, 14059-14063, doi:10.1073/pnas.1003366107 (2010).
69 Eisoldt, L., Smith, A. & Scheibel, T. Decoding the secrets of spider silk. *Materials Today* **14**, 80-86, doi:10.1016/S1369-7021(11)70057-8 (2011).
70 Albertson, A. E., Teulé, F., Weber, W., Yarger, J. L. & Lewis, R. V. Effects of different post-spin stretching conditions on the mechanical properties of synthetic spider silk fibers. *Journal of the Mechanical Behavior of Biomedical Materials* **29**, 225-234, doi:10.1016/j.jmbbm.2013.09.002 (2014).
71 An, B., Hinman, M. B., Holland, G. P., Yarger, J. L. & Lewis, R. V. Inducing β-Sheets Formation in Synthetic Spider Silk Fibers by Aqueous Post-Spin Stretching. *Biomacromolecules* **12**, 2375-2381, doi:10.1021/bm200463e (2011).
72 Renberg, B., Andersson-Svahn, H. & Hedhammar, M. Mimicking silk spinning in a microchip. *Sensors and Actuators B: Chemical* **195**, 404-408, doi:10.1016/j.snb.2014.01.023 (2014).
73 Sutherland, T. D., Weisman, S., Walker, A. A. & Mudie, S. T. The coiled coil silk of bees, ants, and hornets. *Biopolymers* **97**, 446-454, doi:10.1002/bip.21702 (2012).
74 Weisman, S. *et al.* Honeybee silk: Recombinant protein production, assembly and fiber spinning. *Biomaterials* **31**, 2695-2700, doi:10.1016/j.biomaterials.2009.12.021 (2010).
75 Sutherland, T. D. *et al.* Single Honeybee Silk Protein Mimics Properties of Multi-Protein Silk. *PLoS ONE* **6**, e16489, doi:10.1371/journal.pone.0016489 (2011).
76 Wittmer, C. R. *et al.* Production, structure and in vitro degradation of electrospun honeybee silk nanofibers. *Acta Biomaterialia* **7**, 3789-3795, doi:10.1016/j.actbio.2011.06.001 (2011).
77 Elvin, C. M. *et al.* Synthesis and properties of crosslinked recombinant pro-resilin. *Nature* **437**, 999-1002, doi:10.1038/nature04085 (2005).
78 Qin, G., Hu, X., Cebe, P. & Kaplan, D. L. Mechanism of resilin elasticity. *Nature Communications* **3**, 1003, doi:10.1038/ncomms2004 (2012).
79 Dutta, N. K. *et al.* A Genetically Engineered Protein Responsive to Multiple Stimuli. *Angewandte Chemie International Edition* **50**, 4428-4431, doi:10.1002/anie.201007920 (2011).
80 Srokowski, E. M. & Woodhouse, K. A. Evaluation of the bulk platelet response and fibrinogen interaction to elastin-like polypeptide coatings: Bulk Platelet

Response and Fibrinogen Interaction. *Journal of Biomedical Materials Research Part A* **102**, 540-551, doi:10.1002/jbm.a.34699 (2014).
81 Woodhouse, K. A. *et al.* Investigation of recombinant human elastin polypeptides as non-thrombogenic coatings. *Biomaterials* **25**, 4543-4553, doi:10.1016/j.biomaterials.2003.11.043 (2004).
82 McKenna, K. A. *et al.* Mechanical property characterization of electrospun recombinant human tropoelastin for vascular graft biomaterials. *Acta Biomaterialia* **8**, 225-233, doi:10.1016/j.actbio.2011.08.001 (2012).
83 McKenna, K. A. *et al.* Structural and cellular characterization of electrospun recombinant human tropoelastin biomaterials. *Journal of Biomaterials Applications* **27**, 219-230, doi:10.1177/0885328211399480 (2012).
84 Nivison-Smith, L., Rnjak, J. & Weiss, A. S. Synthetic human elastin microfibers: Stable cross-linked tropoelastin and cell interactive constructs for tissue engineering applications. *Acta Biomaterialia* **6**, 354-359, doi:10.1016/j.actbio.2009.08.011 (2010).
85 Bax, D. V., Rodgers, U. R., Bilek, M. M. M. & Weiss, A. S. Cell Adhesion to Tropoelastin Is Mediated via the C-terminal GRKRK Motif and Integrin V 3. *Journal of Biological Chemistry* **284**, 28616-28623, doi:10.1074/jbc.M109.017525 (2009).
86 Benitez, P. L. *et al.* Sequence-Specific Crosslinking of Electrospun, Elastin-Like Protein Preserves Bioactivity and Native-Like Mechanics. *Adv. Healthc. Mater.* **2**, 114-118, doi:10.1002/adhm.201200115 (2013).
87 Huang, L. *et al.* Generation of Synthetic Elastin-Mimetic Small Diameter Fibers and Fiber Networks. *Macromolecules* **33**, 2989-2997, doi:10.1021/ma991858f (2000).
88 Koombhongse, S., Liu, W. & Reneker, D. H. Flat polymer ribbons and other shapes by electrospinning. *Journal of Polymer Science Part B: Polymer Physics* **39**, 2598-2606, doi:10.1002/polb.10015 (2001).
89 Annabi, N. *et al.* Engineered cell-laden human protein-based elastomer. *Biomaterials* **34**, 5496-5505, doi:10.1016/j.biomaterials.2013.03.076 (2013).
90 Annabi, N. *et al.* Highly Elastic Micropatterned Hydrogel for Engineering Functional Cardiac Tissue. *Advanced Functional Materials* **23**, 4950-4959, doi:10.1002/adfm.201300570 (2013).
91 Tu, Y., Wise, S. G. & Weiss, A. S. Stages in tropoelastin coalescence during synthetic elastin hydrogel formation. *Micron* **41**, 268-272, doi:10.1016/j.micron.2009.11.003 (2010).
92 Annabi, N., Fathi, A., Mithieux, S. M., Weiss, A. S. & Dehghani, F. Fabrication of porous PCL/elastin composite scaffolds for tissue engineering applications. *The Journal of Supercritical Fluids* **59**, 157-167, doi:10.1016/j.supflu.2011.06.010 (2011).
93 Tu, Y., Mithieux, S. M., Annabi, N., Boughton, E. A. & Weiss, A. S. Synthetic elastin hydrogels that are coblended with heparin display substantial swelling, increased porosity, and improved cell penetration. *Journal of Biomedical Materials Research Part A* **95A**, 1215-1222, doi:10.1002/jbm.a.32950 (2010).

94 Ford, A. C., Machula, H., Kellar, R. S. & Nelson, B. A. Characterizing the mechanical properties of tropoelastin protein scaffolds. *MRS Proceedings* **1569**, doi:10.1557/opl.2013.1059 (2013).
95 Hu, X. *et al.* Charge-Tunable Autoclaved Silk-Tropoelastin Protein Alloys That Control Neuron Cell Responses. *Advanced Functional Materials* **23**, 3875-3884, doi:10.1002/adfm.201202685 (2013).
96 Hu, X., Wang, X., Rnjak, J., Weiss, A. S. & Kaplan, D. L. Biomaterials derived from silk–tropoelastin protein systems. *Biomaterials* **31**, 8121-8131, doi:10.1016/j.biomaterials.2010.07.044 (2010).
97 Liu, H. *et al.* Biocompatibility of silk-tropoelastin protein polymers. *Biomaterials* **35**, 5138-5147, doi:10.1016/j.biomaterials.2014.03.024 (2014).
98 Trabbic-Carlson, K., Setton, L. A. & Chilkoti, A. Swelling and Mechanical Behaviors of Chemically Cross-Linked Hydrogels of Elastin-like Polypeptides. *Biomacromolecules* **4**, 572-580, doi:10.1021/bm025671z (2003).
99 Wang, E., Desai, M. S. & Lee, S.-W. Light-Controlled Graphene-Elastin Composite Hydrogel Actuators. *Nano Letters* **13**, 2826-2830, doi:10.1021/nl401088b (2013).
100 Orive, G. *et al.* Cell encapsulation: Promise and progress. *Nature Medicine* **9**, 104-107, doi:10.1038/nm0103-104 (2003).
101 McHale, M. K., Setton, L. A. & Chilkoti, A. Synthesis and in vitro evaluation of enzymatically cross-linked elastin-like polypeptide gels for cartilaginous tissue repair. *Tissue engineering* **11**, 1768-1779, doi:10.1089/ten.2005.11.1768 (2005).
102 Lim, D. W., Nettles, D. L., Setton, L. A. & Chilkoti, A. Rapid Cross-Linking of Elastin-like Polypeptides with (Hydroxymethyl)phosphines in Aqueous Solution. *Biomacromolecules* **8**, 1463-1470, doi:10.1021/bm061059m (2007).
103 Lim, D. W., Nettles, D. L., Setton, L. A. & Chilkoti, A. In situ cross-linkinig of elastin-like polypeptide block copolymers for tissue repair. *Biomacromolecules* **9**, 222-230, doi:10.1021/bm7007982 (2008).
104 Chung, C., Lampe, K. J. & Heilshorn, S. C. Tetrakis(hydroxymethyl) Phosphonium Chloride as a Covalent Cross-Linking Agent for Cell Encapsulation within Protein-Based Hydrogels. *Biomacromolecules* **13**, 3912-3916, doi:10.1021/bm3015279 (2012).
105 Cai, L., Dinh, C. B. & Heilshorn, S. C. One-pot synthesis of elastin-like polypeptide hydrogels with grafted VEGF-mimetic peptides. *Biomaterials Science* **2**, 757-765, doi:10.1039/c3bm60293a (2014).
106 Lampe, K. J., Antaris, A. L. & Heilshorn, S. C. Design of three-dimensional engineered protein hydrogels for tailored control of neurite growth. *Acta Biomaterialia* **9**, 5590-5599, doi:10.1016/j.actbio.2012.10.033 (2013).
107 Asai, D. *et al.* Protein polymer hydrogels by in situ, rapid and reversible self-gelation. *Biomaterials* **33**, 5451-5458, doi:10.1016/j.biomaterials.2012.03.083 (2012).
108 Xu, D., Asai, D., Chilkoti, A. & Craig, S. L. Rheological Properties of Cysteine-Containing Elastin-Like Polypeptide Solutions and Hydrogels. *Biomacromolecules* **13**, 2315-2321, doi:10.1021/bm300760s (2012).

109 Baskin, J. M. *et al.* Copper-free click chemistry for dynamic in vivo imaging. *Proceedings of the National Academy of Sciences* **104**, 16793-16797, doi:10.1073/pnas.0707090104 (2007).
110 González de Torre, I. *et al.* Elastin-like recombinamer catalyst-free click gels: Characterization of poroelastic and intrinsic viscoelastic properties. *Acta Biomaterialia* **10**, 2495-2505, doi:10.1016/j.actbio.2014.02.006 (2014).
111 Teeuwen, R. L. M. *et al.* "Clickable" elastins: elastin-like polypeptides functionalized with azide or alkyne groups. *Chemical Communications*, 4022 4024, doi:10.1039/b903903a (2009).
112 Le, D. H. T. *et al.* Self-Assembly of Elastin–Mimetic Double Hydrophobic Polypeptides. *Biomacromolecules* **14**, 1028-1034, doi:10.1021/bm301887m (2013).
113 Morelli, M. A., DeBiasi, M., DeStradis, A. & Tamburro, A. M. An aggregating elastin-like pentapeptide. *Journal of biomolecular structure & dynamics* **11**, 181-190, doi:10.1080/07391102.1993.10508716 (1993).
114 Wright, E., McMillan, A., Cooper, A., Apkarian, R. & Conticello, V. Thermoplastic Elastomer Hydrogels via Self-Assembly of an Elastin-Mimetic Triblock Polypeptide. *Advanced Functional Materials* **12**, 149-154 (2002).
115 Wright, E. R. & Conticello, V. P. Self-assembly of block copolymers derived from elastin-mimetic polypeptide sequences. *Advanced Drug Delivery Reviews* **54**, 1057-1073, doi:10.1016/S0169-409X(02)00059-5 (2002).
116 Moscarelli, P. *et al.* Structural characterization and biological properties of the amyloidogenic elastin-like peptide (VGGVG)3. *Matrix biology: journal of the International Society for Matrix Biology*, doi:10.1016/j.matbio.2014.03.004 (2014).
117 Krishna, U. M., Martinez, A. W., Caves, J. M. & Chaikof, E. L. Hydrazone self-crosslinking of multiphase elastin-like block copolymer networks. *Acta Biomaterialia* **8**, 988-997, doi:10.1016/j.actbio.2011.11.024 (2012).
118 Sallach, R. E. *et al.* Elastin-mimetic protein polymers capable of physical and chemical crosslinking. *Biomaterials* **30**, 409-422, doi:10.1016/j.biomaterials.2008.09.040 (2009).
119 Di Zio, K. & Tirrell, D. A. Mechanical Properties of Artificial Protein Matrices Engineered for Control of Cell and Tissue Behavior. *Macromolecules* **36**, 1553-1558, doi:10.1021/ma0256587 (2003).
120 Liu, J. C. & Tirrell, D. A. Cell Response to RGD Density in Cross-Linked Artificial Extracellular Matrix Protein Films. *Biomacromolecules* **9**, 2984-2988, doi:10.1021/bm800469j (2008).
121 Singh, A. K., Srivastava, G. K., Martín, L., Alonso, M. & Pastor, J. C. Bioactive substrates for human retinal pigment epithelial cell growth from elastin-like recombinamers: Bioactive Substrates for Human Retinal Pigment Epithelial Cell Growth. *Journal of Biomedical Materials Research Part A* **102**, 639-646, doi:10.1002/jbm.a.34726 (2014).
122 Srivastava, G. K. *et al.* Elastin-like recombinamers as substrates for retinal pigment epithelial cell growth. *Journal of Biomedical Materials Research Part A* **97A**, 243-250, doi:10.1002/jbm.a.33050 (2011).

123 Heilshorn, S. C., Di Zio, K. A., Welsh, E. R. & Tirrell, D. A. Endothelial cell adhesion to the fibronectin CS5 domain in artificial extracellular matrix proteins. *Biomaterials* **24**, 4245-4252, doi:10.1016/S0142-9612(03)00294-1 (2003).
124 Liu, J. C., Heilshorn, S. C. & Tirrell, D. A. Comparative Cell Response to Artificial Extracellular Matrix Proteins Containing the RGD and CS5 Cell-Binding Domains. *Biomacromolecules* **5**, 497-504, doi:10.1021/bm034340z (2004).
125 Choi, S.-K., Park, J.-K., Lee, K.-M., Lee, S.-K. & Jeon, W. B. Improved neural progenitor cell proliferation and differentiation on poly(lactide- *co* -glycolide) scaffolds coated with elastin-like polypeptide: Plga Scaffold Functionalization with Thermoresponsive Biomimetic Matrix. *Journal of Biomedical Materials Research Part B: Applied Biomaterials* **101**, 1329-1339, doi:10.1002/jbm.b.32950 (2013).
126 Jeon, W. B., Park, B. H., Wei, J. & Park, R.-W. Stimulation of fibroblasts and neuroblasts on a biomimetic extracellular matrix consisting of tandem repeats of the elastic VGVPG domain and RGD motif. *Journal of Biomedical Materials Research Part A* **97A**, 152-157, doi:10.1002/jbm.a.33041 (2011).
127 Punet, X. *et al.* Enhanced Cell-Material Interactions through the Biofunctionalization of Polymeric Surfaces with Engineered Peptides. *Biomacromolecules* **14**, 2690-2702, doi:10.1021/bm4005436 (2013).
128 Tejeda-Montes, E. *et al.* Bioactive membranes for bone regeneration applications: Effect of physical and biomolecular signals on mesenchymal stem cell behavior. *Acta Biomaterialia* **10**, 134-141, doi:10.1016/j.actbio.2013.09.001 (2014).
129 Nagapudi, K. *et al.* Photomediated Solid-State Cross-Linking of an Elastin−Mimetic Recombinant Protein Polymer. *Macromolecules* **35**, 1730-1737, doi:10.1021/ma011429t (2002).
130 Arnoczky, S. P., Warren, R. F. & Ashlock, M. A. Replacement of the anterior cruciate ligament using a patellar tendon allograft. An experimental study. *The Journal of bone and joint surgery. American volume* **68**, 376-385 (1986).
131 Milthorpe, B. K. Xenografts for tendon and ligament repair. *Biomaterials* **15**, 745-752, doi:10.1016/0142-9612(94)90027-2 (1994).
132 Schwartz, Z. *et al.* Ability of Commercial Demineralized Freeze-Dried Bone Allograft to Induce New Bone Formation. *Journal of Periodontology* **67**, 918-926, doi:10.1902/jop.1996.67.9.918 (1996).
133 Hughes, C. S., Postovit, L. M. & Lajoie, G. A. Matrigel: A complex protein mixture required for optimal growth of cell culture. *PROTEOMICS* **10**, 1886-1890, doi:10.1002/pmic.200900758 (2010).
134 Báez, J., Olsen, D. & Polarek, J. W. Recombinant microbial systems for the production of human collagen and gelatin. *Applied microbiology and biotechnology* **69**, 245-252, doi:10.1007/s00253-005-0180-x (2005).
135 Stein, H. *et al.* Production of Bioactive, Post-Translationally Modified, Heterotrimeric, Human Recombinant Type-I Collagen in Transgenic Tobacco †. *Biomacromolecules* **10**, 2640-2645, doi:10.1021/bm900571b (2009).
136 Shilo, S. *et al.* Cutaneous Wound Healing After Treatment with Plant-Derived Human Recombinant Collagen Flowable Gel. *Tissue Engineering Part A* **19**, 1519-1526, doi:10.1089/ten.tea.2012.0345 (2013).

137 Liu, W. *et al.* Recombinant human collagen for tissue engineered corneal substitutes. *Biomaterials* **29**, 1147-1158, doi:10.1016/j.biomaterials.2007.11.011 (2008).
138 Merrett, K. *et al.* Tissue-Engineered Recombinant Human Collagen-Based Corneal Substitutes for Implantation: Performance of Type I versus Type III Collagen. *Investigative Ophthalmology & Visual Science* **49**, 3887-3894, doi:10.1167/iovs.07-1348 (2008).
139 Fagerholm, P., Lagali, N. S., Carlsson, D. J., Merrett, K. & Griffith, M. Corneal Regeneration Following Implantation of a Biomimetic Tissue-Engineered Substitute. *Clinical and Translational Science* **2**, 162-164, doi:10.1111/j.1752-8062.2008.00083.x (2009).
140 Fagerholm, P. *et al.* A Biosynthetic Alternative to Human Donor Tissue for Inducing Corneal Regeneration: 24-Month Follow-Up of a Phase 1 Clinical Study. *Science Translational Medicine* **2**, 46ra61, doi:10.1126/scitranslmed.3001022 (2010).
141 Pulkkinen, H. J. *et al.* Recombinant human type II collagen as a material for cartilage tissue engineering. *The International journal of artificial organs* **31**, 960-969 (2008).
142 Pulkkinen, H. J. *et al.* Engineering of cartilage in recombinant human type II collagen gel in nude mouse model in vivo. *Osteoarthritis and Cartilage* **18**, 1077-1087, doi:10.1016/j.joca.2010.05.004 (2010).
143 Pulkkinen, H. J. *et al.* Repair of osteochondral defects with recombinant human type II collagen gel and autologous chondrocytes in rabbit. *Osteoarthritis and Cartilage* **21**, 481-490, doi:10.1016/j.joca.2012.12.004 (2013).
144 Werten, M. W. T. *et al.* Precision Gels from Collagen-Inspired Triblock Copolymers. *Biomacromolecules* **10**, 1106-1113, doi:10.1021/bm801299u (2009).
145 Silva, C. I. F. *et al.* Tuning of Collagen Triple-Helix Stability in Recombinant Telechelic Polymers. *Biomacromolecules* **13**, 1250-1258, doi:10.1021/bm300323q (2012).
146 Peng, Y. Y. *et al.* Towards scalable production of a collagen-like protein from Streptococcus pyogenes for biomedical applications. *Microbial Cell Factories* **11**, 146, doi:10.1186/1475-2859-11-146 (2012).
147 Peng, Y. Y. *et al.* A Streptococcus pyogenes derived collagen-like protein as a non-cytotoxic and non-immunogenic cross-linkable biomaterial. *Biomaterials* **31**, 2755-2761, doi:10.1016/j.biomaterials.2009.12.040 (2010).
148 Peng, Y. Y., Stoichevska, V., Schacht, K., Werkmeister, J. A. & Ramshaw, J. A. M. Engineering multiple biological functional motifs into a blank collagen-like protein template from *Streptococcus pyogenes*: New Functional Sites in a Bacterial Collagen. *Journal of Biomedical Materials Research Part A* **102**, 2189-2196, doi:10.1002/jbm.a.34898 (2013).
149 Kundu, B. *et al.* Silk proteins for biomedical applications: Bioengineering perspectives. *Progress in Polymer Science* **39**, 251-267, doi:10.1016/j.progpolymsci.2013.09.002 (2014).
150 Perrone, G. S. *et al.* The use of silk-based devices for fracture fixation. *Nature Communications* **5**, 3385, doi:10.1038/ncomms4385 (2014).

151 Gellynck, K. *et al.* Silkworm and spider silk scaffolds for chondrocyte support. *Journal of Materials Science: Materials in Medicine* **19**, 3399-3409, doi:10.1007/s10856-008-3474-6 (2008).
152 Wendt, H. *et al.* Artificial Skin – Culturing of Different Skin Cell Lines for Generating an Artificial Skin Substitute on Cross-Weaved Spider Silk Fibres. *PLoS ONE* **6**, e21833, doi:10.1371/journal.pone.0021833 (2011).
153 Arcidiacono, S., Mello, C., Kaplan, D., Cheley, S. & Bayley, H. Purification and characterization of recombinant spider silk expressed in Escherichia coli. *Applied Microbiology and Biotechnology* **49**, 31-38, doi:10.1007/s002530051133 (1998).
154 Lazaris, A. Spider Silk Fibers Spun from Soluble Recombinant Silk Produced in Mammalian Cells. *Science* **295**, 472-476, doi:10.1126/science.1065780 (2002).
155 Winkler, S. *et al.* Designing recombinant spider silk proteins to control assembly. *International Journal of Biological Macromolecules* **24**, 265-270, doi:10.1016/S0141-8130(98)00088-9 (1999).
156 Vendrely, C. & Scheibel, T. Biotechnological Production of Spider-Silk Proteins Enables New Applications. *Macromolecular Bioscience* **7**, 401-409, doi:10.1002/mabi.200600255 (2007).
157 Teulé, F. *et al.* Silkworms transformed with chimeric silkworm/spider silk genes spin composite silk fibers with improved mechanical properties. *Proceedings of the National Academy of Sciences* **109**, 923-928, doi:10.1073/pnas.1109420109 (2012).
158 Moisenovich, M. M. *et al.* In vitro and in vivo biocompatibility studies of a recombinant analogue of spidroin 1 scaffolds. *Journal of Biomedical Materials Research Part A* **96A**, 125-131, doi:10.1002/jbm.a.32968 (2011).
159 Moisenovich, M. M. *et al.* Tissue regeneration in vivo within recombinant spidroin 1 scaffolds. *Biomaterials* **33**, 3887-3898, doi:10.1016/j.biomaterials.2012.02.013 (2012).
160 Wong Po Foo, C. *et al.* Novel nanocomposites from spider silk-silica fusion (chimeric) proteins. *Proceedings of the National Academy of Sciences* **103**, 9428-9433, doi:10.1073/pnas.0601096103 (2006).
161 Huang, J., Wong, C., George, A. & Kaplan, D. L. The effect of genetically engineered spider silk-dentin matrix protein 1 chimeric protein on hydroxyapatite nucleation. *Biomaterials* **28**, 2358-2367, doi:10.1016/j.biomaterials.2006.11.021 (2007).
162 Humenik, M., Smith, A. M. & Scheibel, T. Recombinant Spider Silks—Biopolymers with Potential for Future Applications. *Polymers* **3**, 640-661, doi:10.3390/polym3010640 (2011).
163 Rammensee, S., Huemmerich, D., Hermanson, K. D., Scheibel, T. & Bausch, A. R. Rheological characterization of hydrogels formed by recombinantly produced spider silk. *Applied Physics A* **82**, 261-264, doi:10.1007/s00339-005-3431-x (2006).
164 Slotta, U. *et al.* Spider Silk and Amyloid Fibrils: A Structural Comparison. *Macromolecular Bioscience* **7**, 183-188, doi:10.1002/mabi.200600201 (2007).
165 Schacht, K. & Scheibel, T. Controlled Hydrogel Formation of a Recombinant Spider Silk Protein. *Biomacromolecules* **12**, 2488-2495, doi:10.1021/bm200154k (2011).

166 Leal-Egaña, A. *et al.* Interactions of Fibroblasts with Different Morphologies Made of an Engineered Spider Silk Protein. *Advanced Engineering Materials* **14**, B67-B75, doi:10.1002/adem.201180072 (2012).
167 Bauer, F., Wohlrab, S. & Scheibel, T. Controllable cell adhesion, growth and orientation on layered silk protein films. *Biomaterials Science* **1**, 1244-1249, doi:10.1039/c3bm60114e (2013).
168 Schulte, V. A., Díez, M., Möller, M. & Lensen, M. C. Surface Topography Induces Fibroblast Adhesion on Intrinsically Nonadhesive Poly(ethylene glycol) Substrates. *Biomacromolecules* **10**, 2795-2801, doi:10.1021/bm900631s (2009).
169 Widhe, M. *et al.* Recombinant spider silk as matrices for cell culture. *Biomaterials* **31**, 9575-9585, doi:10.1016/j.biomaterials.2010.08.061 (2010).
170 Lewicka, M., Hermanson, O. & Rising, A. U. Recombinant spider silk matrices for neural stem cell cultures. *Biomaterials* **33**, 7712-7717, doi:10.1016/j.biomaterials.2012.07.021 (2012).
171 Widhe, M., Johansson, U., Hillerdahl, C.-O. & Hedhammar, M. Recombinant spider silk with cell binding motifs for specific adherence of cells. *Biomaterials* **34**, 8223-8234, doi:10.1016/j.biomaterials.2013.07.058 (2013).
172 Jansson, R. *et al.* Recombinant spider silk genetically functionalized with affinity domains. *Biomacromolecules* **15**, 1696-1706, doi:10.1021/bm500114e (2014).
173 Qin, G. *et al.* Expression, Cross-Linking, and Characterization of Recombinant Chitin Binding Resilin. *Biomacromolecules* **10**, 3227-3234, doi:10.1021/bm900735g (2009).
174 Qin, G. *et al.* Recombinant exon-encoded resilins for elastomeric biomaterials. *Biomaterials* **32**, 9231-9243, doi:10.1016/j.biomaterials.2011.06.010 (2011).
175 Charati, M. B., Ifkovits, J. L., Burdick, J. A., Linhardt, J. G. & Kiick, K. L. Hydrophilic elastomeric biomaterials based on resilin-like polypeptides. *Soft Matter* **5**, 3412, doi:10.1039/b910980c (2009).
176 Li, L., Teller, S., Clifton, R. J., Jia, X. & Kiick, K. L. Tunable Mechanical Stability and Deformation Response of a Resilin-Based Elastomer. *Biomacromolecules* **12**, 2302-2310, doi:10.1021/bm200373p (2011).
177 Li, L. & Kiick, K. L. Transient dynamic mechanical properties of resilin-based elastomeric hydrogels. *Frontiers in Chemistry* **2**, doi:10.3389/fchem.2014.00021 (2014).
178 McGann, C. L., Levenson, E. A. & Kiick, K. L. Resilin-Based Hybrid Hydrogels for Cardiovascular Tissue Engineering. *Macromolecular Chemistry and Physics* **214**, 203-213, doi:10.1002/macp.201200412 (2013).
179 Renner, J. N., Cherry, K. M., Su, R. S.-C. & Liu, J. C. Characterization of Resilin-Based Materials for Tissue Engineering Applications. *Biomacromolecules* **13**, 3678-3685, doi:10.1021/bm301129b (2012).
180 Kim, Y., Renner, J. N. & Liu, J. C. Incorporating the BMP-2 peptide in genetically-engineered biomaterials accelerates osteogenic differentiation. *Biomaterials Science* **2**, 1110, doi:10.1039/c3bm60333d (2014).
181 Desai, M. S. *et al.* Elastin-Based Rubber-Like Hydrogels. *Biomacromolecules* **17**, 2409-2416, doi:10.1021/acs.biomac.6b00515 (2016).

182 Leggat, P. A., Smith, D. R. & Kedjarune, U. Surgical applications of cyanoacrylate adhesives: A review of toxicity. *ANZ J. Surg.* **77**, 209-213, doi:10.1111/j.1445-2197.2007.04020.x (2007).
183 Singer, A. J., Quinn, J. V. & Hollander, J. E. The cyanoacrylate topical skin adhesives. *The American Journal of Emergency Medicine* **26**, 490-496, doi:10.1016/j.ajem.2007.05.015 (2008).
184 Bouten, P. J. M. *et al.* The chemistry of tissue adhesive materials. *Progress in Polymer Science* **39**, 1375-1405, doi:10.1016/j.progpolymsci.2014.02.001 (2014).
185 Zeng, Q. Y. *et al.* Self-Healing Elastin-Bioglass Hydrogels. *Biomacromolecules* **17**, 2619-2625, doi:10.1021/acs.biomac.6b00621 (2016).
186 Utech, S. & Boccaccini, A. R. A review of hydrogel-based composites for biomedical applications: enhancement of hydrogel properties by addition of rigid inorganic fillers. *Journal of Materials Science* **51**, 271-310, doi:10.1007/s10853-015-9382-5 (2016).
187 Kaur, G. *et al.* A review of bioactive glasses: Their structure, properties, fabrication and apatite formation. *Journal of Biomedical Materials Research Part A* **102**, 254-274, doi:10.1002/jbm.a.34690 (2014).
188 Fan, X. D. & Yun, S. H. The potential of optofluidic biolasers. *Nat. Methods* **11**, 141-147, doi:10.1038/nmeth.2805 (2014).
189 Svelto, O. *Principles of Lasers*. (Springer US, 2010).
190 Quan, H. *Characterization of Optical Whispering Gallery Mode Resonance and Applications*. (Rutgers The State University of New Jersey - New Brunswick, 2006).
191 Chow, D. C., Dreher, M. R., Trabbic-Carlson, K. & Chilkoti, A. Ultra-High Expression of a Thermally Responsive Recombinant Fusion Protein in E. coli. *Biotechnology Progress* **22**, 638-646, doi:10.1021/bp0503742 (2006).
192 Peppas, N. A., Hilt, J. Z., Khademhosseini, A. & Langer, R. Hydrogels in biology and medicine: From molecular principles to bionanotechnology. *Advanced Materials* **18**, 1345-1360, doi:10.1002/adma.200501612 (2006).
193 Peak, C. W., Wilker, J. J. & Schmidt, G. A review on tough and sticky hydrogels. *Colloid and Polymer Science* **291**, 2031-2047, doi:10.1007/s00396-013-3021-y (2013).
194 Yang, Y. & Urban, M. W. Self-healing polymeric materials. *Chemical Society Reviews* **42**, 7446-7467, doi:10.1039/C3CS60109A (2013).
195 Hoffman, A. S. Hydrogels for biomedical applications. *Advanced Drug Delivery Reviews* **64**, 18-23, doi:10.1016/j.addr.2012.09.010 (2012).
196 Mano, J. F. Stimuli-Responsive Polymeric Systems for Biomedical Applications. *Advanced Engineering Materials* **10**, 515-527, doi:10.1002/adem.200700355 (2008).
197 Gong, J. P., Katsuyama, Y., Kurokawa, T. & Osada, Y. Double-Network Hydrogels with Extremely High Mechanical Strength. *Advanced Materials* **15**, 1155-1158, doi:10.1002/adma.200304907 (2003).
198 Brown, H. R. A Model of the Fracture of Double Network Gels. *Macromolecules* **40**, 3815-3818, doi:10.1021/ma062642y (2007).
199 Sun, J.-Y. *et al.* Highly stretchable and tough hydrogels. *Nature* **489**, 133-136, doi:10.1038/nature11409 (2012).

200 Gaharwar, A. K., Dammu, S. A., Canter, J. M., Wu, C. J. & Schmidt, G. Highly Extensible, Tough, and Elastomeric Nanocomposite Hydrogels from Poly(ethylene glycol) and Hydroxyapatite Nanoparticles. *Biomacromolecules* **12**, 1641-1650, doi:10.1021/bm200027z (2011).
201 Gaharwar, A. K., Rivera, C. P., Wu, C. J. & Schmidt, G. Transparent, elastomeric and tough hydrogels from poly(ethylene glycol) and silicate nanoparticles. *Acta Biomaterialia* **7**, 4139-4148, doi:10.1016/j.actbio.2011.07.023 (2011).
202 Liu, J. *et al.* Synthesis of Graphene Peroxide and Its Application in Fabricating Super Extensible and Highly Resilient Nanocomposite Hydrogels. *ACS Nano* **6**, 8194-8202, doi:10.1021/nn302874v (2012).
203 Okumura, Y. & Ito, K. The Polyrotaxane Gel: A Topological Gel by Figure-of-Eight Cross-links. *Advanced Materials* **13**, 485-487, doi:10.1002/1521-4095(200104)13:7<485::AID-ADMA485>3.0.CO;2-T (2001).
204 Ito, K. Novel Cross-Linking Concept of Polymer Network: Synthesis, Structure, and Properties of Slide-Ring Gels with Freely Movable Junctions. *Polymer Journal* **39**, 489-499 (2007).
205 Webber, R. E., Creton, C., Brown, H. R. & Gong, J. P. Large Strain Hysteresis and Mullins Effect of Tough Double-Network Hydrogels. *Macromolecules* **40**, 2919-2927, doi:10.1021/ma062924y (2007).
206 Kato, K., Yasuda, T. & Ito, K. Viscoelastic Properties of Slide-Ring Gels Reflecting Sliding Dynamics of Partial Chains and Entropy of Ring Components. *Macromolecules* **46**, 310-316, doi:10.1021/ma3021135 (2013).
207 Malkoch, M. *et al.* Synthesis of well-defined hydrogel networks using Click chemistry. *Chemical Communications*, 2774-2776, doi:10.1039/B603438A (2006).
208 Meyer, D. E. & Chilkoti, A. Quantification of the Effects of Chain Length and Concentration on the Thermal Behavior of Elastin-like Polypeptides. *Biomacromolecules* **5**, 846-851, doi:10.1021/bm034215n (2004).
209 Cho, Y. *et al.* Effects of Hofmeister Anions on the Phase Transition Temperature of Elastin-like Polypeptides. *Journal of Physical Chemistry B* **112**, 13765-13771, doi:10.1021/jp8062977 (2008).
210 MacKay, J. A., Callahan, D. J., FitzGerald, K. N. & Chilkoti, A. Quantitative Model of the Phase Behavior of Recombinant pH-Responsive Elastin-Like Polypeptides. *Biomacromolecules* **11**, 2873-2879, doi:10.1021/bm100571j (2010).
211 Rodríguez-Cabello, J. C. *et al.* Endothermic and exothermic components of an inverse temperature transition for hydrophobic association by TMDSC. *Chemical Physics Letters* **388**, 127-131, doi:10.1016/j.cplett.2004.03.013 (2004).
212 Zhao, B., Li, N. K., Yingling, Y. G. & Hall, C. K. LCST Behavior is Manifested in a Single Molecule: Elastin-Like polypeptide (VPGVG)n. *Biomacromolecules* **17**, 111-118, doi:10.1021/acs.biomac.5b01235 (2016).
213 Zhang, Y. N. *et al.* A Highly Elastic and Rapidly Crosslinkable Elastin-Like Polypeptide-Based Hydrogel for Biomedical Applications. *Advanced Functional Materials* **25**, 4814-4826, doi:10.1002/adfm.201501489 (2015).
214 Scognamiglio, F. *et al.* Adhesive and sealant interfaces for general surgery applications. *Journal of Biomedical Materials Research Part B: Applied Biomaterials* **104**, 626-639, doi:10.1002/jbm.b.33409 (2016).

215 Joch, C. The safety of fibrin sealants. *Cardiovasc. Surg.* **11**, 23-28, doi:10.1016/s0967-2109(03)00068-1 (2003).
216 Seyednejad, H., Imani, N., Jamieson, T. & Seifalian, A. M. Topical haemostatic agents. *Br. J. Surg.* **95**, 1197-1225, doi:10.1002/bjs.6357 (2008).
217 Waite, J. H. Mussel adhesion - essential footwork. *J. Exp. Biol.* **220**, 517-530, doi:10.1242/jeb.134056 (2017).
218 Liu, Y., Meng, H., Messersmith, P. B., Lee, B. P. & Dalsin, J. L. in *Biological Adhesives* (ed Andrew M. Smith) 345-378 (Springer International Publishing, 2016).
219 Burke, S. A., Ritter-Jones, M., Lee, B. P. & Messersmith, P. B. Thermal gelation and tissue adhesion of biomimetic hydrogels. *Biomedical Materials* **2**, 203-210, doi:10.1088/1748-6041/2/4/001 (2007).
220 Brubaker, C. E. & Messersmith, P. B. Enzymatically Degradable Mussel-Inspired Adhesive Hydrogel. *Biomacromolecules* **12**, 4326-4334, doi:10.1021/bm201261d (2011).
221 Barrett, D. G., Bushnell, G. G. & Messersmith, P. B. Mechanically Robust, Negative-Swelling, Mussel-Inspired Tissue Adhesives. *Adv. Healthc. Mater.* **2**, 745-755, doi:10.1002/adhm.201200316 (2013).
222 Balakrishnan, B., Mohanty, M., Umashankar, P. R. & Jayakrishnan, A. Evaluation of an in situ forming hydrogel wound dressing based on oxidized alginate and gelatin. *Biomaterials* **26**, 6335-6342, doi:10.1016/j.biomaterials.2005.04.012 (2005).
223 Khor, E. & Lim, L. Y. Implantable applications of chitin and chitosan. *Biomaterials* **24**, 2339-2349, doi:10.1016/S0142-9612(03)00026-7 (2003).
224 Lutolf, M. P. & Hubbell, J. A. Synthetic biomaterials as instructive extracellular microenvironments for morphogenesis in tissue engineering. *Nat Biotech* **23**, 47-55, doi:10.1038/nbt1055 (2005).
225 Tan, H., Chu, C. R., Payne, K. A. & Marra, K. G. Injectable in situ forming biodegradable chitosan–hyaluronic acid based hydrogels for cartilage tissue engineering. *Biomaterials* **30**, 2499-2506, doi:10.1016/j.biomaterials.2008.12.080 (2009).
226 Bhattarai, N., Ramay, H. R., Gunn, J., Matsen, F. A. & Zhang, M. PEG-grafted chitosan as an injectable thermosensitive hydrogel for sustained protein release. *Journal of Controlled Release* **103**, 609-624, doi:10.1016/j.jconrel.2004.12.019 (2005).
227 Wang, F. *et al.* Injectable, rapid gelling and highly flexible hydrogel composites as growth factor and cell carriers. *Acta Biomaterialia* **6**, 1978-1991, doi:10.1016/j.actbio.2009.12.011 (2010).
228 Yang, J.-A., Yeom, J., Hwang, B. W., Hoffman, A. S. & Hahn, S. K. In situ-forming injectable hydrogels for regenerative medicine. *Progress in Polymer Science* **39**, 1973-1986, doi:10.1016/j.progpolymsci.2014.07.006 (2014).
229 Van Tomme, S. R., Storm, G. & Hennink, W. E. In situ gelling hydrogels for pharmaceutical and biomedical applications. *Int. J. Pharm.* **355**, 1-18, doi:10.1016/j.ijpharm.2008.01.057 (2008).
230 Yu, L. & Ding, J. D. Injectable hydrogels as unique biomedical materials. *Chemical Society Reviews* **37**, 1473-1481, doi:10.1039/b713009k (2008).

231 He, C. L., Kim, S. W. & Lee, D. S. In situ gelling stimuli-sensitive block copolymer hydrogels for drug delivery. *Journal of Controlled Release* **127**, 189-207, doi:10.1016/j.jconrel.2008.01.005 (2008).
232 Jin, R. *et al.* Synthesis and characterization of hyaluronic acid-poly(ethylene glycol) hydrogels via Michael addition: An injectable biomaterial for cartilage repair. *Acta Biomaterialia* **6**, 1968-1977, doi:10.1016/j.actbio.2009.12.024 (2010).
233 Chang, S. C. N. *et al.* Injection molding of chondrocyte/alginate constructs in the shape of facial implants. *J. Biomed. Mater. Res.* **55**, 503-511, doi:10.1002/1097-4636(20010615)55:4<503::aid-jbm1043>3.0.co;2-s (2001).
234 Urry, D. W. Protein elasticity based on conformations of sequential polypeptides - The biological elastic fiber. *Journal of Protein Chemistry* **3**, 403-436, doi:10.1007/bf01025061 (1984).
235 Betre, H. *et al.* Chondrocytic differentiation of human adipose-derived adult stem cells in elastin-like polypeptide. *Biomaterials* **27**, 91-99, doi:10.1016/j.biomaterials.2005.05.071 (2006).
236 Li, Y. P. *et al.* Hybrid Nanotopographical Surfaces Obtained by Biomimetic Mineralization of Statherin-Inspired Elastin-Like Recombinamers. *Adv. Healthc. Mater.* **3**, 1638-1647, doi:10.1002/adhm.201400015 (2014).
237 Costa, R. R. *et al.* Stimuli-Responsive Thin Coatings Using Elastin-Like Polymers for Biomedical Applications. *Advanced Functional Materials* **19**, 3210-3218, doi:10.1002/adfm.200900568 (2009).
238 Ghosh, K. *et al.* Temperature-dependent morphology of hybrid nanoflowers from elastin-like polypeptides. *Apl Materials* **2**, doi:10.1063/1.4863235 (2014).
239 Costa, R. R., Custodio, C. A., Arias, F. J., Rodriguez-Cabello, J. C. & Mano, J. F. Nanostructured and thermoresponsive recombinant biopolymer-based microcapsules for the delivery of active molecules. *Nanomedicine-Nanotechnology Biology and Medicine* **9**, 895-902, doi:10.1016/j.nano.2013.01.013 (2013).
240 Ding, F. Y. *et al.* A dynamic and self-crosslinked polysaccharide hydrogel with autonomous self-healing ability. *Soft Matter* **11**, 3971-3976, doi:10.1039/c5sm00587f (2015).
241 Zhang, Y. L., Tao, L., Li, S. X. & Wei, Y. Synthesis of Multiresponsive and Dynamic Chitosan-Based Hydrogels for Controlled Release of Bioactive Molecules. *Biomacromolecules* **12**, 2894-2901, doi:10.1021/bm200423f (2011).
242 Wojtecki, R. J., Meador, M. A. & Rowan, S. J. Using the dynamic bond to access macroscopically responsive structurally dynamic polymers. *Nature Materials* **10**, 14-27, doi:10.1038/nmat2891 (2011).
243 Hench, L. L. The story of Bioglass (R). *Journal of Materials Science-Materials in Medicine* **17**, 967-978, doi:10.1007/s10856-006-0432-z (2006).
244 Gorustovich, A. A., Roether, J. A. & Boccaccini, A. R. Effect of Bioactive Glasses on Angiogenesis: A Review of In Vitro and In Vivo Evidences. *Tissue Engineering Part B-Reviews* **16**, 199-207, doi:10.1089/ten.teb.2009.0416 (2010).
245 Hu, S., Chang, J., Liu, M. Q. & Ning, C. Q. Study on antibacterial effect of 45S5 Bioglass(A (R)). *Journal of Materials Science-Materials in Medicine* **20**, 281-286, doi:10.1007/s10856-008-3564-5 (2009).

246 Jones, J. R. Review of bioactive glass: From Hench to hybrids. *Acta Biomaterialia* **9**, 4457-4486, doi:10.1016/j.actbio.2012.08.023 (2013).
247 Miguez-Pacheco, V., Hench, L. L. & Boccaccini, A. R. Bioactive glasses beyond bone and teeth: Emerging applications in contact with soft tissues. *Acta Biomaterialia* **13**, 1-15, doi:10.1016/j.actbio.2014.11.004 (2015).
248 Zeng, Q. Y., Han, Y., Li, H. Y. & Chang, J. Design of a thermosensitive bioglass/agarose-alginate composite hydrogel for chronic wound healing. *Journal of Materials Chemistry B* **3**, 8856-8864, doi:10.1039/c5tb01758k (2015).
249 Stamboulis, A., Hench, L. L. & Boccaccini, A. R. Mechanical properties of biodegradable polymer sutures coated with bioactive glass. *Journal of Materials Science-Materials in Medicine* **13**, 843-848, doi:10.1023/a:1016544211478 (2002).
250 Zeng, Q. Y., Han, Y., Li, H. Y. & Chang, J. Bioglass/alginate composite hydrogel beads as cell carriers for bone regeneration. *Journal of Biomedical Materials Research Part B-Applied Biomaterials* **102**, 42-51, doi:10.1002/jbm.b.32978 (2014).
251 Kaur, G. *et al.* A review of bioactive glasses: Their structure, properties, fabrication, and apatite formation. *Journal of Biomedical Materials Research Part A* **102**, 254-274, doi:10.1002/jbm.a.34690 (2014).
252 Vollenweider, M. *et al.* Remineralization of human dentin using ultrafine bioactive glass particles. *Acta Biomaterialia* **3**, 936-943, doi:10.1016/j.actbio.2007.04.003 (2007).
253 Wu, C. T., Zhu, Y. F., Chang, J. A., Zhang, Y. F. & Xiao, Y. Bioactive inorganic-materials/alginate composite microspheres with controllable drug-delivery ability. *Journal of Biomedical Materials Research Part B-Applied Biomaterials* **94B**, 32-43, doi:10.1002/jbm.b.31621 (2010).
254 Wheeler, T. S., Sbravati, N. D. & Janorkar, A. V. Mechanical & Cell Culture Properties of Elastin-Like Polypeptide, Collagen, Bioglass, and Carbon Nanosphere Composites. *Annals of Biomedical Engineering* **41**, 2042-2055, doi:10.1007/s10439-013-0825-3 (2013).
255 Stoor, P., Söderling, E. & Salonen, J. I. Antibacterial effects of a bioactive glass paste on oral microorganisms. *Acta Odontologica Scandinavica* **56**, 161-165, doi:10.1080/000163598422901 (1998).
256 Wang, E., Desai, M. S., Heo, K. & Lee, S.-W. Graphene-Based Materials Functionalized with Elastin-like Polypeptides. *Langmuir* **30**, 2223-2229, doi:10.1021/la404333b (2014).
257 Maltby, J. G. & Primavesi, G. R. The Estimation of aldehydes, ketones and acetals by means of the hydroxylamine hydrochloride method. *Analyst* **74**, 498-502, doi:10.1039/an9497400498 (1949).
258 Haldar, U., Bauri, K., Li, R., Faust, R. & De, P. Polyisobutylene-Based pH-Responsive Self-Healing Polymeric Gels. *Acs Applied Materials & Interfaces* **7**, 8779-8788, doi:10.1021/acsami.5b01272 (2015).
259 Jin, Y. H., Wang, Q., Taynton, P. & Zhang, W. Dynamic Covalent Chemistry Approaches Toward Macrocycles, Molecular Cages, and Polymers. *Accounts of Chemical Research* **47**, 1575-1586, doi:10.1021/ar500037v (2014).

260 Wei, Z. *et al.* Novel Biocompatible Polysaccharide-Based Self-Healing Hydrogel. *Advanced Functional Materials* **25**, 1352-1359, doi:10.1002/adfm.201401502 (2015).
261 Blaiszik, B. J. *et al.* in *Annual Review of Materials Research* Vol. 40 *Annual Review of Materials Research* (eds D. R. Clarke, M. Ruhle, & F. Zok) 179-211 (2010).
262 Deng, G. H., Tang, C. M., Li, F. Y., Jiang, H. F. & Chen, Y. M. Covalent Cross-Linked Polymer Gels with Reversible Sol-Gel Transition and Self-Healing Properties. *Macromolecules* **43**, 1191-1194, doi:10.1021/ma9022197 (2010).
263 Canadell, J., Goossens, H. & Klumperman, B. Self-Healing Materials Based on Disulfide Links. *Macromolecules* **44**, 2536-2541, doi:10.1021/ma2001492 (2011).
264 Ghosh, S. K. *Self-healing Materials: Fundamentals, Design Strategies, and Applications*. (Wiley, 2009).
265 Livant, D. L. *et al.* The PHSRN sequence induces extracellular matrix invasion and accelerates wound healing in obese diabetic mice. *Journal of Clinical Investigation* **105**, 1537-1545, doi:10.1172/jci8527 (2000).
266 Miyamoto, T. *et al.* An integrin-activating peptide, PHSRN, ameliorates inhibitory effects of conventional peritoneal dialysis fluids on peritoneal wound healing. *Nephrology Dialysis Transplantation* **25**, 1109-1119, doi:10.1093/ndt/gfp601 (2010).
267 Hersel, U., Dahmen, C. & Kessler, H. RGD modified polymers: biomaterials for stimulated cell adhesion and beyond. *Biomaterials* **24**, 4385-4415, doi:10.1016/s0142-9612(03)00343-0 (2003).
268 Smith, G. P. & Petrenko, V. A. Phage display. *Chemical Reviews* **97**, 391-410, doi:10.1021/cr960065d (1997).
269 Hoppe, A., Guldal, N. S. & Boccaccini, A. R. A review of the biological response to ionic dissolution products from bioactive glasses and glass-ceramics. *Biomaterials* **32**, 2757-2774, doi:10.1016/j.biomaterials.2011.01.004 (2011).
270 Rabiee, S. M., Nazparvar, N., Azizian, M., Vashaee, D. & Tayebi, L. Effect of ion substitution on properties of bioactive glasses: A review. *Ceramics International* **41**, 7241-7251, doi:10.1016/j.ceramint.2015.02.140 (2015).
271 Lopez-Noriega, A., Arcos, D. & Vallet-Regi, M. Functionalizing Mesoporous Bioglasses for Long-Term Anti-Osteoporotic Drug Delivery. *Chemistry-a European Journal* **16**, 10879-10886, doi:10.1002/chem.201000137 (2010).
272 Xia, W. & Chang, J. Well-ordered mesoporous bioactive glasses (MBG): A promising bioactive drug delivery system. *Journal of Controlled Release* **110**, 522-530, doi:10.1016/j.jconrel.2005.11.002 (2006).
273 Miyawaki, A., Sawano, A. & Kogure, T. Lighting up cells: labelling proteins with fluorophores. *Nat. Rev. Mol. Cell Biol.*, S1-S7, doi:10.1038/ncb1031 (2003).
274 Giepmans, B. N. G., Adams, S. R., Ellisman, M. H. & Tsien, R. Y. Review - The fluorescent toolbox for assessing protein location and function. *Science* **312**, 217-224, doi:10.1126/science.1124618 (2006).
275 Alford, R. *et al.* Toxicity of Organic Fluorophores Used in Molecular Imaging: Literature Review. *Mol. Imaging* **8**, 341-354, doi:10.2310/7290.2009.00031 (2009).

276 van de Linde, S., Heilemann, M. & Sauer, M. in *Annual Review of Physical Chemistry* Vol. 63 *Annual Review of Physical Chemistry* (eds M. A. Johnson & T. J. Martinez) 519-540 (Annual Reviews, 2012).
277 Foreman, M. R., Swaim, J. D. & Vollmer, F. Whispering gallery mode sensors. *Advances in Optics and Photonics* **7**, 168-240, doi:10.1364/aop.7.000168 (2015).
278 Jonas, A. *et al.* In vitro and in vivo biolasing of fluorescent proteins suspended in liquid microdroplet cavities. *Lab on a Chip* **14**, 3093-3100, doi:10.1039/c4lc00485j (2014).
279 Sun, Y. Z. & Fan, X. D. Distinguishing DNA by Analog-to-Digital-like Conversion by Using Optofluidic Lasers. *Angewandte Chemie-International Edition* **51**, 1236-1239, doi:10.1002/anie.201107381 (2012).
280 Gather, M. C. & Yun, S. H. Single-cell biological lasers. *Nat. Photonics* **5**, 406-410, doi:10.1038/nphoton.2011.99 (2011).
281 Humar, M. & Yun, S. H. Intracellular microlasers. *Nat. Photonics* **9**, 572-576, doi:10.1038/nphoton.2015.129 (2015).
282 Gather, M. C. & Yun, S. H. Lasing from Escherichia coli bacteria genetically programmed to express green fluorescent protein. *Optics Letters* **36**, 3299-3301, doi:10.1364/ol.36.003299 (2011).
283 Toffanin, S. *et al.* Low-threshold blue lasing from silk fibroin thin films. *Applied Physics Letters* **101**, doi:10.1063/1.4748120 (2012).
284 Michalet, X. *et al.* Quantum dots for live cells, in vivo imaging, and diagnostics. *Science* **307**, 538-544, doi:10.1126/science.1104274 (2005).
285 Reis, C. P., Neufeld, R. J., Vilela, S., Ribeiro, A. J. & Veiga, F. Review and current status of emulsion/dispersion technology using an internal gelation process for the design of alginate particles. *Journal of Microencapsulation* **23**, 245-257, doi:10.1080/02652040500286086 (2006).
286 King, N. P. *et al.* Accurate design of co-assembling multi-component protein nanomaterials. *Nature* **250**, 103-108, doi:10.1038/nature13404 (2014).
287 King, N. P. *et al.* Computational Design of Self-Assembling Protein Nanomaterials with Atomic Level Accuracy. *Science* **336**, 1171-1174, doi:10.1126/science.1219364 (2012).